SSD

SCIENCE FOR A SUSTAINABLE DEVELOPMENT

A DECISION SUPPORT TOOL TO MANAGE CLIMATE CHANGE RISKS TO FOREST ECOSYSTEMS

"ECORISK"

G. DECKMYN, T. AL MAHAINI, E. ANDIVIA, M. BORTIER, A. DECKMYN, J.G. GENON, O. GIOT, R. HAMDI, M. JONARD, Q. PONETTE, S. SARIOGLU, J. VIVES I BATLLE & R. CEULEMANS

ENERGY

TRANSPORT AND MOBILITY

AGRO-FOOD

HEALTH AND ENVIRONMENT

CLIMATE

BIODIVERSITY

ATMOSPHERE AND TERRESTRIAL AND MARINE ECOSYSTEMS

TRANSVERSAL ACTIONS

.be

SCIENCE FOR A SUSTAINABLE DEVELOPMENT
(SSD)

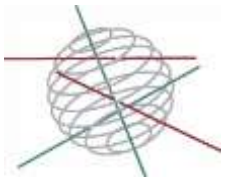

Thematic risks

FINAL REPORT

A DECISION SUPPORT TOOL TO MANAGE CLIMATE CHANGE RISKS TO FOREST ECOSYSTEMS

"ECORISK"

SD/RI/06A

Promotors
R. CEULEMANS (UAntwerpen)
Q. PONETTE (UCL)
R. HAMDI & A. DECKMYN (RMI)
J. VIVES I BATLLE (SCK•CEN)

Authors
G. DECKMYN[1], T. AL MAHAINI[4], E. ANDIVIA[2], M. BORTIER[1], A. DECKMYN[3], J.G. GENON[2], O. GIOT[1,3], R. HAMDI[3], M. JONARD[2], Q. PONETTE[2], S. SARIOGLU[4], J. VIVES I BATLLE[4] & R. CEULEMANS[1]

[1] UAntwerpen, Universiteitsplein 1, 2610 Antwerpen
[2] UCL, Croix du Sud 2, 1348 Louvain-la-Neuve
[3] RMI, Ringlaan 3, 1180 Ukkel
[4] SCK•CEN, Boeretang 200, 2400 Mol

Universiteit Antwerpen
UCL Université catholique de Louvain
SCK•CEN STUDIECENTRUM VOOR KERNENERGIE CENTRE D'ETUDE DE L'ENERGIE NUCLEAIRE
KMI

Published in 2017 by the Belgian Science Policy
Avenue Louise 231
Louizalaan 231
B-1050 Brussels
Belgium
Tel: +32 (0)2 238 34 11 – Fax: +32 (0)2 230 59 12
http://www.belspo.be

Contact person: Christine MATHIEU
+32 (0)2 238 34 93

G. Deckmyn, T. Al Mahaini, E. Andivia, M. Bortier, A. Deckmyn, J.G. Genon, O. Giot, R. Hamdi, M. Jonard, Q. Ponette, S. Sarioglu, J. Vives i Batlle & R. Ceulemans. ***A decision support tool to manage climate change risks to forest ecosystems "ECORISK"***. Final Report. Brussels: Belgian Science Policy 2017 – 103 p. (Research Programme Science for a Sustainable Development)

Table of Contents

SUMMARY

A. Context

In the global change context, forest ecosystems are key components for successful mitigating strategies. At the Belgian scale, the major roles of forest ecosystems have been highlighted in the National Climate Plan (NCP, 2008) for the period 2009-2012, through a series of strategic axes. Briefly, the plan includes the following aims along six strategic axes: (1) to optimize energy production; (2) to make a rational use of energy within the buildings; (3) to act on industrial processes; (4) to develop sustainable forms of transport; (5) to promote sustainable management of agricultural and forest ecosystems; (6) to increase efforts in waste management.

In addition to being central in climate issues, forests also provide the human society with goods and services fundamental to human well-being. These include provisioning services, regulating services, cultural services and supporting services (Millennium Ecosystem Assessment, 2005).

The extent to which forest ecosystems will be able to effectively ensure these roles in the future remains, however, poorly documented, due to an intricate web of factors related to both direct and indirect effects of global change.

Direct effects are due to a combination of stress events (e.g. extreme droughts) and of diffuse pollution (contamination, nutritional unbalances), which may act at different time scales and with different intensities.

Indirect effects are those generated by alternative energy sources used to mitigate climate change impacts. Among these options, woodfuel and nuclear energy are of special concern due to their potentially drastic effects on forest ecosystems. The impacts of the expected increased biomass harvesting on forest ecosystems will strongly depend on final wood utilization as the latter largely dictates management decisions such as species selection, rotation length, and harvesting strategies. The impact of radionuclides on forests is also to be considered as a possible side effect of mitigation strategies, whatever final decision on nuclear energy use at the Belgian scale will be, as their emissions are clearly a transnational issue.
Due to their perennial character, forest vegetation systems affect dispersion of pollutants, including radionuclides, and their distribution in the biosphere.

B. Objectives

The aim of this project was to design a methodology capable of modelling scenarios of forest growth, nutrient uptake and pollutant behaviour under different forest, soil, groundwater and climate conditions in Belgian forests. Although originally this was envisaged to take the form of a decision support tool, eventually it was decided that an integrated modelling platform should be developed first. Emphasis is not only on forest growth and productivity, but also on the soil carbon and nutrient status and the possible changes in the distribution of a number of elements, including pollutants and radioactive substances.

C. Conclusions

We developed a fully integrated modelling platform able to simulate detailed responses of forest ecosystems to changes in climate, pollution and management. The model can explore the feedback mechanisms between growth, management, climate and nutrient status of the soil and simulate the transfer of nuclear pollutants through the soil and the ecosystem. The downscaled climate scenarios developed within this project can be used for many other modelling studies. Main innovations in the models are the detailed soil water (including upward capillar flow), and the detailed soil nutrient cycling (active decay of soil organic matter, detailed uptake from the soil solution, allocation to tree compartments, interaction with the soil substrate and weathering).

We have used the model for specific stand scale applications in intensively monitored sites. This has led to an increased process understanding and the following main conclusions from a set of case studies:

- Not only the average climate, but also the climate interannual variability is important for ecosystem stability.
- By running many random weather variations from each climate scenario, we can calculate the risk of an 'unlucky' weather sequence resulting in severely reduced growth.
- Changes in ground water or in soil temperature have important effects on soil nutrient status (by effects on decomposition) which impacts stand growth.
- Soil nutrient status is crucial for stand development of forests in Belgium and nutrient availability constrains forest response to climate change.
- Changes in forest management affects soil chemical fertility through nutrient removal by harvesting (leaving dead branches/ bark at harvest).

- Radionuclides disperse in the forest ecosystem through soil water fluxes and diffusion within the soil and eventually enter plant roots.

D. Contribution of the project in a context of scientific support to a sustainable development policy

The modelling platform is available for decision support and climate change impact at stand scale applications on request to the project coordinators. It can serve as a benchmark to more empirical models with larger spatial coverage, but less detailed process descriptions. As such, the modelling platform can contribute to sustainable development under climate change:

- The climate simulations will be used for analyzing climate impact at European and Belgian scales within the CORDEX framework.
- The simulations can be used to optimise forest management options as to yield a sustainable production of woody biomass without disturbing soil carbon and nutrient stocks.
- The carbon budget simulations are useful to understand and evaluate the current role of the forests in sequestering CO_2.
- Optimisation of radiation protection of the environment by improving risk assessment of the impact of radionuclides from contaminated soils to vegetation.

E. Keywords

forests – global climate change – soil nutrients – radionuclides – modelling – feedbacks – impact

1. INTRODUCTION

In the global change context, forest ecosystems are key components for successful mitigating strategies. In addition to being central in climate issues, forests also provide the human society with goods and services fundamental to human well-being. These include provisioning services, regulating services, cultural services and supporting services (Millennium Ecosystem Assessment, 2005).

The extent to which forest ecosystems will be able to effectively ensure these roles in the future remains, however, poorly documented (Campioli *et al.*, 2012), due to an intricate web of factors related to both direct and indirect effects of global change.
Direct effects are due to a combination of stress events (e.g. extreme droughts) and of diffuse pollution (contamination, nutritional unbalances), which may act at different time scales and with different intensities. These factors could drastically alter the expected positive impacts on forest productivity associated with the observed trends in environmental drivers as increased length of the vegetation period, increased CO_2 concentration and increasing nitrogen supply (Lindner *et al.*, 2010). Although increased forest productivity has been observed in Western Europe (e.g. Bontemps *et al.*, 2009; Charru *et al.*, 2010; Bontemps *et al.*, 2011), the sustainability of this increase remains indeed largely unknown as it depends on a series of biotic and abiotic climate-mediated factors acting through a complex array of feedbacks (e.g. Hyvönen *et al.*, 2007).

Indirect effects are those generated by alternative energy sources used to mitigate climate change impacts. Among these options, woodfuel and nuclear energy are of special concern due to their potentially drastic effects on forest ecosystems. The impacts of the expected increased biomass harvesting on forest ecosystems strongly depends on final wood utilization (biomass *vs*. long-term carbon sink materials) as the latter largely dictates management decisions as species selection, rotation length, and harvesting strategies. The impact of radionuclides on forests is also to be considered as a possible side effect of mitigation strategies, whatever final decision on nuclear energy use at the Belgian scale is. Due to their perennial character, forest vegetation systems affect dispersion of pollutants, including radionuclides, and their distribution in the biosphere.

Extreme climate events can play an important role in altering the fluxes and storage of these substances in the ecosystem, but these have been overlooked, i.e. there is still a high degree of uncertainty on estimations of long-term pollutant risks. On the other hand, long-lived radionuclides released from an underground nuclear waste repository

may reach the vegetation via the groundwater and also constitute a potential risk for humans and biota through different pathways potentially affected by extreme events.

The aim of the ECORISK project was to design a tool capable of modelling scenarios of forest growth, nutrient uptake and pollutant behaviour under different forest, soil, groundwater and climate conditions in Belgian forests. Emphasis was not only on forest growth and productivity, but also on the soil C and nutrient status and the potential changes in the distribution of a number of elements, including pollutants and radioactive substances.

2. METHODOLOGY AND RESULTS

The consortium already had ample experience in modelling of several aspects related to simulating the effects of global change on forest services. The models that were available at the start of the project (2012) were:

ALARO-0 is a new model version of the ALADIN model, which is the Limited Area Model (LAM) version of the Action de Recherche Petite Echelle Grande Echelle Integrated Forecast System (ARPEGE-IFS) (Bubnová *et al.*, 1995; ALADIN international team, 1997). Since the 1990s the ALADIN model has been widely used in the numerical weather prediction community and, more recently, in regional climate modelling (e.g. De Troch *et al.*, 2013; Hamdi *et al.*, 2012, Giot *et al.* 2016). In the research department of the RMI, the model is used for regional climate simulations since 2010.

PHREEQC is a geochemical equilibrium and reaction code that has been developed by USGS since the 1990's and is still evolving: Parkhurst and Appelo (2013), Charlton and Parkhurst (2011).

ANAFORE is a stand-scale forest model that was developed by UAntwerpen and simulates forest C, nitrogen (N) and H_2O fluxes in function of climate, soil, stand characteristics and forest management (Deckmyn *et al.* 2008). At the start of the project other nutrients/pollutants (besides N) were not simulated by ANAFORE.

A five work package (WP) framework was used to add and improve on the already existing individual models (see Figure 1).

1. In the first WP the newly developed model ALARO-0 (Gerard *et al.* 2009) was used to downscale the latest IPCC global projections of the global ARPEGE model on a European domain with a very high 12.5 km resolution within the context of the CORDEX initiative, an international effort for Intercomparison of regional climate models.
2. The ecophysiological ANAFORE model (Deckmyn *et al.* 2008, 2011) developed by the UA team deals with water, carbon and nitrogen cycles in forest stands, focusing on soil organic pools and processes. In WP2 a more detailed representation of the mineral soil processes and of the behaviour of an additional set of nutrients – mainly phosphorus, calcium, magnesium and potassium – was developed by coupling the existing ecophysiological model with a geochemical equilibrium and reaction model (PhreeqC). A much more detailed allocation of elements within the tree was developed as well as a better representation of the pathway of all elements in the soil organic matter (SOM) as new modules in the ANAFORE forest model.

3. The third WP dealt with the integration of pollutants into the modelling system by simulation of the water transfer and the transfer of dissolved elements/pollutants by the water incorporating the transport of solutes in a simplified way by means of a parametric K_d approach. An improved and more detailed soil description and hydrology model was added to the ANAFORE model (half-hourly time-steps and 1 cm soil layers) to enable this. For radionuclides a module was added to ANAFORE to calculate the radioactive dose (Bq) of a polluted forest. Radionuclides are simulated by linking them to the most similar nutrient and following the same pathway as the nutrient (with the option to introduce selectivity coefficients).

4. The fourth WP involved running different climate scenarios with parameterisations for spruce and Scots pine, and validating the combined model including the effects of micro- and macro-nutrients and pollutants. The influence of forest management on the response of forests was also analysed in this WP.

5. Finally, the last WP was devoted to the development of the final tools and conclusions. At the start of this project it was not sure whether we would be able to have a single system running in real time including all the calculations or a database with results from runs using separate tools.
   The end product is a fully functional improved ecosystem model ANAFORE that can be dynamically linked to the PhreeqC soil geochemical code or used with a simpler, empirical model for P solubility. This model can be used to make risk-maps for different climate and management options and examples for a few key questions are included in this report.

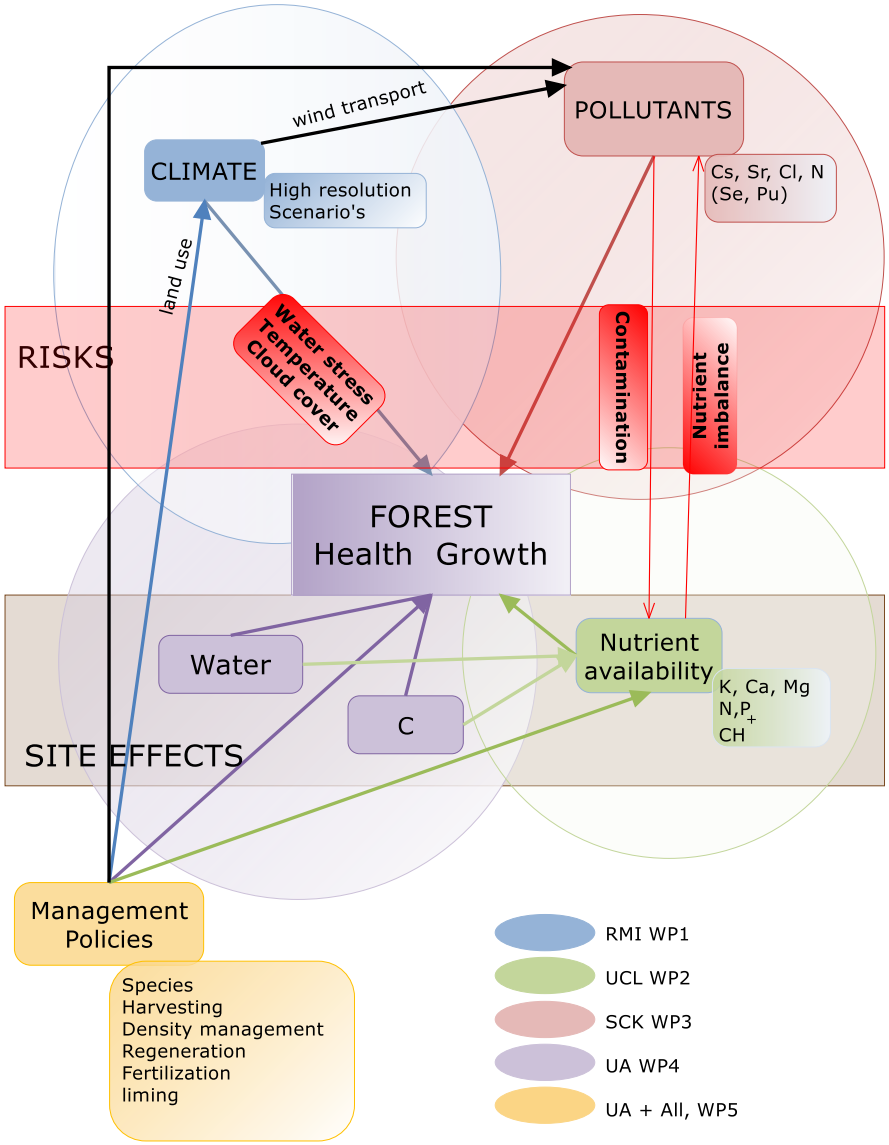

Figure 1. General model flow and interaction among WPs

The first step in the analysis was to assess the exposure of Belgian forest ecosystems. Exposure related to direct effects of global change was dealt with by deriving regionalized climatic impact factors from a newly-developed Regional Climate Model (WP1). Exposure related to indirect effects (alternative energy selection) was considered by designing policy and forest management scenarios (WP5). Based on these scenarios, the impacts of global climate change on forest ecosystems was assessed in terms of resource availability (nutrients, WP2) and pollution/contamination (radio-isotopes and other contaminants; WP3) through the development of specific modules that were integrated in the existing ANAFORE mechanistic forest stand model.

In a second step, the sensitivity of forest ecosystems to climate change exposure and the likely impacts on forest services was considered. A more realistic description of forest response in terms of growth and health was obtained by designing a specific nutrient module, allowing to take into account major soil feedbacks instead of considering only single factor responses (WP2 and WP4). The possible changes in the uptake action of forests on pollutants (radioisotopes, heavy metals) was approached with a specific sub-model allowing the quantification of pollutant distribution in the soil-plant-water continuum (WP3 and WP4), while taking climate change impacts on forest productivity into account.

Change in nutrient availability as a result of both direct (e.g. increased N deposition) and indirect (increased biomass harvesting) effects of global change were quantified by coupling the newly developed nutrient sub-model, allowing to quantify the distribution of nutrients between the tree and the soil (through modelling of nutrient uptake and returns), and within the tree tissues (WP2 and WP4). Changes in carbon storage and forest yield are direct output of the upgraded ANAFORE model.

The third step consisted of a detailed assessment of uncertainties and variability of risks attached to management decisions, for supporting policymakers (WP5). This was performed by running various versions of the ANAFORE model (WP4) under a set of selected climatic scenarios and policy/management options on specific sites using randomised weather variations and statistical input parameter distributions to create a robust output with uncertainty and risk evaluation.

This report starts with a short model description (section 2.1), followed by a descriptions of the used sites (section 2.2) and an overview of the necessary parameterisations (section 2.3). Then, model testing and verification (section 2.4) and final results (section 2.5) are given. In section 3 the policy support is discussed.

2.1. Model descriptions

2.1.1. Climate modelling

The climate projections used in the Fifth Assessment Report (AR5) of the Intergovernmental Pan el on Climate Change (IPCC, 2013) are based on the set of Global Climate Model (GCM) simulations performed within the fifth Coupled Model Intercomparison Project (CMIP5; Taylor et. al 2012). Over the last centuries these GCMs have been developed in order to study the response of the Earth's climate to changes in its composition, such as an increase in carbon dioxide concentrations, or changes at its boundaries, such as an increased insulation or volcanic activity. These

models, which are based on Numerical Weather Prediction (NWP) models, have at their core a set of equations that describes the motion of the atmosphere. Unfortunately, solving this set analytically is impossible and a numerical solution is required.

This means that (i) one needs to choose a grid, i.e. select a few points in space and time where the state of the atmosphere is a representative for the region around it, and (ii) to choose a numerical solver for the equations, i.e. select a mathematical approach which focuses on stability, efficiency and obviously correctness. Ideally, one would choose a very fine grid as this would lead to a more detailed model, but that also implies a large number of grid points and therefore a large number of computations. In order for the complete 100-year simulations to be finished within a few months, the horizontal resolution (i.e. the distance between two grid points) is limited to 50-200 km for state-of-the-art GCMs by this computational constraint. Dozens of different research institutes from all over the world have proposed and developed different approaches and solutions to this problem. Therefore, the climate community now possesses a rich variety of GCMs, which can be compared to observations and one another. One such a GCM, which is used in this project, is ARPEGE-Climat (Déqué *et al.*, 1998), developed by Météo-France.

For local impact studies, more detailed information in both space and time than can be provided through GCMs is required on many key regional and local aspects and underlying physical subgrid scale processes, such as extreme precipitation, which are of particular interest for impact researchers, stakeholders, and policy makers (Rummukainen, 2010; Prein *et al.*, 2015, Teutschbein and Seibert, 2010). In this case, Regional Climate Models (RCMs; Giorgi and Mearns, 1999) can provide a solution. RCMs are based on the same principles as GCMs, with the major difference that the former only covers a part of the globe, for example Europe. For the smaller study area, the same number of grid points can therefore be positioned closer to one another, increasing the resolution. This technique introduces a new challenge: by defining the study area, arbitrary boundaries are introduced on the Earth's sphere across which one has no idea what is going on, for example when a front is coming in. Therefore, the coarser GCM data is interpolated and used as lateral boundary condition (LBC) for the RCM. The RCM is said to be *coupled* to the GCM and the GCM is *downscaled* by the RCM.

2.1.1.1 ALARO-0

The ALARO-0 model is developed and maintained mainly through a collaboration between the Royal Meteorological Institute of Belgium (RMI) and the Regional Cooperation for Limited Area modelling for Central Europe (RC-LACE).
The model finds its origins in Numerical Weather Prediction (NWP) and it runs operationally in a number of countries of the ALADIN and HIRLAM consortia for the national NWP applications, the first of them already since 2008. More recently, the model is also used for climate simulations. At the research department of the RMI, the model is used for regional climate simulations since 2010.

ALARO-0 is a new model version of the ALADIN model, which is the Limited Area Model (LAM) version of the Action de Recherche Petite Echelle Grande Echelle Integrated Forecast System (ARPEGE-IFS) (Bubnová *et al.*, 1995; ALADIN international team, 1997). Since the 1990s the ALADIN model has been widely used in the NWP community and, more recently, in regional climate modelling. The model uses a diagnostic-type deep convection and microphysics parameterisation with upgrades from Gerard and Geleyn (2005). The new physical parameterisations within the ALARO-0 model as proposed by Gerard *et al.* (2009) were specifically designed to be used from the mesoscale to the convection-permitting scales (so-called *grey-zone* scales) and are built around an improved convection and cloud scheme, 3MT. The main feature of 3MT is scale awareness, i.e. the parameterisation itself works out which processes are unresolved at the current resolution, in contrast to traditional parameterisations which are switched on or off or have differently tuned parameter values at different resolutions. This allows 3MT to generate consistent results across scales, as shown by De Troch *et al.* (2013), to which we also refer for full model details.

2.1.1.2 CORDEX

The Coordinated Regional Climate Downscaling Experiment (CORDEX; Giorgi *et al.*, 2009) is an international effort for comparing the performance of several RCMs. By imposing a common experiment design, CORDEX simulations and thus RCMs can be compared to one another, which is an important model development and improvement stage. The EURO-CORDEX domain is prescribed in detail by the CORDEX community (see Figure 2) and consists of 501 by 501 grid points which are 12.5 km apart, a very high resolution for such a large domain. As in De Troch *et al.* (2013), 46 vertical levels were used. For these high resolution simulations, the time step of the model is small (180 s) for numerical stability reasons, implying that more time steps and thus calculations are required. Considering the high computational demand, the tier-1 supercomputer of the Flemish Supercomputer Centre was used to

perform these simulations. Using 64 double octacores, totalling to 1024 cores, a typical 30 year simulation would take several months and output tens of terabytes.

Figure 2. The EURO-CORDEX domain has the green box as borders. The analysis subdomains of Giot *et al.* (2016) are shown by the black areas.

2.1.1.3 Climate simulations overview

For this project the ALARO-0 model has been used to perform the EURO-CORDEX validation, recent past and RCP simulations (see Table 1 for an overview).

For the validation experiments the ERA-Interim reanalysis (Dee *et al.*, 2011) is used as LBCs for the 32-year period 1979-2010, abbreviated as "ERA". The ERA-Interim reanalysis produces a database of the state of the atmosphere at six-hourly intervals by starting a global atmospheric model integration and constantly nudging the atmosphere towards observations (e.g. temperature or wind speed) that were made. As such, in places where there were no observations, the model has a best guess of its state by integrating its governing equations. Every six hours, all fields are stored and can be used as LBCs for ALARO-0.

For the recent past experiment, the CNRM-CM5 historical simulation (Voldoire *et al.*, 2011) is used as LBCs for the 30-year period 1976-2005, abbreviated as "HIST".
The CNRM-CM5 model produces a database of the state of the atmosphere at six-hourly intervals by integrating the governing equations under a set of initial conditions

and observed external forcings. Initial conditions include ice mass, water reserves, soil conditions and external forcings include surface properties, greenhouse gases, aerosols, and solar irradiance. By using a set of different external forcings evolutions in time, the response of the atmosphere to those forcings can be quantified.

The major difference between the ERA and HIST simulation is that by construction the ERA states are correlated to the observed day-to-day weather. Or said differently, suppose that 1st of January 1983 was a very cold day, it should also be very cold in the ERA-Interim LBCs. On the other hand, the HIST simulations are constructed more like very long weather "predictions" started in 1850, but of course it is impossible to predict whether in a 100 years the 1st of January will be very cold or not. What one can do, however, is use the HIST simulation as a "climate prediction", also known as a *projection*. As such, the HIST simulations should be able to produce the climate (the distribution of weather events, e.g. the average number of frost days in January) but not the weather conditions of a specific year. Therefore, the ERA simulations serve as a first test for the model: given almost-perfect LBCs, can the RCM produce the correct local sequence of weather events? The HIST simulations are then a second test: can the RCM produce the correct local climate given LBCs from a GCM with observed external forcings? After withstanding these tests, the focus can shift to the future.

For the RCP experiments, three possible future evolutions of a set of external forcings are used to run CNRM-CM5 for the period 2005-2100. Three scenarios were used, (i) in RCP2.6 the GHG concentrations reach a peak mid-century and then gradually decrease as a consequence of the evolution to renewable energy (van Vuuren *et al.*, 2007), (ii) RCP4.5 projects a stabilization of GHG concentrations by the end of the century by employment of a range of technologies and strategies for reducing greenhouse gas emissions (Wise *et al.*, 2009), (iii) RCP8.5 assumes minor technological advances, a large energy demand and low climate change policies and thus a continuing increase in GHG emissions (Riahi *et al.*, 2007). The numbers 2.6, 4.5 and 8.5 denote the projected radiative forcing, i.e. the difference in incoming solar radiation and the energy radiated back in space. A larger positive radiative forcing implies that more energy is added to the Earth system, leading to an increase in temperatures.

Table 1. Climate simulations overview. The first column shows the experiment abbreviation as will be used in the text and figures, the second the global model used at the boundaries as LBCs and the third the period for which the simulation was performed. All experiments are on the domain shown in Figure 2 with a 12.5 km horizontal resolution.

experiment abbreviation	***GCM model + reference***	***period***
ERA	ERA-Interim (Dee *et al.*, 2011)	1979-2010
HIST	CNRM-CM5 historical simulation (Voldoire *et al.*, 2011)	1976-2005
RCP26	CNRM-CM5 RCP2.6 simulation (Voldoire *et al.*, 2011; van Vuuren *et al.*, 2007)	2005-2100
RCP45	CNRM-CM5 RCP4.5 simulation (Voldoire *et al.*, 2011; Wise *et al.*, 2009)	2005-2100
RCP85	CNRM-CM5 RCP8.5 simulation (Voldoire *et al.*, 2011; Riahi *et al.*, 2007)	2005-2100

All produced data are available through the Earth System Grid Federation data nodes (ESGF, website: http://esgf.llnl.gov/)

2.1.1.4 Coupling to ANAFORE

The climate simulations produce a huge set of tens of terabytes of climatic fields given on the RCMs grid and with an hourly temporal frequency. ANAFORE requires as climate input (i) 2-meter air temperature, (ii) rainfall, (iii) solar irradiance, (iv) CO_2 concentrations, (v) relative humidity. These are provided to ANAFORE as monthly mean or daily input values in a text file. In order to provide this file, a scripting procedure was developed to extract the data in the correct format from the ALARO-0 output. To obtain the model data for the three sites that are used in this report, we use the closest grid point to the given coordinates.

2.1.2. Water and pollutant transport modelling

This section deals with the modelling done under the third WP. This includes the integration of pollutants into the modelling system by simulation of the water transfer and the transfer of dissolved elements/pollutants by the water within a hydrological model incorporating solute transport in a simplified way by means of a parametric K_d approach. Additionally we developed as a new initiative, a very simplified soil-vegetation-atmospheric transfer model, ECOFOR, separate from the ANAFORE model, to initially test the concept of a parametric K_d for ECORISK, to help us to generate model parameters for the main model and (having fulfilled its purpose) as a platform for future sensitivity analyses and model abstraction in the search beyond this project

for a simple radioecological assessment model for forests. At the end of the project we produced a code to simulate water flow and solute transport in the variably saturated zone of the soil column. The conceptual model is shown in Figure 3.

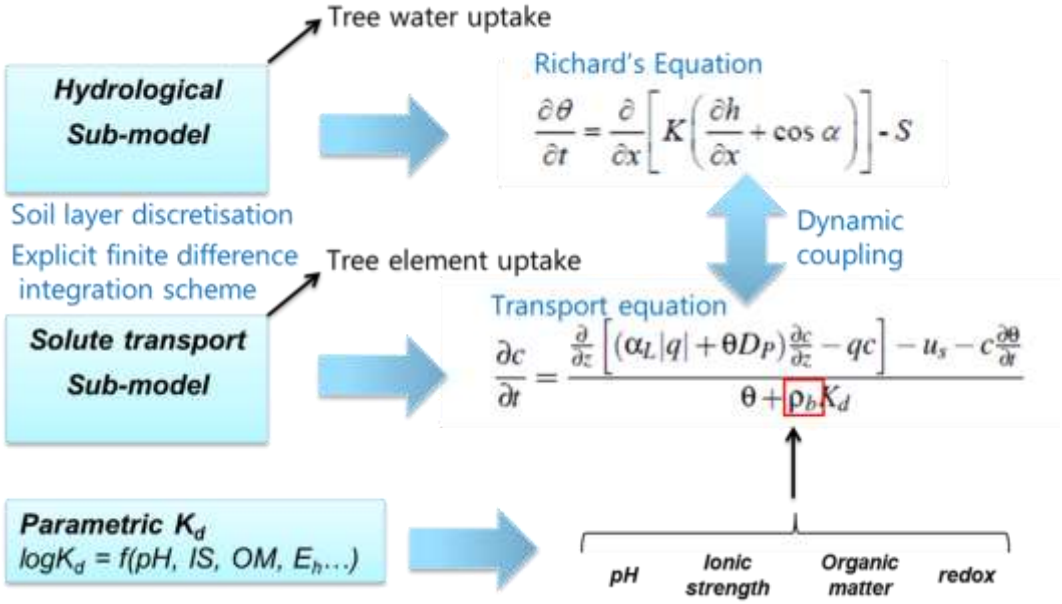

Figure 3: Conceptual model for the water and solute transport model developed at SCK-CEN for the ECORISK project.

2.1.2.1. Water transport through the unsaturated zone

The code accounts for the effects of short- and long-term changes in atmospheric conditions on soil water flow and distribution, the effect of the variation in soil physico-chemical properties on solute transport and includes a sink term to simulate removal of water from the root zone by root uptake. The model can be finally coupled to the ANAFORE forest model, which was well developed for its specific domain but did not explicitly account for the mechanisms that affect the availability of the water in the root zone (the vadose zone and the root zone are overlapping and indeed the two processes are strongly coupled).

The code implements a hydrological representation of water in the variably saturated zone below the tree roots (i.e. the depth of the soil column between land surface and the water table), in the form of a physically-based one-dimensional water flow model. This uses a finite difference approximation to Richards equation; specifically the one-dimensional pressure head based form of this, with root water uptake represented as a sink term:

$$C\frac{dh}{dt}=\frac{\partial}{\partial z}\left(K\left(\frac{\partial h}{\partial z}-1\right)\right)-U$$

where C = C(h) = dθ/dh is the moisture capacity (m^{-1}), θ is the volumetric water content ($m^3\ m^{-3}$), h is the soil water pressure head (m), t is time (s), z is the soil depth (directed positive downward) (m), K is the hydraulic conductivity ($m\ s^{-1}$), and U is the root water uptake rate (s^{-1}). This is a complex equation to solve because it requires knowledge of the constitutive relationships between θ, K, and h. The resolution of the equation is extremely difficult due to the fact that is a strongly non-linear partial differential equation, which is often difficult to approximate since it does not have a closed-form analytical solution.

A key aspect of hydrological models of this nature is how to represent the hydraulic conductivity. Initially, our code implemented the Brooks and Corey parameterisation of the hydraulic conductivity, applied to a multi-layered soil column (Figure 4). This approach represents the balance between the simplest soil-water balance models based on the "tipping-bucket" approach to more complex hydrological models. Later in the project we adopted the more refined Van Genuchten parameterisation:

$$S_e = \frac{\theta - \theta_r}{\theta_s - \theta_r} = \begin{cases} 1 \text{ if } \Psi \geq 0 \\ \dfrac{1}{\left[1 + (\alpha|\Psi|)^n\right]^{1-\frac{1}{n}}} \text{ if } \Psi < 0 \end{cases} \qquad K = K_S S_e^l \left[1 - \left(1 - S_e^{\frac{n}{n-1}}\right)^{\frac{n-1}{n}}\right]^2$$

where Se is the soil effective saturation, θr and θs are the residual and saturated soil moisture contents, respectively, α and n are empirical parameters that affect the shape of the hydraulic functions, Ks is the saturated hydraulic conductivity [LT^{-1}], and l is the pore connectivity parameter, equal to 0.5. We used pedotransfer functions to estimate the parameters (see Section 2.3).

In each time step, the water flow module numerically solves Richards' equation to determine the vertical distribution of soil water content and velocity in response to changes in weather conditions (i.e. precipitation and evaporation). The code is designed to simulate the hydrology of homogeneous and heterogeneous soils by allowing soil hydraulic properties to vary with depth. The code handles situations where the water table is shallow (i.e. the soil column is bounded by the water table) or deep enough to allow free drainage.

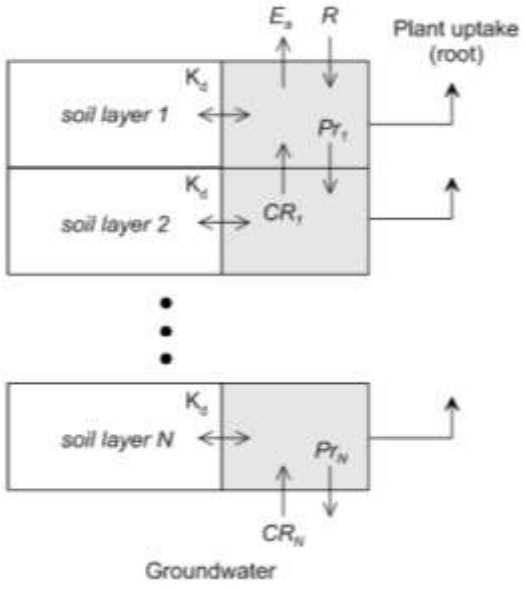

Figure 4. Typical solute-coupled groundwater representation. The soil is divided in to a number of discrete layers.

2.1.2.2. Solute transport through the unsaturated zone

The outputs of the water transport calculations, namely the soil water content and velocity, are passed as inputs to the solute transport submodule. Solute transport is modelled by the advection-dispersion equation:

$$R\frac{\partial C}{\partial t} = D\frac{\partial^2 C}{\partial t^2} - v\frac{\partial C}{\partial x}$$

where D is the diffusion coefficient, [m^2 s^{-1}], $v = q/\theta$ is the mean flow velocity or the transport velocity of a non-adsorbing solute [m s^{-1}], q is the 'Darcy velocity' [m s^{-1}] and θ is the volumetric water content [m^3 m^{-3}].

This equation also contains the dimensionless retardation for absorbing solute $R = 1 + \frac{\rho K_d}{\theta}$, here with a constant partition coefficient, or K_d [m^3 kg^{-1}] and factorising also the bulk density of soil ρ [kg m^{-3}]. The transport velocity is R times lower and the arrival time R times longer than for a non-adsorbed (conservative) solute. The K_d is calculated here using a parametric K_d-approach which obviates the need for complex geochemical model, and reduces the number of parameters required by the model to the level of what is available in environmental situations.

The one-dimensional advection-dispersion module is solved (numerically) with the appropriate initial and boundary conditions to calculate the vertical distribution of solutes. The transport of the solutes is driven by advection (with flowing water) and

hydrodynamic dispersion (combined effect of mechanical dispersion and molecular diffusion). A term is included for the removal of solutes by the plant.

The water and solute transport submodel accounts for the retardation of solute transport due to interactions with soil constituents by using a retardation factor. This factor is a measure of the reduction in solute velocity relative to that of water due to sorption and it is a function of soil water content, bulk density, porosity, and solid-liquid distribution coefficient (K_d). For the K_d, we use a parametric approach to estimate its value from basic soil physicochemical properties (e.g. pH, clay, and organic matter content, are used. This method allows the code to simulate changes in the pollutant sorption with depth due to changes in soil physicochemical properties by changing its K_d value.

The code as developed can deal with 34 elements for which there are parametric K_d equations: As, Cd, Ce, Cl, Co, Cr, Cs, Cu, Fe, Ho, I, La, Mn, Mo, Nb, Nd, Ni, Np, Pa, Pb,Pu, Ra, Sb, Se, Sm, Sn, Sr, Tc, Th, Tl, Tm, U, W and Yb. However, for this project we did not focus on all these elements, but on those for which the relationships are strongest and bearing in mind that the elements that have more radioecological significance are ^{137}Cs and ^{90}Sr, with the additional advantage that they can be coupled to K and Ca nutrient fluxes for which there already exists history in the ANAFORE model. The remaining elements are there to render the model future-ready for other projects.

2.1.2.3. Simplified model ECOFOR

The ECOFOR model is a simplified one-dimensional compartment model, which adopts a more simplified version of the hydrology than adopted in the ANAFORE model. It assumes a quasi-steady-state of water (laminar) flow, whereupon the higher kinetic terms of Richard's equation can be neglected and hydraulic conductivity is approximately constant. A 'tipping-bucket' approach is used whereby different soil layers in a 10 m soil column gradually fill-up as adjacent layers become saturated. The volumetric water content in each layer can fluctuate between a minimum, defined by the soil field capacity, and a maximum, defined by the soil porosity, until the resulting water table occupies the whole soil column, leading to runoff.

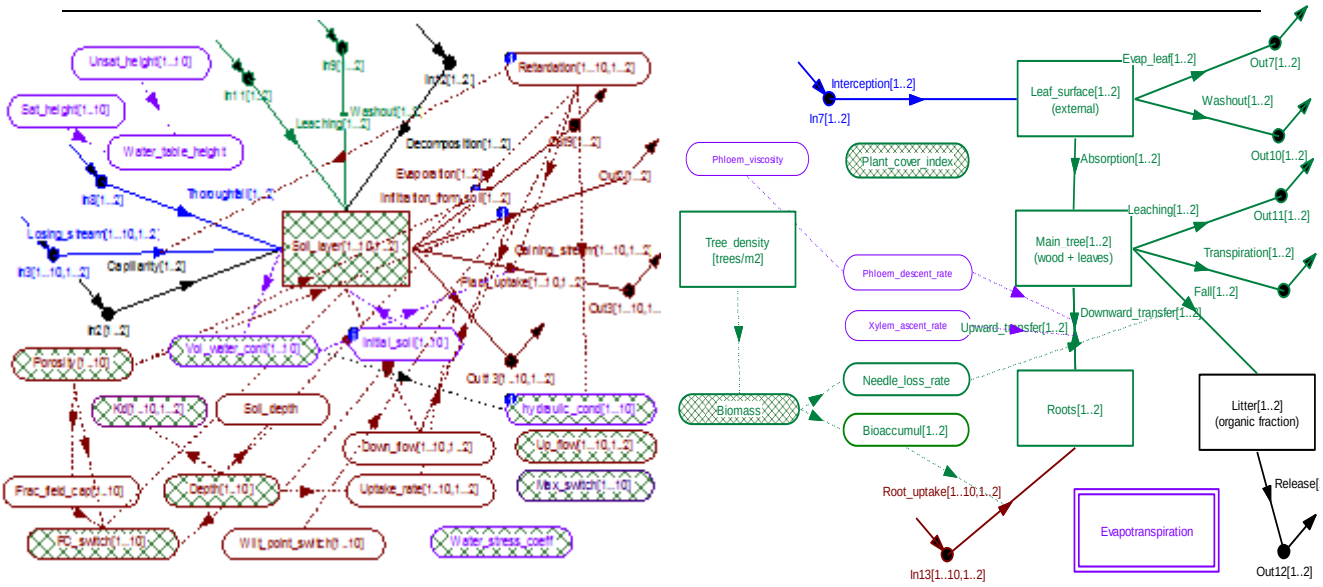

Figure 5: Conceptual model including compartments (rectangles), variables (rounded rectangles), definitions (polygons), flows (arrow lines) and influences (dotted arrow lines).

Downward water migration through the soil was modelled by Darcy's law and upper capillary transport is described by Newton dynamics' equation for a viscous non-compressible liquid, assuming quasi-steady Poiseuille flow, approximated by Phillip's law (1957). Though the model is one-dimensional, the effect of a nearby river is modelled by a simple losing or gaining stream with lateral flow calculated using Darcy or Torricelli flows, respectively.

Plant root water uptake was represented by an exponential root water uptake model (Li, Boisvert *et al.*, 1999), with the total root uptake rate balanced against the total evaporation demand and provision for soil drying (wilting point) or water logging (anaerobiosis, using a water stress coefficient).

Vertical transport is modelled as the ascent of xylem across a hydraulic potential gradient (Poiseuille equation) and the descent of the phloem – a 20% sucrose solution (Saupe, 2009) along an osmotic pressure gradient. The model calculates the combined effect of soil evaporation and plant transpiration using the Penman-Monteith equation (Monteith and Unsworth, 2007). Evaporation and transpiration are separated using a plant cover index, which according to Beer's Law is a function of the leaf area index.

The model apportions precipitation to different parts of the plant by the relevant interception, washout, absorption and leaching factors. Litterfall is assumed to be continuous, using an annually averaged, moisture-corrected needle mass turnover rate. Return of radionuclides to the soil is modelled by a constant decomposition rate. The model incorporates a simple logistic model for stand density, quantifying the effect of water availability on tree density.

From a hydrological point of view, Cl is usually considered to be a conservative element; hence the K_d is virtually 0 and there should be in principle no retardation in soil transport. However, the model provides a generic retardation approach linked to a K_d function of volumetric water content (Perez-Sanchez, Thorne *et al.*, 2012) applied to both infiltration and capillarity flows. We also assumed that radionuclide transfer from soil, and subsequent circulation within the tree, follow the water fluxes multiplied by the radionuclide concentrations in water and corrected by a selectivity coefficient Sc (Casadesus, Sauras-Yera et al,. 2008). Based on analogue chemistry, Sc for ^{36}Cl would arguably be equal to 1 but this coefficient was adjusted for each compartment to match the previous ^{36}Cl model.

2.1.2.4. Adaptation of ANAFORE for radionuclides and interaction of radionuclides with canopy

The main difference between simulating normal elements compared to radioactive elements is the radioactive decay. As output from the model values in Bq per surface area and per tree are calculated from the content of the different pools in the soil, the soil water and all tree compartments.

$$\frac{dRX_C[Bq]}{dt} = X_C[kg]\left(\frac{N_A\left[\frac{N}{mol}\right]}{10^{-3}\ x\ M_X\left[\frac{g}{mol}\right]}\right)\left(1-\frac{\lambda_X\ [d^{-1}]}{24\ x\ 60\ x\ 60}\right)$$

RX_C is the radioactivity of compartment C of radioactive element RX. X is element biomass in kg. M_X is molar mass (136,907g mol^{-1} ^{137}Cs). N_A is Avogadro's number, 6,022 x 1023 N mol^{-1}. The decay constant λ_X equals ln(2)/$t_{0,5}$X. ^{137}Cs has a half-life $t_{0,5}$ of 30,2 years so λ equals 6,29. 10^{-5} d^{-1}. Few data are available concerning the uptake and distribution of radionuclides in plants. For this study we opted to link each radionuclide to it's closest nutrient (in size) and assume that the radionuclide follows the same pathway. In a next stage this can be improved by including a selectivity coefficient S that reduces the uptake of the radionuclide compared to its 'sister' nutrient. For example Cs is linked to K.

$$\frac{dC_{RCs}}{dt} = \frac{dC_K}{dt}.\frac{[RCs]}{[K]}.S$$

Within the tree, the distribution is again coupled to the distribution of the sister element. When there is a nutritional shortage there is more uptake of the radionuclide and this is allocated to the needles/leaves where the nutrient is needed. While under nutrient rich conditions allocation is towards storage tissues and bark.

2.1.3. Nutritional constraints modelling

Nutrient availability exerts a tight control on forest ecosystem response to climate change. In densely populated and industrialized regions, forest ecosystems have been enriched by nitrogen deposition and are therefore gradually moving from nitrogen to phosphorus limitation (Peñuelas *et al.*, 2013). Other nutrients such as magnesium (Mg) and potassium (K) could also become or are already limiting in forests growing on acid soils (Jonard et al,. 2012). Therefore eco-physiological models of forest stand growth such as ANAFORE have to account for the processes regulating nutrient availability, in the short and in the long run, in order to correctly predict forest response to climate change (e.g. C sequestration) and to evaluate the impact of different adaptation and mitigation strategies.

In the biogeochemical cycle, the soil solution is the central nutrient pool in the soil, through which most of the nutrient flux passes. It is supposed to be in equilibrium with the soil ion exchange complex. Together they make a nutrient pool easily available to plants. Besides biologically driven processes leading to nutrient release or immobilization associated to transformation of the soil organic matter, the weathering or precipitation reactions of soil minerals are an additional source or sink of chemical elements.
Soil solution is also the compartment in which nutrients are taken up by roots and mycorrhizae before being distributed in the tree compartments and returned to the soil through litterfall and root death as a closure of the cycle.

Initially not widely developed in ANAFORE, the above mentioned chemical elements and groups of processes need to be modelled in the soil and have been added to ANAFORE by coupling the original model with a geochemical equilibrium and reaction calculation code (section 2.1.3.1), and with a simpler model for P only (section 2.1.3.2). Another submodel was added to account for soil organic matter mineralization and mineral element release (section 2.1.3.3). Finally, in order to assess potential nutrient limitations of tree growth, a refined nutrient uptake, allocation and cycling in the tree has been added to ANAFORE (section 2.1.3.4).

2.1.3.1. Chemical processes in the mineral soil

Figure 6 shows a general description of the chemical processes at layer/horizon level, based on a pool and flux approach. Inputs to the soil solution are the flux of elements produced by litter mineralization and the solute transfer from the upper or lower layer, or atmospheric deposition for the top layer. The mineral soil system re-equilibrates by ion-exchange and/or mineral dissolution/precipitation reactions, yielding an updated composition of the soil solution, exchangeable elements, and mineralogy. The

resulting new solution composition is then used to calculate the outputs of elements from the layer/horizon by uptake and solute transfer. The chemical processes associated with the mineral components of the soil were added to ANAFORE by interfacing its original code with the IPhreeqc library version of the geochemical equilibriums and reaction calculation code PHREEQC (Charlton and Parkhurst, 2011). Three groups of processes in the mineral soil are modelled with PHREEQC: (i) equilibrium within the soil solution itself, (ii) equilibrium between the soil solution and the soil ion exchangers, (iii) equilibrium or kinetic dissolution and/or precipitation of minerals.

The modules describing this submodel are closely interrelated with ANAFORE, as they receive input data from ANAFORE (water transfer and litter mineralization fluxes), and feed the updated chemical composition of mineral soil pools back to ANAFORE. The resulting soil solution is then directly used as an input to the uptake routine of the module dealing with element distribution and cycling in tree.

From the elements solution concentrations, exchangeable concentrations, mineralogy, soil-to-solution ratio and soil layer temperature, an IPhreeqc command string is composed that submits the solution, exchangers and minerals to the IPhreeqc chemical equilibrium and reaction functions. It is out of the scope to detail the working of PHREEQC itself. In short and classically for that kind of code, it solves a set of chemical equilibrium and kinetic reaction equations together with mass balance equations for each element. The parameters of the chemical reactions are read in the associated PHREEQC database. Then still according to the composed IPhreeqc command string, the results of the calculations are retrieved from the memory workspace of PHREEQC and output to ANAFORE.

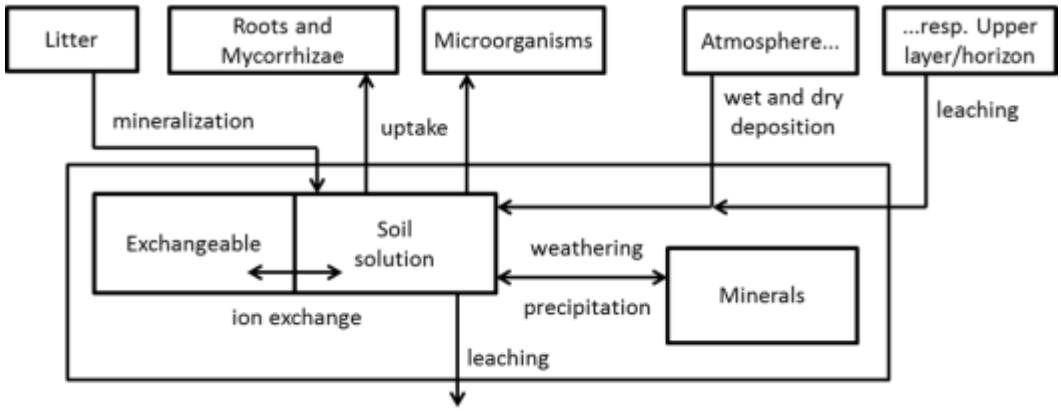

Figure 6. Chemical processes, pools and fluxes in the mineral soil layers.

2.1.3.2. Simple model for mineral phosphorus

Besides the general scheme dealing with a greater number of chemical elements and reactions, a lighter version of the augmented ANAFORE code works with carbon, nitrogen and phosphorus only. A simple model of phosphorus equilibriums and reactions in the mineral soil component was devised for this version (Figure 7).

The principles are the same as described for the more general case. However this model is inspired from a three-pool model involving fast-, medium- and slow-reacting pools of P (resp. labile, active and stable), plus a P-containing primary mineral. The fluxes of P between the pools are proportional to the source pool and controlled by the parameters K1-K5, which may be computed according to various equations.

$$P\ flux_{pool1,pool2} = K_{pool1,pool2} \quad P_{pool1}$$

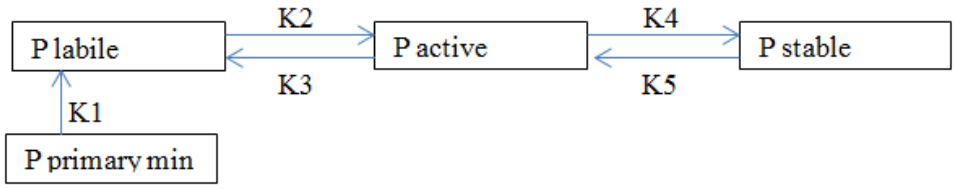

Figure 7. Phosphorus pools and fluxes in the mineral soil layers.

Within the labile pool, a solution and an adsorbed P subpools are in equilibrium, which is modelled with a Langmuir relation:

$$Pads = Pmax \frac{Psolu}{(Kp + P\ solu)}$$

Pads = adsorbed P (mass P / mass soil)

Pmax = maximum soil P sorption capacity (mass P / mass soil)

Psolu = solution P (mass P / volume soil solution)

Kp = Langmuir constant (mass P / volume soil solution)

Psolu + Pads = Plabile.

2.1.3.3. Mineral soil elements in SOM

New elements

The ANAFORE soil module already included cycling of C and N through the soil, and soil processes in function of humidity, soil texture, soil organic matter content and quality, temperature and pH. For the ECORISK project the ANAFORE soil module was expanded to include more elements. Because P is in many ecosystems co-limiting and is well studied in many forests, emphasis was on getting the P-cycle included and validated and assuming all other elements can be simulated using the same methodology if the required parameters are known. New elements concern both the

litter decay and the ectomycorrhizal uptake. Detailed description of the model can be found in the publication project (Bortier *et al.*, 2017, in preparation).

Litter decay

SOM decay is simulated as an active process by fungi and bacteria, in function of their requirements. In addition to energy and N, these microbes also need enough P to maintain their C:P ratio. Decay of SOM pools is initiated by all these requirements. This unique and novel way of describing litter decay can simulate known effects such as increased decay of recalcitrant matter under low-nutrient conditions (i.e. when P or N are limiting to the microbes, not energy), and is in line with the latest views on ecosystem functioning (Vereecken *et al.*, 2016).

Ectomycorrhizal (EM) uptake and transfer

Ectomycorrhizae (EM) fungi are very important for plant nutrient uptake, but most ecosystem models do not include this, so nutrient limitation is overestimated because EM can take up nutrients from SOM while plants need the nutrients to be in the soil solution. Transfer from the EM to the plants is simulated as a michaelis-menten type function, above a threshold nutrient content of the EM.

2.1.3.4. Element cycling in trees

General description: background and novelties

The uptake of elements (from soil water and through EM fungi) is modelled in more detail. A completely new allocation module of elements in the tree was added including more detailed description of pools to allow distinction between old and new tissues. For some elements the effects on photosynthesis, growth and allocation are known and were included in the model.

Most existing stand models empirically compare soil nutrient availability with tree demand and reduce growth to available nutrient levels in case of limitation (e.g. de Vries and Posch, 2011). In addition, tree nutrient demand is often calculated from average tree nutrient content or foliage nutrient content (e.g. Blanco *et al.*, 2005; de Vries and Posch, 2011), and the ability of trees to overcome nutrient limitations by remobilizing nutrient reserves is neglected. Moreover, ectomycorrhizae are on the whole rarely included in ecosystem models, resulting in an underestimation of the total element uptake, especially P, at tree level (Deckmyn *et al.*, 2014; Mollier *et al.*, 2008). Altogether, the lack of consideration of the ability of plants to react to nutrient deficiency in forest ecosystem models may result in an overestimation of plant growth, and therefore failure to accurately predict forest dynamics under climate change

scenarios (Fernandez-Martinez *et al.*, 2014; Jonard *et al.*, 2015). It is within this context that a complete process-based description of the nutrient cycling and its limiting effect on tree growth in forest models becomes crucial in order to understand the magnitude and direction of forest stands response to future changes.

Our nutrient cycling module is based on the law of mass conservation assuming that allocations and transfers of nutrients between tree compartments is regulated by the balance between source and sink-driven recycling and remobilization (Millard and Grelet 2010), which is ultimately controlled by soil nutrient availability.
The general description of element cycling in the model provides an excellent basis to simulate different elements, other than N and P, in forest ecosystem models. Indeed, nutrients such as K, Mg, or Ca could be easily simulated by adapting the uptake parameters and the effect of limitation on tree growth, and toxic elements such as Cd or Pb among others by adapting this mechanism to the effect of toxicity on tree growth.

Module description

a. Pools

Three different essential pool types are considered in the nutrient cycling module: soil pools, microorganism pools and tree pools. Here, we focus our description in those pools involved in element cycling in trees. Trees are divided in the following tissue pools: current year leaves or needles (l_0), old leaves or needles of evergreen species (l_1), dead bark of branches (bra_{bark}) and stem ($stem_{bark}$), current year sapwood of branches (bra_0), stem ($stem_0$) and coarse roots (cr_0), old sapwood of branches (bra_1), stem ($stem_1$) and coarse roots (cr_1), heartwood of branches (bra_{heart}), stem ($stem_{heart}$) and coarse roots (cr_{heart}), fine roots (fr) and fruits ($fruits$). These element pools are broadly classified into two groups, on one hand the functional tissue pools, that require elements to grow, comprising current year leaves or needles and sapwood, bark, and fruits; and on the other hand the internal reserves tissue pools, comprising old leaves or needles and old sapwood, whose element content can be depleted in case of nutrient deficiency. Furthermore, heartwood does not belong to either of these two categories, since it consists of dead tissue from which elements are retranslocated before its formation (Meerts, 2002).

All organ pools are characterized by their carbon content (C_{pool}), which is provided by the main ANAFORE model, element content (X_{pool}) and the derived element concentration on carbon content basis ($[X]_{pool}$). In addition to the actual element concentration in the pools, the deficient ($[X]_{def,pool}$), optimal ($[X]_{opt,pool}$) and toxic ($[X]_{tox,pool}$) concentrations are defined for each pool as input parameters. Besides these tissue

pools we define two non-physical pools at tree level. First there is the reserve pool (*res*) in which retranslocation from litterfall and element uptake over requirements are stored and which is only defined by its current and maximum element content (X_{res} and $X_{res,max}$ respectively). Elements stored in this pool are allocated to functional tissue pools in case of deficiency.

Secondly there is the temporary pool (*tem*) in which nutrients from internal reserves tissue pools are translocated before being distributed among functional pools in case of severer nutrient deficiency.

b. Growth requirements and tree element demand

The amount of elements demanded by trees is a central part of the element module because it determines the nutritional status of trees and may limit element uptake. Regarding this, we define two different levels of element needs: requirement and demand. At tree level, element requirement ($X_{req,T}$) is the amount of a specific element needed to support new growth at optimal concentration and to maintain the functionality of all tissues, i.e. keep all tissues at optimal concentrations.

$$X_{req,T} = \sum[(\Delta C_{pool} \times [X]_{opt,pool}) + C_{pool}([X]_{opt,pool} - [X]_{pool})]$$

Tree nutrient demand (X_{dem}) is the amount of a specific element needed to not only meet growth requirements but also to fill the reserve pool.

$$X_{dem} = X_{req,T} + X_{res,max} - X_{res}$$

The maximum element content of the reserves pool ($X_{res,max}$) is the maximum amount of elements that can be stored in this pool. This is physically limited to the amount of the element that corresponds to toxic concentrations in all tree tissue pools.

$$X_{max,res} = \sum C_{pool}([X]_{tox,pool} - [X]_{opt,pool})$$

c. Fluxes

In this section we briefly describe the internal elements fluxes accounted for in the module (Figure 8). For each specific element a series of inputs and outputs to the system are considered. We consider that elements in solution are absorbed by trees through three pathways (see Deckmyn *et al*. 2008; 2011): (i) by mycorrhizae ($X_{up,myc(i)}$) and (ii) fine roots ($X_{up,fr,dif(i)}$) through a combination of diffusion and active transport, and (iii) through the fine roots along with water uptake ($X_{up,fr,sol(i)}$). Part of the elements taken up by the mycorrhizae is transferred from the mycorrhizal reserve pool to the target trees (X_{trans}). In case that potential tree element uptake, consisting of these three components, is in one time step greater than the demand, total tree element uptake ($X_{up,T}$) is limited to the demand.

Next, the absorbed nutrient amount is allocated to the different tissue pools according to their requirements after which any excess is allocated to the reserve pool. When growth requirements are not met by uptake, elements are translocated from the reserve pool to the functional tissue pools. If translocation from the reserve pool is not sufficient to meet the growth requirements of the functional tissue pools, elements are remobilized from the internal reserves pools (the old tissue pools) and allocated to the temporary pool. Then, the remobilized amount of this element is redistributed among the functional pools. The amount of an element that is lost from each tissue pool through litterfall ($X_{lit,pool}$) is determined according to the litter biomass, which is simulated by ANAFORE, yet a fraction of this amount is retranslocated before litterfall occurs ($X_{retran\_in,pool}$) and allocated to the reserve pool. The element contents of litter from needles, branches and stems are then added to the litter pools in the surface organic layer, while litter from roots is added to the litter pools of both the organic and the mineral soil layers.

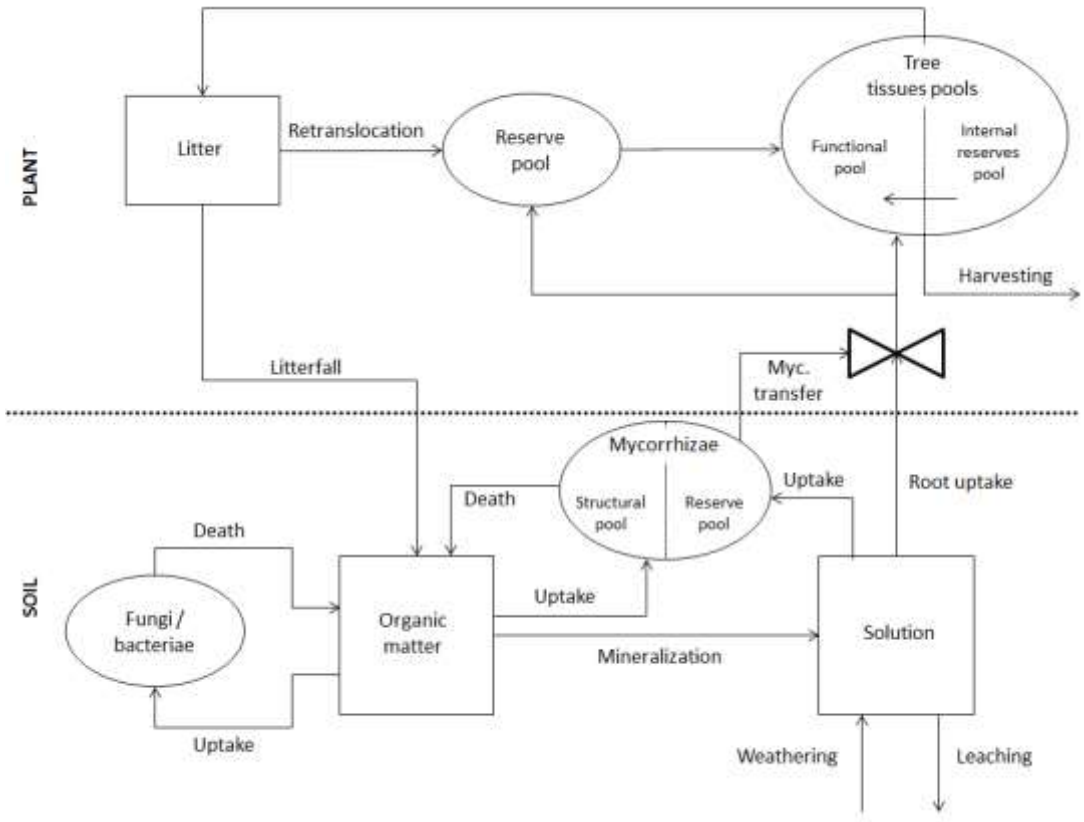

Figure 8. Nutrient pools and fluxes at tree level.

On the first day of the year, before the start of the growing season, elements from current year sapwood pools are transferred to their corresponding old sapwood pools (i.e; bra_0, $stem_0$ and cr_0 to bra_1, $stem_1$ and cr_1, resp.), from old sapwood to heartwood pools (i.e. bra_1 and $stem_1$ to bra_{bark} and $stem_{bark}$, resp.) and from current year needles (l_0) to old needles (l_1). If a sufficient amount is present in the initial tissue pool, the

corresponding older pool is supplemented till its optimal concentration. Since the optimal concentration of older tissues is typically lower any remaining amount from the initial tissues is then added to the tree reserves pool.

d. Element status

Five different situations according to the balance between on the one hand the element supply (element uptake and tree element reserves), and on the other hand the element requirement and demand by the tree are considered (Figure 9). In situation 1, the daily potential nutrient uptake exceeds the demand so the uptake is limited to the demand and the excess of elements is returned to the soil solution and mycorrhizal reserve pool proportionally to the contribution of the absorption mechanisms to the total potential uptake. In this case all tissue pools are at optimum conditions and the reserve pool is filled to maximum. In situation 2, the uptake is greater than requirements but lower than the demand. Accordingly, all tissues pools growth at optimal conditions and the rest of elements are allocated to the reserve pool. In situation 3, element uptake is lower than the requirement and, therefore, retranslocation occurs from the reserve pool to the tissues pools, which will growth at optimal concentrations. In situation 4 element uptake is also lower than requirement but the elements stored in the reserve pool are not sufficient to meet the requirements. In this case, requirements are met by translocating elements from the internal reserves tissue pools, those tissue pools that can be depleted in case of shortage, and allocating them to the temporary pool, from where the remobilized quantity is redistributed among the functional tissue pools at the same time step. The maximum amount of nutrients that can be remobilized from these internal reserves tissue pools in one day (X_{temp}) (old leaves/needles and sapwood) is calculated as:

$$X_{temp} = f_{X,temp} \sum C_{pool}([X]_{opt,pool} - [X]_{def,pool})$$

where $f_{x,temp}$ is a parameter that limits the amount of element that can be mobilized at each model time step from old tissues. The last situation (situation 5) implies that, in spite of all nutrients being taken from the reserves pool at tree level and the internal reserves tissue pools, the amount of nutrients supplied is not enough to achieve optimal concentrations.

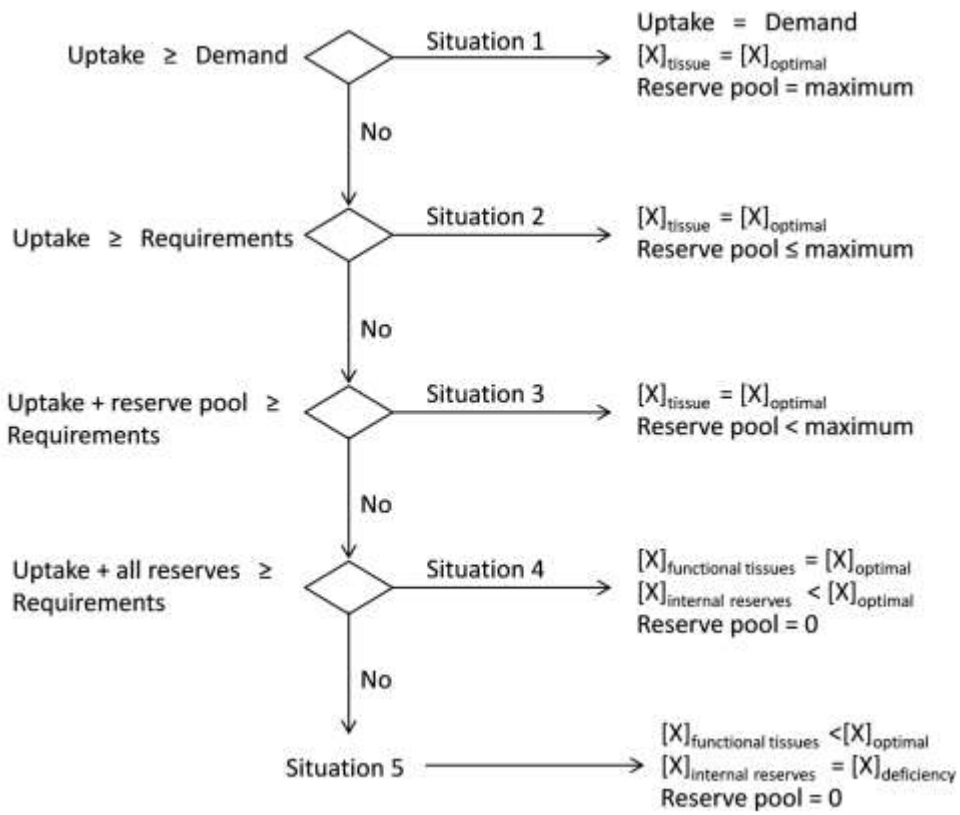

Figure 9. Decision diagram describing the different model situations according to tree nutritional status

e. Element shortage effect on trees

In general the effect of element shortage, or toxicity in the case of toxic elements such as pollutants, is implemented in the model according to the degree of the shortage or toxicity. In the case of essential elements, i.e. nutrients, these effects are implemented as the modification of biomass allocation and the limitation of photosynthesis and growth. Firstly, C allocation is modified by increasing the normal root to shoot growth ratio up to a maximum ratio when the element uptake is lower than the growth requirements, even if nutrient reserves are sufficient to fulfill the deficiency. When element concentration drops below the deficiency level, and in order to reduce growth, the construction respiration costs of each pool are increased proportionally (Deckmyn *et al*. 2008). We also define a critical concentration (i.e. minimum element level in leaves) below which growth is stopped altogether.

For N and P, parameter values exist to describe this, for other elements the model can be used if/when parameters for species-specific effects of the element are included. Other element-specific effects can be easily implemented in the module.

2.2. Site descriptions

For the initial testing and calibration of the models, we focused on four well-described forest stands where we had all necessary information to validate the new parts of the models.

2.2.1. Brasschaat

The experimental forest 'De Inslag' (51°18'33"N and 4°31'14"E) is located in Brasschaat in the Belgium Campine region. 'De Inslag' is a 1.3 ha plot that is dominated by Scots pine planted in 1929, and that belongs to the level-II observation plot of the European Programme for Intensive Monitoring of Forest Ecosystems. Since 1995 several studies concerning tree physiology, cycling of nutrients, CO_2 and water fluxes, forest vitality and air pollution have been conducted in the plot. The location has a temperate maritime climate, with a long term mean annual temperature of 9.8°C and 767 mm of precipitation. The soil consists of a moderately wet sandy soil characterized by a distinct humic and/or iron B-horizon on top of an impermeable clay layer at a variable depth between 1.5 and 2 m. The soil is classified as umbric regosol (F.A.O. classification). The organic soil layer has an average P content of 446 mg kg^{-1} and the P concentration in the underlying mineral layers ranges from 62 to 20 mg kg^{-1} top down (Overloop and Meiresonne, 1999).

2.2.2. Mol

The second stand was an experimental Scots pine (*P. sylvestris* L.) stand located in Mol (51°81'10" N, 58°50' E) in the Belgian Campine region (Fig. 9). The topography of the forest is flat and the altitude is 15 m. The climate is humid temperate. Mean annual PET is 616 mm per year, mean annual precipitation is 767 mm per year and the mean annual temperature is 9.8 °C. The stand is 45 acres in surface, was planted with Scots pine in 1949 on a former tilled soil.

The forest is dominated by Scots pine, but with small patches of Black Pine. In autumn 2004, the mean circumference of Scots pine was 91 cm, mean height was 22 m, stand basal area was 24.4 m^2 ha^{-1} and there were 359 trees ha^{-1}. The understory vegetation is mainly constituted by *Sorbus aucuparia*. The soil is a podzol, classified as a distric Cambisol. Seven distinct horizons exist, with one of them (IIIA) variable in thickness. The water table appears at low depth in spring (0.50–1.20 m), and has a strong seasonal variation (between 1 and 1.5 m of amplitude). A detailed description of the forest has been provided by Vincke (2006).

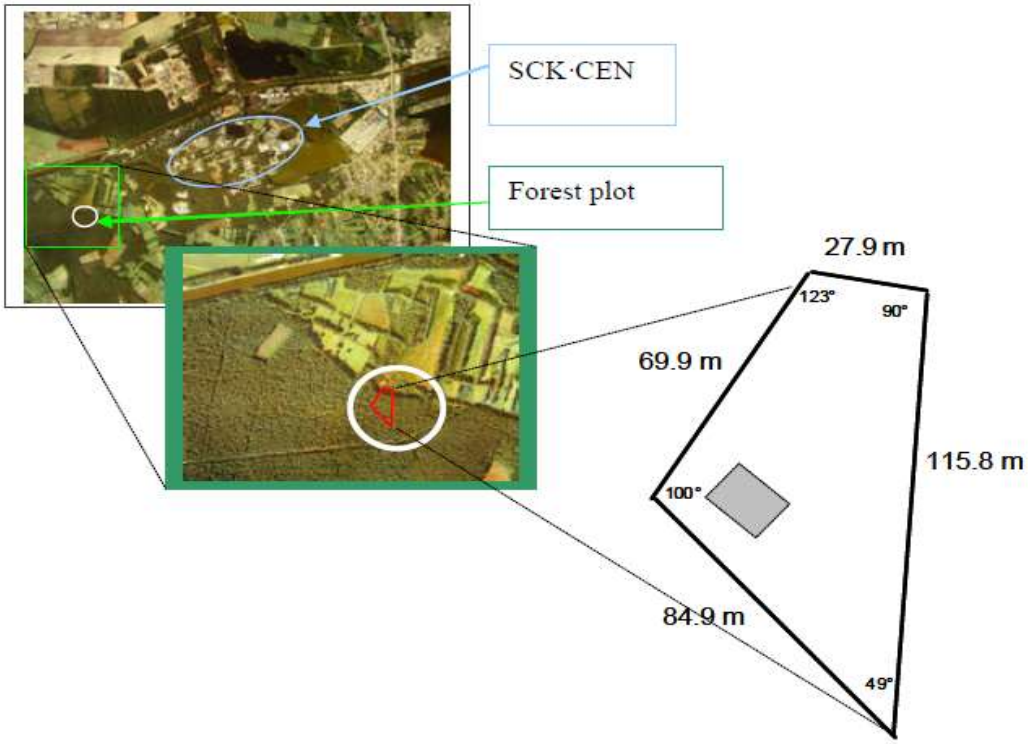

Figure 10. Location of the studied pine forest in Mol (Vincke 2006)

Previous research (Vincke and Thiry, 2008) quantified the water table cycle in Scots pines in the plot studied here. Continuous monitoring in 2005 revealed a shallow water table. Pine transpiration was estimated to be < 1.85 mm d^{-1}, 25% of the potential evapotranspiration (PET). Understorey transpiration was estimated as 18 – 20% of the stand water use. The maximum soil water reserve measured over the soil rooted zone was 250 mm, in which 145 mm was extractable water. The contribution of the water table to forest transpiration reached 61% (98.5% in dry periods).

Six pine trees were randomly chosen as part of a forest management plan to form a sample consistent with the average diameter of trees in the plot, reflecting its typical even-aged distribution.
The trees chosen have a circumference of 93 ± 16 cm and a mean height of 22.3 ± 0.6 m). These trees are therefore below 55 years old, an important consideration given that, in older trees (e.g. 65 years) the total content of N, P, and K in Scots pine would fall, whilst the Ca content would to rise due to progressive heartwood development (Wright and Will 1958). According to these authors, P and K contents in the heartwood of pine trees is very low, but Ca accumulates, contrary to the sapwood zone immediately surrounding the heartwood, where higher levels of all nutrients are found.

Stable element cycling in the forest was measured as part of this project (Gielen, 2013, Gielen; Vives i Batlle *et al.*, 2016) using a purposely-installed monitoring sampling

station, leading to improved parameters for radionuclide transport modelling. Specifically, Ca, K, Mg, Al, Cl and Mn were measured in tree components fractionated into 8 classes (heart and sapwood, inner and outer bark, living branches, twigs and younger/older than 1 y needles). For the trunk, discs of 5 cm thickness were cut at several heights above the ground (0, 6, 12 and 18 m). Soil and root samples were also taken. The soil vertical profile was as follows: humus layer, 0-23 cm, 23-53 cm, 53-66 cm, 66-89 cm or 89-110 cm. Stable element contents were measured analytically. At the same time, continuous hydrological monitoring (climate, throughfall, moisture, tree transpiration and water table variations) was maintained. From this information, we derived the necessary data to parameterise the water and pollutant transport module for the unsaturated zone (see parameterisation section 2.3.9 below).

2.2.3. Gedinne

The spruce stand of Gedinne is a level II core plot of the ICP-Forest network, located in the Ardenne (49°57'N, 4°50'E), at 460 m altitude. The trees grew from natural regeneration in 1949. The soil developed in weathered Upper Cambrian shale mixed with a solifluction sheet of Quaternary periglacial loess and classifies as a Cambisol (WRB) or Ghbfi/Gbbr (Belgian soil map legend).

Tree growth, litterfall mass and litterfall chemistry, rainfall, throughfall and soil solutions (at 20 and 70 cm depth) are monitored since the late 1990's, and a soil analysis was performed twice, according to the ICP Forests harmonized protocols available at http://icp-forests.net/page/icp-forests-manual (accessed Nov. 2016).
Table 2 presents the basic soil physicochemical characteristics by layers determined in 2011.

Layer	Depth	C_{org}	N	C/N	pH		Ca	Mg	K	Al	EA[1]	ECEC[2]	EBS[3]
	cm	g kg^{-1}			H_2O	$CaCl_2$	exchangeable, cmolc kg^{-1}						%
OL-OF		512	20.5	25	3.7	3.0	5.09	1.40	0.77	0.86	4.10	11.37	64
OH		462	20.4	23	3.4	2.6	3.03	1.21	0.47	4.93	9.34	14.06	33
	0-10	81	4.6	18	3.8	3.2	0.24	0.15	0.10	7.78	9.72	10.20	5
	10-20	34	2.3	15	4.2	3.9	0.09	0.05	0.04	3.74	4.52	4.71	4
	20-40	20	1.6	12	4.4	4.2	0.08	0.03	0.03	2.04	2.43	2.57	5

1. Exchangeable Acidity
2. Effective Cation Exchange Capacity = sum of exchangeable base cations + EA
3. Effective Base Saturation = sum of exchangeable base cations / ECEC

Table 2. Basic soil characteristics of the Gedinne profile by layers in 2011.

2.2.4. Baileux

The experimental site of Baileux is located near Chimay in Lower Ardenne (50°01'N, 4°24'E), at 300 m altitude. Average yearly precipitation is 1040 mm and temperature 8°C. The stands consist of pure oak, pure beech, and two levels of oak-beech mixing. They probably originate from an oak coppice that was converted into a high forest by the end of the 19th century and then invaded by beech.

The soil developed in weathered Lower Devonian sandstone and schist mixed with a solifluction sheet of Quaternary periglacial loess, and classifies as a Cambisol (WRB) or Dystrochrept (USDA Soil Taxonomy), with a moder-type humus under beech and closer to mull under oak. Table 2presents the basic soil physicochemical characteristics by horizons determined in 2004 in the pure oak stand (Jonard, 2005).

Layer	Depth	Corg	N	pH	Ca	Mg	K	Al	H	ECEC	EBS
	cm	g kg^{-1}		H_2O	exchangeable, cmolc kg^{-1}						%
Ah	0-6	79.0	7.0	4.0	0.43	0.55	0.50	8.34	0.98	12.51	21
Bw1	6-27	17.4	0.9	4.3	0.55	0.09	0.09	3.91	0.07	4.90	15
Bw2	27-42	7.2	0.9	4.4	0.47	0.11	0.10	3.97	0.13	5.14	18
2Bw3	42-55	6.8	0.8	4.4	0.56	0.24	0.12	6.79	0.00	7.81	13
2Bg1	55-75	5.5	0.7	4.5	0.47	0.36	0.12	6.84	0.26	8.32	14.
2Bg2	75-119	2.4	0.8	4.7	0.53	0.63	0.11	5.32	0.76	7.46	18.
2Bg3	119-160	2.3	0.9	4.8	1.38	0.84	0.13	5.99	0.41	8.13	21

Table 3. Basic soil characteristics of the Baileux oak profile in 2004.

2.3. Model parameterisation

2.3.1. Climate

The ALARO-0 model is a well established, tested and optimized model. Most of these optimizations were done within a NWP context, by assessing scores of daily weather forecasts. In de Troch *et al.* (2013) and Hamdi *et al.* (2012), it was shown that ALARO-0 also serves well as a climate model. Therefore, within this project no further

optimizations were performed and the exact model description of De Troch et. al (2013) was used for consistency.

2.3.2. Water and pollutant transport in unsaturated soil

The water transport model requires the following input parameters: soil hydrological data, weather data (temperature, precipitation), root-distribution, initial and dynamic boundary conditions. The outputs of the model (serving as inputs to the pollutant transport module) are time and depth water profiles, and water fluxes (infiltration, percolation, root uptake, drainage and actual evapotranspiration). The pollutant transport module requires also as inputs soil geochemical characteristics (expressed in the parameters of the parametric K_d equations), in order to produce as outputs time and depth profiles of solutes, and give the solute uptake by plants.

2.3.2.1. Parameterisation of the water transport submodule

The water transport submodel was parameterised using data from our own measurements in the Scots pine forest stand in Mol. The soil physico-chemical properties required by the model were derived from the following information, as shown in Table 4. A soil morphological description is given in Table 5.

The water table properties are described elsewhere (Vincke and Thiry 2008) (see Mol scenario description in Section 2.1.3 for a summary).

Table 4: Physico-chemical properties of Mol forest soil (Vincke, 2006)

Horizons	Depth (cm)	Sand (%)	Size class	Silt (%)	Clay (%)	pH (KCl)	pH (H2O)	Organics (%)
Ap	0-23	92,3	Coarse	6,1	1,5	3,4	4,21	2,03
B	23-41	91,5	Thin	6,5	2,0	3,97	4,73	0,61
IIAB	41-53	91,1	Thin	7,3	1,6	4,15	4,84	0,72
BC	53-66	91,7	Thin	8,0	0,3	4,35	4,96	0,43
IIIA	66-89	92,3	Peat	6,4	1,2	4,02	4,64	6,55
IIIB	89-110	91,9	Coarse	7,1	1,0	4,18	4,72	0,46
IVC	>110	91,9	Coarse	7,5	0,7	4,25	4,62	0,34

Table 5: Morphological properties of the Mol forest soil (Vincke, 2006)

Soil layer	Depth	Description
Ol	+5/+12–0 cm	Annual litter.
Ap	0 – 23 cm	Plowed Horizon. Not sticky, not plastic, non few small gravel. 10YR3/2. Textural class Z. Numerous thin roots (Æ 2-3 mm), few coarse roots, coarse sand.
Bw	23 – 41 cm	No structure, not sticky, not plastic, friable. Textural class Z. Almost no roots. 10YR6/4 with spots 10YR4/1 and spots 10YR2/1. Thin sand.
II AB	41 – 53 cm	No structure, not sticky, not plastic, few coarse roots (Æ 1 cm), 10YR5/3. BC (53 – 66 cm) No structure, not sticky, not plastic, no roots, thin sand.
IIIA	66 – 89 cm	Tourb (4.5YR2/0), greasy lime, structured, slightly firm, little, sticky and plastic, in bands with coarse sand (10YR4/2). A lot of roots, thin (mm) and mean (0.5 cm).
IIIB	89 – 110 cm	No structure, not sticky, not plastic, textural class Z, no roots. 10YR4/3, sand.
IVC	110 cm	Glauconifer sand (glauconite), 5Y5/2 No structure, not sticky, not plastic. Few roots channels with brown-red spots. Very coarse sand, very humid.

Based on this information, and additional data from the general literature, a complete parameter set for a model with the 7 soil layers given in Table 5 could be derived.

As an improvement to the earlier version of water flow module, the parameters of the hydraulic (van Genuchten) functions needed to solve Richards' equation are now calculated from basic soil properties (particle size distribution, dry bulk density, and carbon content), available through ANAFORE, using the pedotransfer functions of Vereecken *et al*. (1989):

$$\theta_s = 0.81 - 0.283\rho + 0.001C$$
$$\theta_r = 0.015 + 0.005C + 0.014O$$
$$\log(\alpha) = -2.486 + 0.025S - 0.351O - 2.617\rho - 0.023C$$
$$\log(n) = 0.053 - 0.009S - 0.013C + 0.00015S^2$$

where θ_s (-) is the soil saturated water content, θ_r(-) is the soil residual water content, α (cm^{-1}) and n (-) are van Genuchten parameter, ρ (g cm^{-3}) is dry bulk density, C (%), O (%), and S(%) are respectively clay, organic matter, and sand content of the soil.

It should be noted that the particle size distribution and dry bulk density are input parameters, whereas organic matter content is a variable which is calculated by ANAFORE as the forest grows. In order to account for the change that occurs in the

organic matter content as the tree grows, this is calculated at each time step, assuming that the dry bulk density remains constant.

Table 6: Hydrological parameters for model in the case of the Mol forest

Soil horizon	Parameter	Value
General	Water table depth in winter (m)	0.7
	Water table depth in summer (m)	1.3
	Soil density (kg m^{-3})	1300
1	Horizon thickness (m)	0.23
	Fraction of sand	0.923
	Fraction of clay	0.015
	Initial water (kg m^{-2})	20
	Saturation water (kg m^{-3})	118
	Maximum total water (kg m^{-3})	250
	Saturated soil hydr. cond. (m h^{-1})	0.00005933
2	Horizon thickness (m)	0.18
	Fraction of sand	0.915
	Fraction of clay	0.02
	Initial water (kg m^{-2})	54.4
	Saturation water (kg m^{-3})	67
	Maximum total water (kg m^{-3})	250
	Saturated soil hydr. cond. (m h^{-1})	0.000044637
3	Horizon thickness (m)	0.22
	Fraction of sand	0.911
	Fraction of clay	0.016
	Initial water (kg m^{-2})	44.2
	Saturation water (kg m^{-3})	131
	Maximum total water (kg m^{-3})	250
	Saturated soil hydr. cond. (m h^{-1})	0.000042451
4	Horizon thickness (m)	0.13
	Fraction of sand	0.917
	Fraction of clay	0.003
	Initial water (kg m^{-2})	68
	Saturation water (kg m^{-3})	148
	Maximum total water (kg m^{-3})	250
	Saturated soil hydr. cond. (m h^{-1})	0.000047881
5	Horizon thickness (m)	0.23
	Fraction of sand	0.923
	Fraction of clay	0.012
	Initial water (kg m^{-2})	50
	Saturation water (kg m^{-3})	250
	Maximum total water (kg m^{-3})	260
	Saturated soil hydr. cond. (m h^{-1})	0.000048526
6	Horizon thickness (m)	0.21
	Fraction of sand	0.919
	Fraction of clay	0.01
	Initial water (kg m^{-2})	19
	Saturation water (kg m^{-3})	111
	Maximum total water (kg m^{-3})	260
	Saturated soil hydr. cond. (m h^{-1})	0.000048547
7	Horizon thickness (m)	0.30
	Fraction of sand	0.919
	Fraction of clay	0.075
	Initial water (kg m^{-2})	19
	Saturation water (kg m^{-3})	111
	Maximum total water (kg m^{-3})	260
	Saturated soil hydr. cond. (m h^{-1})	0.000048547

2.3.2.2. Parameterisation of the solute transport submodule

The water and solute transport submodel accounts for the retardation of solute transport due to interactions with soil constituents by using a retardation factor. This factor is a measure of the reduction in solute velocity relative to that of water due to sorption and it is a function of soil water content, bulk density, porosity, and solid-liquid distribution coefficient (K_d). The K_d is a compound parameter that cannot be simply modelled at the geochemical model unless employing geochemistry codes, but these require parameters not generally available in environmental measurements. A practical alternative is the parametric K_d approach.

The IAEA Technical document 1616 (IAEA 2009) and, particularly, the papers by Vidal *et al*. (Vidal, Rigol *et al*. 2009) in this document gave us a good basis for this. We also found a particularly good review of regression relationships for many elements (Sheppard 2011), all of which commonly take the form of a nonlinear polynomial expression:

$$\log(K_d) = A + B \times pH + C \times \log[\text{organic carbon}] + D \times [\text{clay}] + E \times [\text{clay}] \times pH$$

Leading to tables of formulae such as the extract given in Table 7, each of which is determined statistically based on a large number of studies (typically > 50 and in several cases > 200).

Elem.	Regression equation	N	GSD	Soil organic carbon (%) 5th/95th percentiles
As	Log(Kd) = 2.39 + 0.085·(pH)	178	1.8	1.1/4.7
Cd	Log(Kd) = 2.35 + 0.114·(pH)	150	1.4	0/5.0
Ce	Log(Kd) = 1.84 + 0.469·(pH) − 0.00162·(clay)·(pH)	209	2.0	0.0/4.7
Cl	1.4 L kg^{-1} for mineral soils, 150 L kg^{-1} for organic soils	11/3	na	na
Co	Log(Kd) = 1.46 + 0.247·(pH) + 0.00709·(clay)	342	7.5	0.27/30
Cr	Log(Kd) = 1.61 + 0.290·(pH) + 0.381·log(organic carbon) where CrIII	83	3.0	0.29/30
	9.4 L kg^{-1} where possibly CrVI	51	2.0	0.06/8.0
Cs[a]	Log(Kd) = 3.03[a] + 0.101·(pH) + 0.0117·(clay)	470	5.6	0.09/40
Cu	Log(Kd) = 2.47 + 0.0656·(pH) + 0.00726·(clay)	205	1.4	0/4.7
Fe	Log(Kd) = 2.01 + 0.00442·(clay)·(pH)	44	3.2	0.81/31
Ho	Log(Kd) = 2.15 + 0.338·(pH) − 0.00094·(clay)·(pH)	161	1.7	0.0/4.8
I	Log(Kd) = 0.953 +0.701·log(organic carbon)	114	8.1	0.19/49
La	Log(Kd) = 3.26 + 0.234·(pH) − 0.0448·(clay) + 0.00517·(clay)·(pH)	227	1.8	0.0/4.7
Mn[b]	Log(Kd) = −0.330[b] + 0.457·(pH)	402	15	0.4/7.7
Mo	Log(Kd) = 3.22–0.212·(pH) + 0.0125·(clay)	215	1.9	0.44/4.8
Nb	Log(Kd) = 2.45 + 0.348·(pH) + 0.0960·(clay) − 0.0159·(clay)·(pH)	92	2.8	0.0/8.6
Nd	Log(Kd) = 2.98 + 0.271·(pH) − 0.0112·(clay) + 0.204·log(organic carbon)	228	1.9	3.5/5.5
Ni[c]	Log(Kd) = 0.816[c] + 0.229·(pH)	410	2.5	0.3/14
Np	Log(Kd) = −1.71 + 0.322·(pH) + 0.960·log(organic carbon) +	159	5.7	0.42/40
	0.00740·(clay)·(pH)			

Table 7: Parametric relationships for Kd from Sheppard (2011): example

In the context of our modelling, the element-dependent K_d equations predict the partitioning of solutes between the soil solution and the soil solid phase. We found that the correlations by Sheppard (2011) are not strong in some cases. Hence, we assembled a dataset with extensive information available at SCK-CEN on K_ds for different elements in soils. The database contains soil K_d's for Cs, Se, U, Th, Ra, Po, Ni, Nb and Tc, based on our previous work. We then tested the calibration of the parametric K_d equation:

$$\log(K_d) = A + B \times pH + C \times \log[\text{organic carbon}] + D \times [\text{clay}] + E \times [\text{organic matter}]$$

For one of the most environmentally relevant radionuclides ^{137}Cs, we already have simple and multiple regressions calculated between K_d (Cs) and soil properties (pH, OM, sand and clay content), using our updated dataset (n = 598). All regressions were calculated not only for the whole dataset but for three sub-datasets:

- Indigenous group: K_d values of stable Cs determined either "in-situ" or from soil solution (desorption).
- RN sorption group (batch): K_d values determined either by batch method with radioactive or stable Cs (at very low concentrations, such as the lowest concentration point of sorption isotherms) or calculated from soil properties.
- RN in-situ group: K_d values determined from in-situ, soil solution (desorption) or column experiments with radiocaesium.

The best simple regressions were obtained for pH and Clay content. When log transformed data of soil variables are used, only the correlation between K_d and Clay content slightly improves. Regarding the regressions for the different sub-datasets, better correlations were obtained than using the whole dataset. Nevertheless, there is no common trend for all the sub-datasets, as the variable that best correlates with K_d values depends on the sub-dataset used.

Multiple regressions with two variables were also tested, using both original and log transformed data. From the results obtained, only the combination of pH + clay (r^2 = 0.37) or pH + log clay (r2 = 0.40) improved the results of simple regressions for the whole dataset. When multiple regressions were calculated by using sub-datasets, only a slightly improvement for the RN in-situ group was obtained when using pH + clay (r2 = 0.48). Finally, a multiple regression which involved the three main variables (pH, Clay and OM) does not improve results. In order to complete this evaluation, for a limited number of radionuclides, we will be applying the "cofactors" approach or a filter to reduce data variability. For instance, in the case of radiocaesium, the radiocaesium interception potential RIP (or the RIP corrected by potassium in soil solution) will be considered.

2.3.2.3. Parameterisation of the simplified ECOFOR model

The ECOFOR model was set-up in the ModelMaker 4 software (Rigas 2000) (Table 8) using the Gear integration method (Gear 1971). The main parameters are given in Table 8.

Table 8: ECOFOR model parameters

Parameter	Symbol	Value
Allometric factor a for tree biomass	a, b	0.152 kg, 2.234 (Xiao and Ceulemans 2004)
Amplitude of energy radiation	Rn-G	237.3 J m^2 s^{-1} (Ceulemans, Kowalski *et al.* 2003)
Diameter of tree at breast height	DBH	0.2897 m (Van den Hoof and Thiry 2011)
Extinction coefficient from Beer's law	γ	0.526 (Brission, Seguin *et al.* 1992)
Forest stand density	Σ	3.59×10^{-2} m^{-2} (Van den Hoof and Thiry 2011)
Fractional field capacity of sandy soil	ξ	0.19 (Brakensiek, Rawls *et al.* 1984, Schroeder, Dozier *et al.* 1994)
Fractional needle mass	N_m	0.22 – 0.36 (Pausas 1997, Xiao and Ceulemans 2004)
Leaching, decomposition and needle fall rates	$k_{63,}$ K_{dec}, k_{64}	4.93×10^{-5} d^{-1}, 4.22×10^{-3} d^{-1} , 5.27×10^{-1} d^{-1} (Pausas 1997, Van den Hoof and Thiry 2012)
Phloem drag coefficient	χ	0.5 (Nonweilwer 1975)
Plant absorption, intercption & washout	$k_{76,}$ $f_{int}^{p,}$ w_f	0.15, 0.29, 0.85 (Van den Hoof and Thiry 2012)
Ratio below/above ground biomass	κ	0.26 (Xiao and Ceulemans 2004)
Hydraulic conductance	H_c	0.710 m d^{-1} (typical for sand)
Root depth & extinction coefficient	h_{root}, b	1.4 m (Vincke and Thiry 2008), 2 d^{-1} (Li, Boisvert *et al.* 1999)
Runoff coefficient	r_c	0.1 (ODOT, 2005)
Soil bulk and particle density	ρ_0, ρ_{soil}	1880, 2650 kg m^{-3} (Baes and Sharp 1983)
Sorptivity constant (undisturbed soil)	S	3.79×10^{-2} m $d^{-1/2}$ (Fuentes, Bustamante *et al.* 2010)
Pine tree density & tree height	ρ_{tree}, h_{tree}	700 kg m^{-3} (Ketterings, Coe *et al.* 2001), 35 m (Rushforth 1981)
Xyleem density & viscosity	ρ_{xyl}, η_{xyl}	1.08×10^3 kg m^{-3} (Lane 2012), 1.68×10^2 kg m^{-2} d^{-1} (Hölttä, Vesala *et al.* 2006)

2.3.3. Nutritional constraints

The data for Brasschaat originate from the ICP-Forests monitoring by the Instituut voor Natuur- en Bosbeheer (Verstraeten and Cools, pers. com.) The data for Gedinne originate from the ICP-Forests monitoring by UCL-Forest Sciences. Although we used data from plots that are integrated in networks and intensively monitored some additional properties describing the chemical reactivity of the soil materials that are needed by our model had not been characterized. In points 2.3.3.1 and 2 below, we outline procedures for estimating those properties. The new model for nutrient allocation and cycling in the tree also requires a more detailed parameterisation, which is explained in point 2.3.3.3.

2.3.3.1. Simple model for P

The simple model for phosphorus chemistry in the mineral soils requires the knowledge of the mineral P pools and of their reaction parameters. No detailed fractionation of the P pools is available. The P concentrations in the holorganic layer(s)

and total P concentrations in the soil horizons are known. A fractionation of these P pools was calculated on the basis of average Hedley fractions for the USDA soil orders reported by Yang and Post (2011), with the values for a Spodosol in Brasschaat and an Inceptisol in Gedinne. No information is available on the reactivity of these estimated mineral P pools either, so two options were considered:
(i) the reactive mineral P pool is the labile one (see Figure 6), with the Langmuir equilibrium between the adsorbed and solution phases. The Langmuir maximal P sorption capacity is estimated from the oxalate-extracted Al + Fe content with an affinity factor (Van der Zee *et al*. 1987) of 0.25, and the Langmuir constant is set to reproduce the known growth of the stand;
(ii) the reactive mineral P pool is the active one (see Figure 6), with a single reaction constant set to reproduce the known growth of the stand.

2.3.3.2. General model for mineral soil chemistry

Use of the PHREEQC code requires the knowledge of a larger parameter set. While the reaction constants for the solution ion species are quite well established and available in the databases delivered with the PHREEQC software, the parameters related to ion exchange and soil minerals weathering needed to be estimated, as well as the amount of these two element pools in the soil. Also in order to compute the contribution of weathering mineral to the nutrient biogeochemical cycle, the concentrations and reactivity of the minerals present in the soil material needed to be estimated.

a. Ion exchange

In practice we used from 1 to 3 cation exchangers and one anion exchanger. The cation exchangers are (i) in the holorganic horizon 1 organic exchanger, (ii) in the hemiorganic horizons 1 organic exchanger combined with 1 or 2 mineral exchangers, (iii) in the mineral horizons 1 or 2 mineral exchangers. Two mineral cation exchangers were considered when the presence of certain ion-specific (namely K) exchange sites was known or could be inferred. The concentration and selectivity coefficients of the exchangers need to be determined. Estimation of the exchangers concentrations and selectivity coefficients: The concentration of the organic exchanger is set by considering an average charge of 3 cmolc/kg Corg, reduced by an average of 0.5 cmolc/kg Corg per pH unit below 7 (e.g. Helling *et al*. 1964, Appelo 1994, Curtin and Rostad 1997). The cation exchange capacity arising from organic matter is then subtracted from the soil cation exchange capacity, yielding the exchange capacity of the mineral exchanger(s). If more than one mineral exchanger is used, their relative contributions need to be estimated (see below).

The estimation of the selectivity coefficients is straightforward if there is one single exchanger in the soil material: they are calculated from the measured cation composition and the composition of the soil solution collected at or around the time of the soil sampling (Cosby *et al.* 1985). If there is more than one exchanger, values from the PHREEQC database and/or literature are assigned to the selectivity coefficients. The concentrations of exchangeable cations on each exchanger are then computed using the soil solution composition.

Finally the contribution of each exchanger is estimated by applying a weight fraction (from literature or itself adjusted) to their cation composition in order to sum up to the exchangeable cations measured on the whole soil material. If the best proportions found nonetheless cause discrepancies for some of the cations, the selectivity coefficients and exchanger fractions are adjusted accordingly and the procedure is iterated.

Three exchangers were defined for the test sites of Brasschaat and Baileux: an organic, a mineral non-specific and a mineral K-specific (Baileux only) exchanger. The calculated Gaines-Thomas exchange coefficients are reported in Table 9.

	Organic exchanger		Non-specific mineral exch.		K-specific mineral exch.	
Reaction	Kgt	Prefered	Kgt	Prefered	Kgt	Prefered
Ca++/NaX	0.56	(Na)	0.63	(Na)	6.31	Ca
Ca++/KX	0.45	(K)	0.16	K	0.00006	K
Ca++/HX	0.0001	H	10	Ca	16	Ca
Ca++/NH4X	0.45	(NH4)	0.25	NH4	0.000002	NH4
Ca++/MgX2	3.98	Ca	1	-	1.58	Ca
Ca++/AlX3	0.48	(Al)	0.04	Al	38	Ca
K+/NH4X	1	-	1.26	(K)	0.16	NH4

Table 9. Exchanger types and exchange coefficients.

The organic exchanger shows a strong affinity for H, slightly prefers Al over Ca, and prefers Ca over Mg, as expected for this type of material. The non-specific exchanger prefers Al over Ca, and also the monovalent cations (except H) over Ca. The K-specific exchanger has a strong preference for K over Ca, and an even stronger preference for NH_4.

b. Mineralogy and mineral reactivity

The quantitative mineralogy of the soil horizons was reconstructed with the dedicated software A2M from their elemental analysis (Posch and Kurz 2007). The elemental analysis consists of either a total analysis by a tri-acidic dissolution or an *aqua regia* digestion which is considered as an approximation of the total contents and where the difference to 100% is ascribed to SiO_2 content (overestimate). Some qualitative

mineralogical information was available for Brasschaat, which enabled us to constrain the minerals present in the soil material (Van Ranst *et al*. 2002). Table 10 reports the tentative quantitative reconstruction of the soil minerals for Brasschaat (a) and Baileux (b). The PHREEQC thermodynamic database was augmented with solubility products and/or kinetic reactions of relevant minerals whenever possible.

Table 10. Reconstructed quantitative mineralogy, expressed as w/w percentage of the mineral soil material.

Brasschaat	
Quartz	98
Na-plagioclase	0.2
Al oxides	0.4-0.6
Fe oxides	0.1-0.3
Ca-plagioclase	0.1
Mica	0.2-0.3
P-bearing	0.2-0.3
Vermiculite	0.1

(a) Brasschaat (Boldfaced minerals are attested by X-ray diffractometry)

	Ah	Bw1	Bw2	2Bw3	2Bg1	2Bg2	2Bg3
Quartz	75	71	66	58	60	58	53
Plagioclase	3	4	4	4	4	4	4
K-Feldspar	5	6	7	9	8	9	10
Mica	8	10	12	15	13	14	16
P-bearing	0.4	0.2	0.3	0.3	0.3	0.3	0.4
Chlorite	5	6	7	11	12	12	13
Vermiculite	1	2	2	2	2	2	3
Smectite	2	2	1	1	1	1	1

(b) Baileux

The mineralogy of the Brasschaat soil material is poor and nearly exclusively dominated by quartz. The X-ray diffractometric analysis by Van Ranst *et al*. (2002) only revealed Na-plagioclase. The other minerals are hypothesised to account for the remaining elements (Ca, Mg, K, P) in the total analysis. The mineralogy does not vary much between the horizons.

No X-ray diffractometric analysis has been performed on the soil material in Baileux. The minerals considered here are common in the mineralogy of the Ardenne soils (e.g. Brahy and Delvaux 2000). The quartz fraction is high but not exclusive. The proportion of the other minerals increases in the deeper horizons, as does the clay-sized fraction of the material.

2.3.3.3. Element cycling in the tree

The optimal nutrient concentration in all the tree pools defined in 2.1.3.4.a were derived for pine, spruce, oak and beech from an intensive literature review and are reported in Table 11.

The feedback of leaf N and P concentration on photosynthesis was implemented using the equations and parameter value of Reich *et al*. 2009.

BEECH						OAK					
	N	P	Ca	Mg	K		N	P	Ca	Mg	K
L0	4.30E-02	2.70E-03	1.20E-02	2.50E-03	1.50E-02	L0	4.00E-02	2.80E-03	1.10E-02	3.50E-03	1.50E-02
L1	---	---	---	---	---	L1	---	---	---	---	---
StBark	1.47E-02	1.00E-03	4.10E-02	1.18E-03	4.68E-03	StBark	1.24E-02	1.01E-03	6.19E-02	1.15E-03	4.68E-03
StCurSap	2.61E-03	2.35E-04	1.16E-03	6.04E-04	2.83E-03	StCurSap	4.04E-03	4.66E-04	7.56E-04	3.02E-04	2.83E-03
StOldSap	2.37E-03	1.91E-04	2.09E-03	4.74E-04	1.62E-03	StOldSap	3.66E-03	3.79E-04	1.36E-03	2.37E-04	1.62E-03
StHeartw	2.35E-04	8.40E-05	2.30E-03	6.25E-04	1.60E-03	StHeartw	1.90E-03	2.42E-05	7.08E-04	3.50E-05	1.60E-03
BrBark	5.19E-02	4.80E-03	4.10E-02	1.70E-03	7.55E-03	BrBark	4.10E-02	2.19E-03	6.19E-02	4.06E-03	7.55E-03
BrCurSap	9.22E-03	1.13E-03	4.90E-03	8.70E-04	4.57E-03	BrCurSap	1.34E-02	1.01E-03	5.38E-03	1.06E-03	4.57E-03
BrOldSap	8.37E-03	9.18E-04	8.82E-03	6.82E-04	2.61E-03	BrOldSap	1.21E-02	8.22E-04	9.68E-03	8.34E-04	2.61E-03
BrHeartw	4.53E-03	4.03E-04	9.73E-03	9.00E-04	2.58E-03	BrHeartw	6.30E-03	5.26E-05	5.04E-03	1.23E-04	2.58E-03
CR0	6.55E-03	8.24E-03	3.28E-03	1.04E-03	4.08E-03	CR0	8.01E-03	6.35E-04	4.96E-03	9.67E-04	4.08E-03
CRSap	5.94E-03	6.69E-03	5.90E-03	8.15E-04	2.33E-03	CRSap	7.27E-03	5.16E-04	8.93E-03	7.58E-04	2.33E-03
CrHeartw	3.21E-03	2.94E-03	6.51E-03	1.08E-03	2.30E-03	CrHeartw	3.78E-03	3.30E-05	4.65E-03	1.12E-04	2.30E-03
FRoot	1.43E-02	1.20E-03	1.06E-02	1.48E-03	4.36E-03	FRoot	1.49E-02	1.48E-03	1.24E-02	2.12E-03	4.36E-03
Fruit	6.50E-02	6.00E-03	1.00E-02	3.00E-03	1.25E-02	Fruit	ND	ND	ND	ND	ND
PINE						SPRUCE					
	N	P	Ca	Mg	K		N	P	Ca	Mg	K
L0	3.00E-02	3.00E-03	5.50E-03	2.10E-03	1.35E-02	L0	3.00E-02	3.00E-03	7.50E-03	2.10E-03	1.25E-02
L1	2.58E-02	2.30E-03	8.97E-03	2.04E-03	1.02E-02	L1	2.67E-02	2.30E-03	1.22E-02	2.04E-03	9.47E-03
StBark	7.70E-03	9.20E-04	1.01E-02	1.22E-03	4.16E-03	StBark	1.03E-02	1.30E-03	1.63E-02	1.54E-03	5.66E-03
StCurSap	2.03E-03	1.76E-04	7.93E-04	7.25E-04	2.53E-03	StCurSap	1.79E-03	1.41E-04	8.54E-04	2.66E-04	1.40E-03
StOldSap	1.84E-03	1.43E-04	1.43E-03	5.69E-04	1.44E-03	StOldSap	1.63E-03	1.15E-04	1.54E-03	2.09E-04	8.00E-04
StHeartw	1.38E-03	3.80E-05	1.30E-03	5.80E-04	8.80E-04	StHeartw	8.30E-04	6.00E-06	1.64E-03	3.39E-04	3.04E-04
BrBark	2.83E-02	4.05E-03	1.01E-02	3.21E-03	1.01E-02	BrBark	6.53E-02	1.41E-02	1.63E-02	7.42E-03	2.94E-02
BrCurSap	7.47E-03	7.76E-04	4.17E-03	1.91E-03	6.12E-03	BrCurSap	1.13E-02	1.53E-03	4.06E-03	1.28E-03	7.27E-03
BrOldSap	6.78E-03	6.31E-04	7.51E-03	1.50E-03	3.50E-03	BrOldSap	1.03E-02	1.24E-03	7.31E-03	1.00E-03	4.16E-03
BrHeartw	5.08E-03	1.67E-04	6.84E-03	1.53E-03	2.13E-03	BrHeartw	5.24E-03	6.50E-05	7.79E-03	1.63E-03	1.58E-03
CR0	3.82E-03	4.94E-04	1.18E-03	7.25E-04	3.29E-03	CR0	8.94E-03	8.71E-04	1.94E-03	7.25E-04	4.20E-03
CRSap	3.47E-03	4.01E-04	2.13E-03	5.69E-04	1.88E-03	CRSap	8.11E-03	7.07E-04	3.49E-03	5.69E-04	2.40E-03
CrHeartw	2.60E-03	1.06E-04	1.94E-03	5.80E-04	1.15E-03	CrHeartw	4.14E-03	3.70E-05	3.72E-03	9.24E-04	9.11E-04
FRoot	1.49E-02	1.24E-03	5.66E-03	9.00E-04	2.94E-03	FRoot	2.15E-02	1.96E-03	5.22E-03	1.10E-03	4.36E-03
Fruit	ND	ND	ND	ND	ND	Fruit	ND	ND	ND	ND	ND

Table 11. Optimal nutrient concentrations in the tree pools (C:nutrient ratio).

2.4. Model verification and testing

2.4.1. Climate modelling

2.4.1.1. ERA-Interim forced simulations

In order to test the model for its performance in downscaling, we simulated the period 1979-2010 using ERA-Interim as LBCs. We denote these simulations as "ERA simulations", or more shortly, "ERA". The details of this study can be found in Giot *et al.*, (2016), in which the ALARO-0 simulation is compared to a set of other RCMs which were analyzed by Kotlarski *et al.* (2014) for near-surface air temperature and precipitation. The main conclusion of Giot *et al.* (2016) is that "ALARO-0 is able to represent both seasonal mean near-surface air temperature and accumulated precipitation amounts well". More specifically, the study revealed that ALARO-0 suffers from some issues in representing near-surface air temperatures (but not in Belgium) which need to be addressed by the model developers. However, it is very good in representing the precipitation field, outperforming the other models on several occasions.

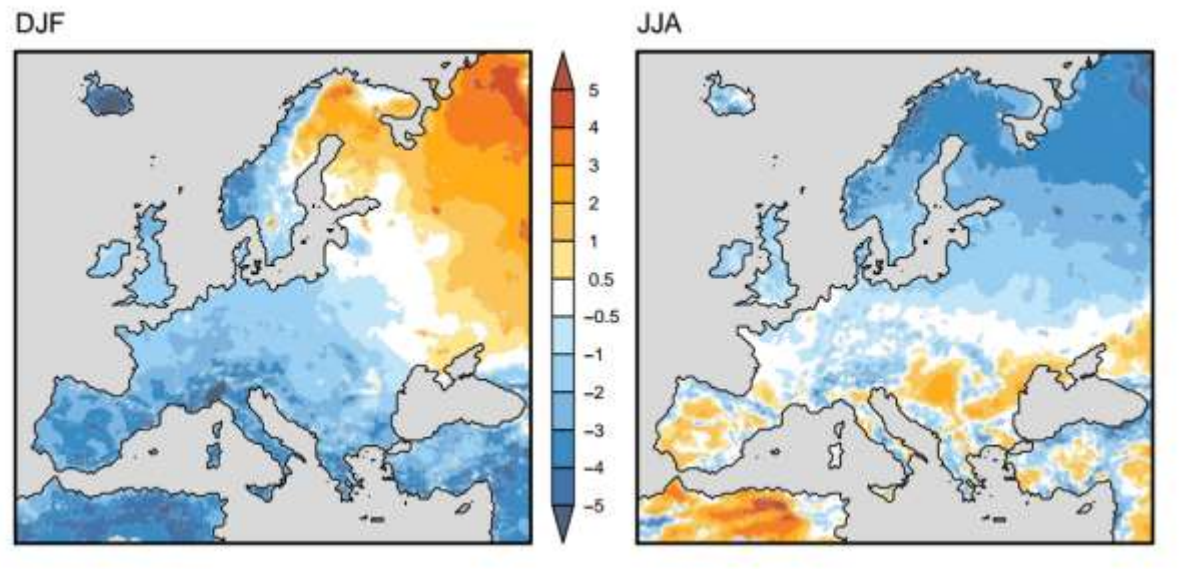

Figure 11. Seasonally mean temperature bias, i.e. model-obs in °C, for the ALARO-0 ERA simulations (from Giot *et al.*, 2016) for winter (DJF, left) and summer (JJA, right)

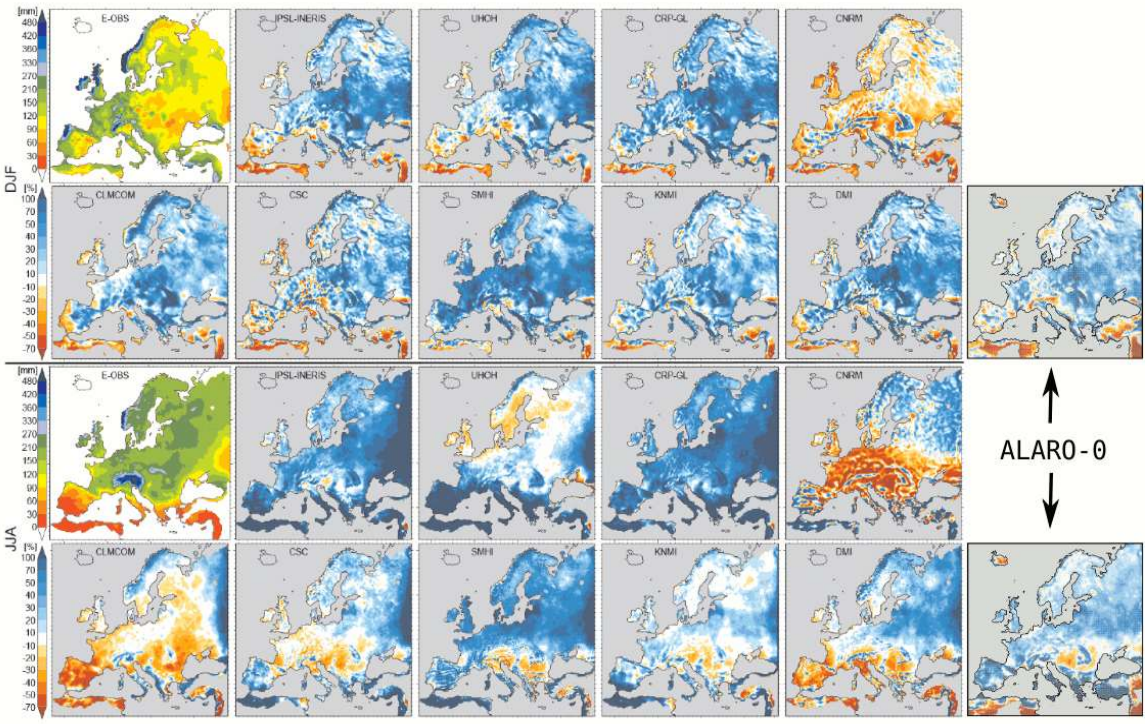

Figure 12. Comparison of the mean relative spatial bias, i.e. (model-obs)/obs in %, of ALARO-0 and other climate models for winter (DJF, top two rows) and summer (JJA, bottom two rows). The top left panes show observed values, The other panes show different models' performance. The right most panes show ALARO-0 results.

For example, the absolute spatial bias, i.e. the mean difference between modelled and observed values (model – obs, °C), of near-surface air temperature for winter (the months December, January and February, "DJF") and summer (the months June, July and August, "JJA") reveals for Western Europe a considerable cold bias in winter and very small cold bias in summer (Figure 11).

The relative spatial bias, i.e. the mean relative difference between modelled and observed values ((model – obs)/obs, %), of precipitation reveals a slight wet bias for Western Europe, both in winter and summer (Figure 12). The right-most panes in Figure 12 show the bias of ALARO-0, the other panes are the observed mean (top left) and the biases of 9 other models. The wet bias of ALARO-0 is common to almost all models. This is a long standing issue in climate modelling, called the drizzle effect, i.e. too many days with very light rain. In conclusion, the ALARO-0 EURO-CORDEX simulations withstand the comparison with many renowned and well-established climate models and can thus with confidence be employed as climate model.

2.4.1.2. CNRCM-CM5 forced simulations

In this section we will analyze the CNRM-CM5 forced simulations in more detail, focusing directly on the three sites Brasschaat ("BRA"), Gedinne ("GED") and Mol ("MOL"). Model output can be compared to both observations ("OBS") and ERA output. As observations, the corresponding closest grid point from the E-OBS dataset was used (Haylock *et al.*, 2008). The results for temperature and precipitation of the historical simulations (HIST in black) and future scenario simulations (RCP4.5 in green, RCP8.5 in red), are summarized in Figure 13 as histograms of the 30 year periods 1976-2005 for HIST (black), 2071-2100 for the RCPs (RCP4.5 in green, RCP8.5 in red), 1976-2005 for OBS (grey) and 1979-2008 for ERA (yellow; ERA-Interim is only available from 1979 onwards) for near surface air temperature (top row) and daily precipitation (middle row DJF; bottom row JJA) for BRA (left column), GED (middle column) and MOL (right column). We omit RCP2.6 from the analysis since its response is rather small and in order to keep clarity to the figures. The three past climate histograms HIST, OBS and ERA provide insight in how well the model can represent climatic features. Ideally, both the ERA and the HIST simulations coincide with the observed values as this means that both when forced by ERA-Interim and the CNRM-CM5 historical simulation, the model is able to reproduce the observed weather over a 30 year period.

For near surface air temperature (T2m), on every pane the distribution of both winter (left) and summer (right) temperature is shown. The vertical segments at the bottom of each subplot denote the average values of the distributions. In summer, the ERA simulations represent well the mean and the distribution of the observed temperatures.

In winter, the ERA simulation is consistently too cold and for Gedinne the distribution shape also differs. This could be attributed to known issues with temperature inversion in the ALARO-0 model. The HIST simulation is even more cold biased, in winter at all three locations the bias is around -3°C, which is most likely due to already biased

LBCs from CNRM-CM5. As expected, RCP45 has a warmer climate (mean +3°C in winter and +1°C in summer with respect to HIST) and RCP85 even warmer (mean +4°C in winter and +3°C in summer with respect to HIST).

For precipitation, the top/bottom row shows the winter/summer (DJF/JJA) frequency distribution. The first two bins are 1 mm/day wide, the others are 2 mm/day wide.
The first bin (between 0 and 1 mm/day) contains the dry days and the second bin the so-called drizzle days. For all locations and seasons the ERA and HIST simulation underestimate the number of dry days and overestimate the number of drizzle days (except for ERA in Gedinne). This is a well-known issue with climate models, called the drizzle effect. Generally, the winter frequency distributions are well reproduced by the past model runs ERA and HIST for Brasschaat and Mol. In summer, there is a minor overestimation of light to heavy rain days (5-30 mm/day) for Brasschaat and Mol. For Gedinne, light to heavy rain days are overestimated severely for both seasons, possibly due to orographic effects. Comparing the RCP simulations to HIST, the response to climate change can be quantified. In winter, a decrease in drizzle days and an increase in light to heavy rain days appears, while in summer the distribution does not change significantly. This is also seen in the daily mean amounts of precipitation, which are given in Table 12. In winter, both ERA and HIST represent mean amounts well for BRA and MOL, but for GED there is a large bias and for all locations there is a considerable increase in mean precipitation for both RCP45 and even more so for RCP85. In summer, again BRA and MOL are represented well in ERA and HIST, while GED is overestimated, but here, no clear change for the RCPs is found. This implies that the RCPs project wetter winters, but no change for summer.

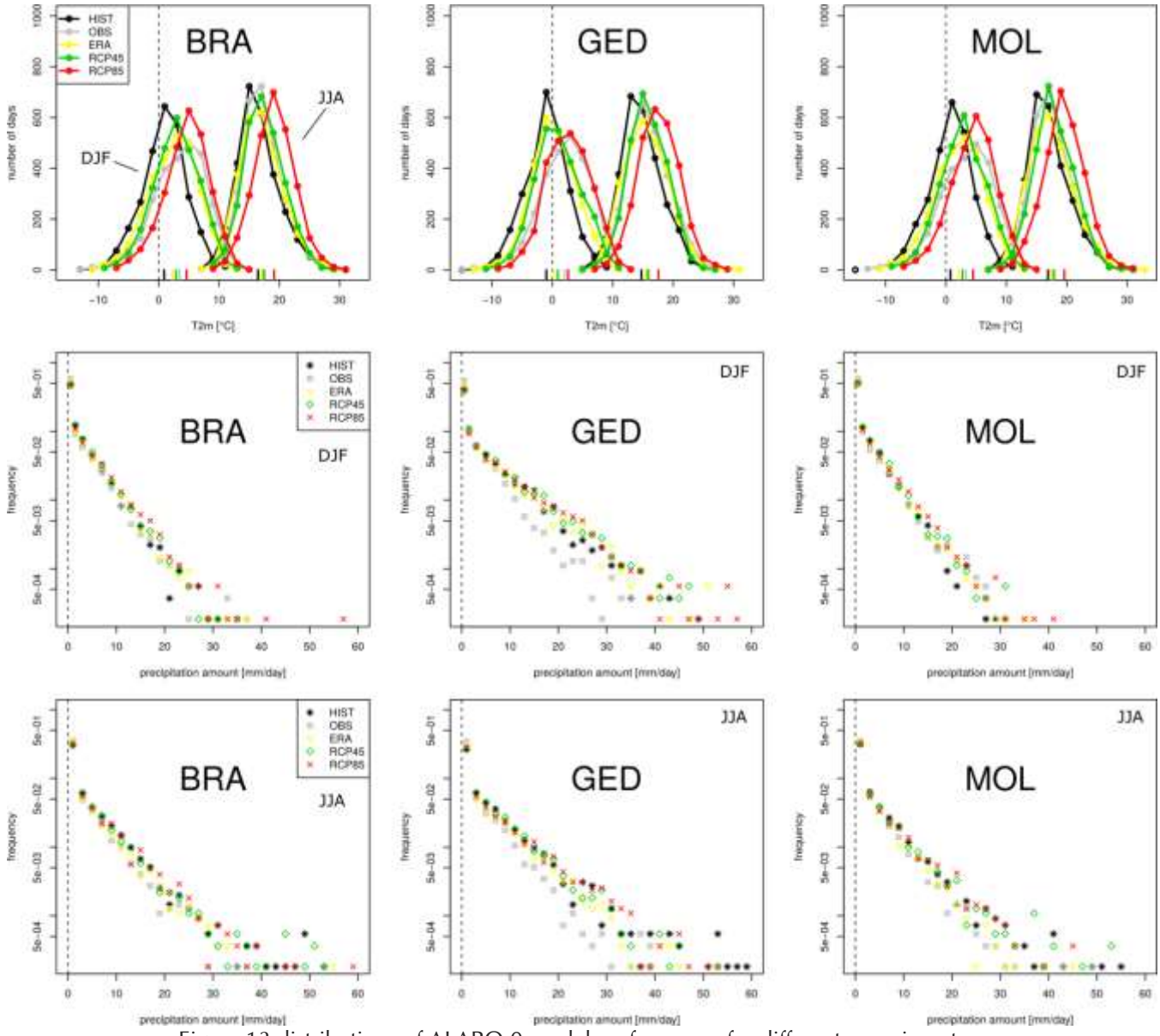

Figure 13 distributions of ALARO-0 model performance for different experiments

Table 12. Daily mean precipitation [mm/day] in winter (DJF) and summer (JJA) for the three locations BRA, GED and MOL for the five sets of data.

DJF	*OBS*	*ERA*	*HIST*	*RCP45*	*RCP85*
BRA	2.25	2.72	2.64	2.96	3.19
GED	2.63	4.54	4.60	5.26	5.32
MOL	2.27	2.47	2.47	2.78	2.93
JJA	*OBS*	*ERA*	*HIST*	*RCP45*	*RCP85*
BRA	2.21	2.53	3.33	3.21	3.26
GED	2.39	3.50	4.42	4.39	4.35
MOL	2.19	2.35	3.02	3.04	3.01

2.4.2. Effects of climate uncertainty on forest growth

2.4.2.1. Biases in climate models

One major problem are the biases (difference between modelled and observed, MOD - OBS) in the HIST simulation, which are sometimes as large as the climate change signal (RCP – HIST). There exist two major approaches to this issue in the literature: the delta method and the scaling method (Teutschbein and Seibert, 2010). In the delta method approach, first the change between RCP and HIST is calculated and added to past observations OBS(p) to obtain the future "observed" climate OBS(f):

$$OBS(f) = OBS(p) + delta = OBS(p) + \text{"RCP – HIST"}$$

In the scaling method, first the difference between HIST and OBS(p) is calculated and then the RCP output is corrected by this difference:

$$OBS(f) = RCP - scaling = RCP - \text{"HIST – OBS(p)"}$$

The quotation marks can denote a set of different approaches, such as pdf or cdf corrections, quantile mapping and many others (for an overview, see Teutschbein and Seibert, 2010) and/or different periods in time which are used to calibrate and define the delta or scaling functions. These bias correction methods all suffer from (i) the fact that the change of scaling is defined based on statistics and this implies that a large set of observations and simulations are needed, (ii) the delta or scaling is assumed constant under climate change, (iii) effects of the correction on extreme events, which are rare by definition are badly defined, (iv) the statistical correction breaks the physical equilibrium as calculated by the model, both in time (autocorrelation) and between different variables (dependencies in governing equations). An example of the latter is that when correcting temperature, one should also account for a change in relative humidity and radiative fluxes. All these issues impose extra errors, which possibly cancel the other benefits of performing a bias correction (Teutschbein and Seibert, 2013).

Therefore, it was decided to use the raw output of the climate model and to assume that the response of the forest ecosystem to a warming climate is not very dependent on the state itself. By this we mean that the difference in ANAFORE due to RCP and HIST climates is the same as the difference due to the OBS(f) and OBS(p) if RCP – HIST $\sim$ OBS(f) – OBS(p) and thus that only changes in climate play a role, not the climate itself. For this to be the case, processes should react linearly to a change in climate. This is obviously not always the case. For example, the bias in the number of frost days due the cold bias of HIST in winter, will lead to significantly longer winters, a later bud burst and therefore a major change in the forest ecosystem dynamics. However, if the climate changes are in the "same direction", i.e. a decrease in frost days due to climate

change, the response will also be in the "same direction", for example an increase in biomass due to a prolonged summer season. Therefore, we will interpret our final results not quantitatively, but rather qualitatively.

2.4.2.2. Coupling to ANAFORE

Since we run ANAFORE simulations as a continuous run of 80 years long, we need to create a time series of this length. Naively, one would sample a 80-year long time series from the 95-year long RCP simulations. There are however two issues we need to take into account when doing this, which is (i) "the transient climate issue": in a period of 80 years, in which climate change is assumed, the climate is not constant, but transient from one climatic state into another and (ii) "the inter-annual variability issue": the sequence of weather events obtained by a single realization of an RCM is random and therefore this should not have a consequence for downstream models.

The first issue implies that the climate over the next century will gradually evolve and that the largest changes will be seen only by the end of the century. The forest is thus forced by a so-called transient climate. Here, we are more interested in the forest state given a certain climate state. Also, the sensitivity of the forest under transient conditions might be rather small, as a large portion of its growing phase is under small climatic changes (2005-2050). Therefore, we have decided to investigate the response of forest growth in a different climate, using the 30-year (2071-2100) end-of-the-century pool of RCP4.5 and RCP8.5. We omit RCP2.6 for clarity. This climate state is used as an alternative climate, which is overall warmer and wetter in winter as shown before. This poses a new challenge: we need a 80-year long sequence of daily climate, but only 30 years are available. This is resolved together with the second issue.

The second issue addresses the fact that climate models do not intend, cannot and never will be able to predict sequences of events, i.e. from within the pool of statistics (e.g. in 10 out of 30 daily temperatures of 1st July exceed 35°C) being able to tell exactly which years.
At most, the model can predict inter-annual variability, i.e. how do certain fields change year-to-year (the distribution of 1st July temperatures). Of course, from the climate model output we can tell which years the warm years were, because to compute the statistic we need to get the sequence first by integrating the climate model. However, it is of utmost importance not to attribute skill to the climate models, where they do not have any. And thus, using the daily temperature series from a climate model in a downstream model should be done with reservation. Specifically for ANAFORE, this is the case as forest growth is very sensitive to climatic conditions. In Figure 14, the biomass evolution as a function of time of 80 ANAFORE simulations

is shown. The lines with the same colour only differ by climate sequence input. They have the same "climate", which means that their statistics (e.g. the histograms shown in section 2.4.1.2) do not significantly differ, but have a different sequence of events by shifting the starting date of the sequence (20 per colour). Or viewed differently, the forest was initialized in different years. The different colours show different parameter sets of the forest processes within the model, acquired from a Bayesian optimization. The drops in biomass are due to the forest management scenario. A different parameter set forces the forest into a different evolution, but it is also sensitive to the climate sequence, shown by the spread of the same-colour lines. This is important, because if we would perform a simulation with a given parameter set for both a historical climate sequence and a RCP sequence, the response might not be due to the changed climate but due to the changed climate sequence.

In conclusion, the transient simulation is interesting from a climate change policy view; "How will temperature change, given this scenario" is a societal relevant question. To study the response of forest growth however it is more interesting to create a set of climate states and see how the forest ecosystem evolves under these climates. Additionally, climate models can project inter-annual variability, but not the exact sequence of days or years. To solve these two issue simultaneously, we have used the following approach in the modelling process. A set of climate sequences was created from the different climate states (HIST 1976-2005; RCPs 2071-2100). This is done by taking from the 30 years of climate a set of random sampled years to create a 80 year long sequence of events. In this way, the climate is by construction constant, not transient. The sensitivity to the sequence of events can be assessed by generating multiple sequences for each climate and analyzing the response of both mean and spread of the forest ecosystem.

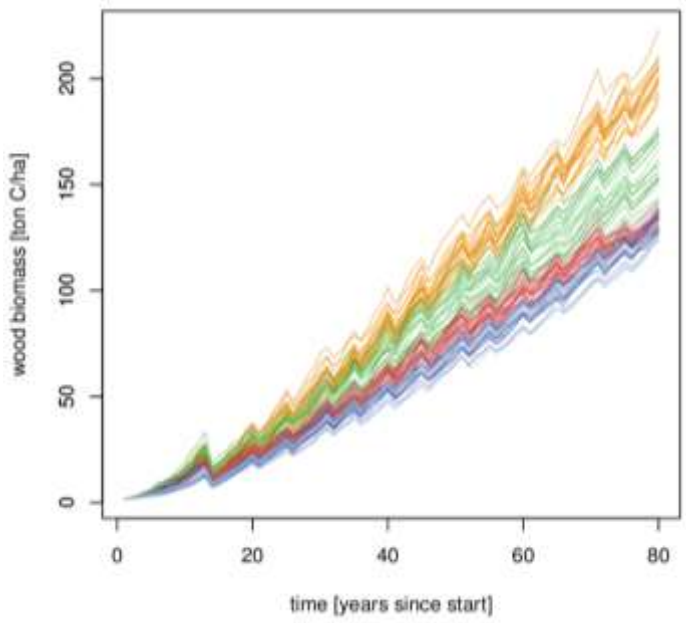

Figure 14: Example of influence of climate variability. Same colour curves show the forest wood biomass evolution as it grows for the exact same parameters set and climate, but for different climate sequences.

2.4.3. Water and pollutant transport in unsaturated soil

2.4.3.1. Testing and validation of water transport submodel

The water transport submodel was tested in a series of benchmarking exercises with other models. Specifically, the model output was compared with the output of HYDRUS-1D (Šimůnek, Van Genuchten *et al*. 2008), an industry-standard hydrological model which allows the simulation of volumetric water content (θ) at various observation nodes. Satisfactory tests for constant boundary conditions are shown below by way of example (Figure 15). There is a remarkable agreement between the two models for the types of soil considered. Additional HYDRUS vs. ECOFLOW tests for different layer thicknesses and time step lengths confirmed the stability of the numerical algorithm (Figure 16).

Several other tests were carried out to give additional verification after the finalised version of the code was developed. An example is shown in Figure 16. The conditions of the test are as follows. Upper and lower flow boundary conditions: atmospheric with runoff and free drainage, respectively. Upper and lower contaminant transport boundary condition: constant concentration; constant precipitation and evapotranspiration; heterogeneous (layered) soil with no plant uptake. The resulting match between our model and the model HYDRUS (used for benchmarking purposes) is indeed satisfactory (Šimůnek, Van Genuchten *et al*. 2008).

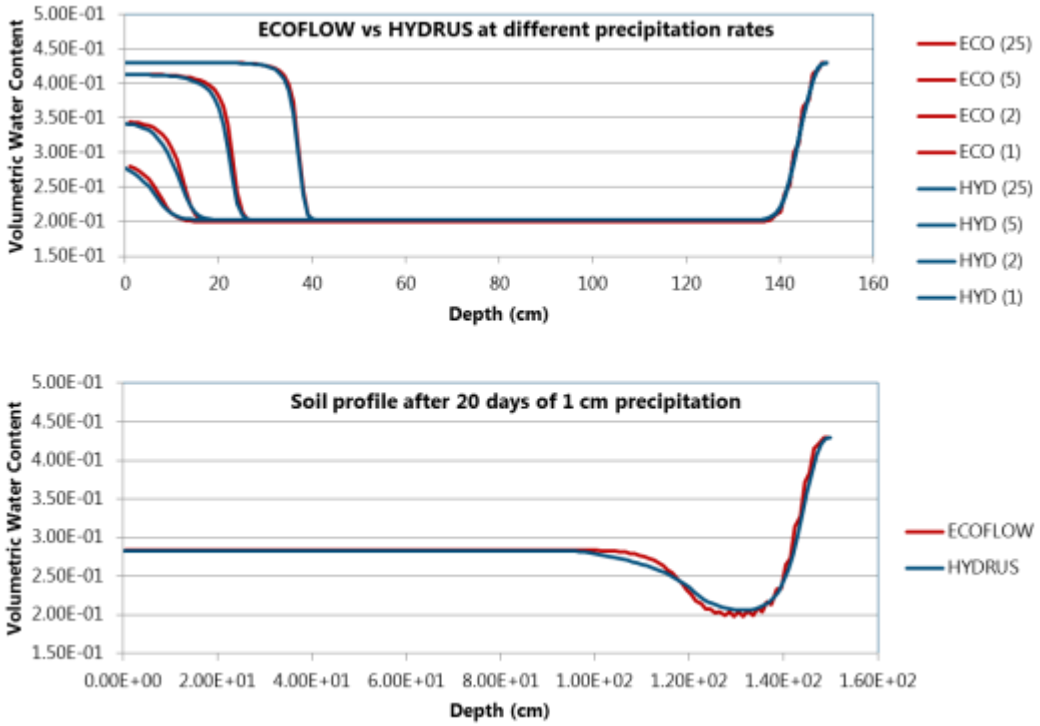

Figure 15. Comparison between the ECOFLOW (red line) and HYDRUS-1D (blue line) models for soil profile

More advanced tests included the comparison between our code and HYDRUS for static water table versus free drainage, under conditions of real (time-variable) precipitation in the Mol forest site, with successful results as shown in Figure 17.

Coupling with ANAFORE means that the Van Genuchten parameters (alpha, n) used to represent hydraulic conductivity are now calculated using soil parameters including organic content. The code runs well under simplified conditions; namely homogeneous soil (sand, loam, silt, and clay), atmospheric boundary conditions, static water table or free drainage, and no or constant plant uptake.

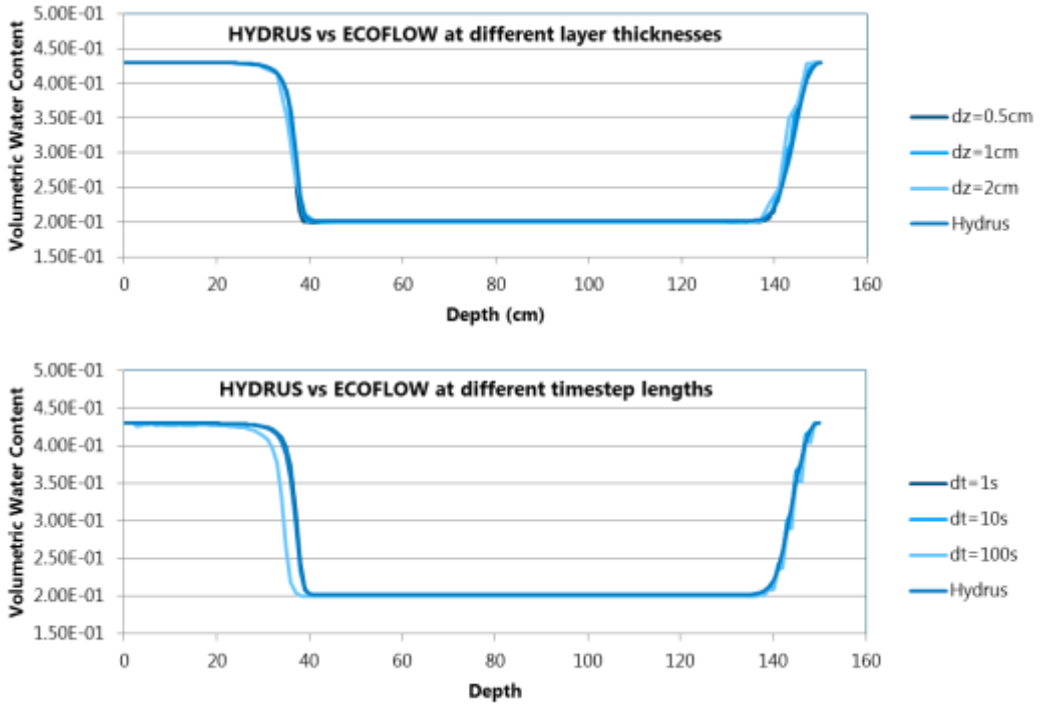

Figure 16. Comparison between ECOFLOW (red line) and HYDRUS-1D (blue line) models for different layer thicknesses and time steps

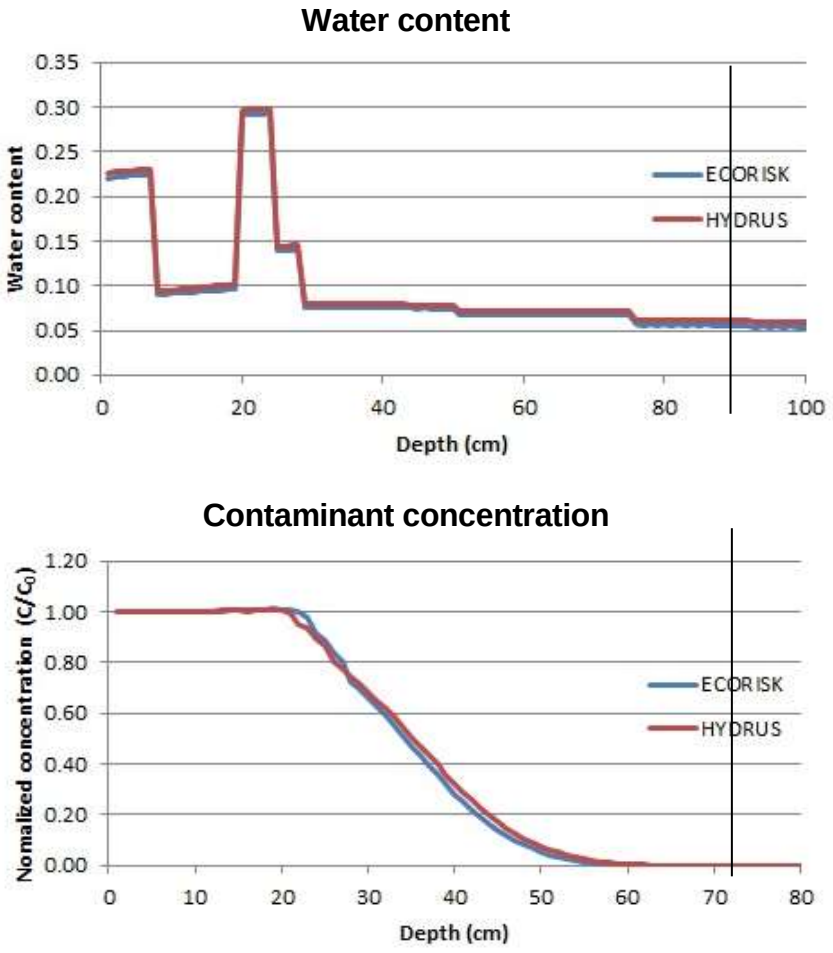

Figure 17: Examples of code verification in respect of water content and contaminant concentration

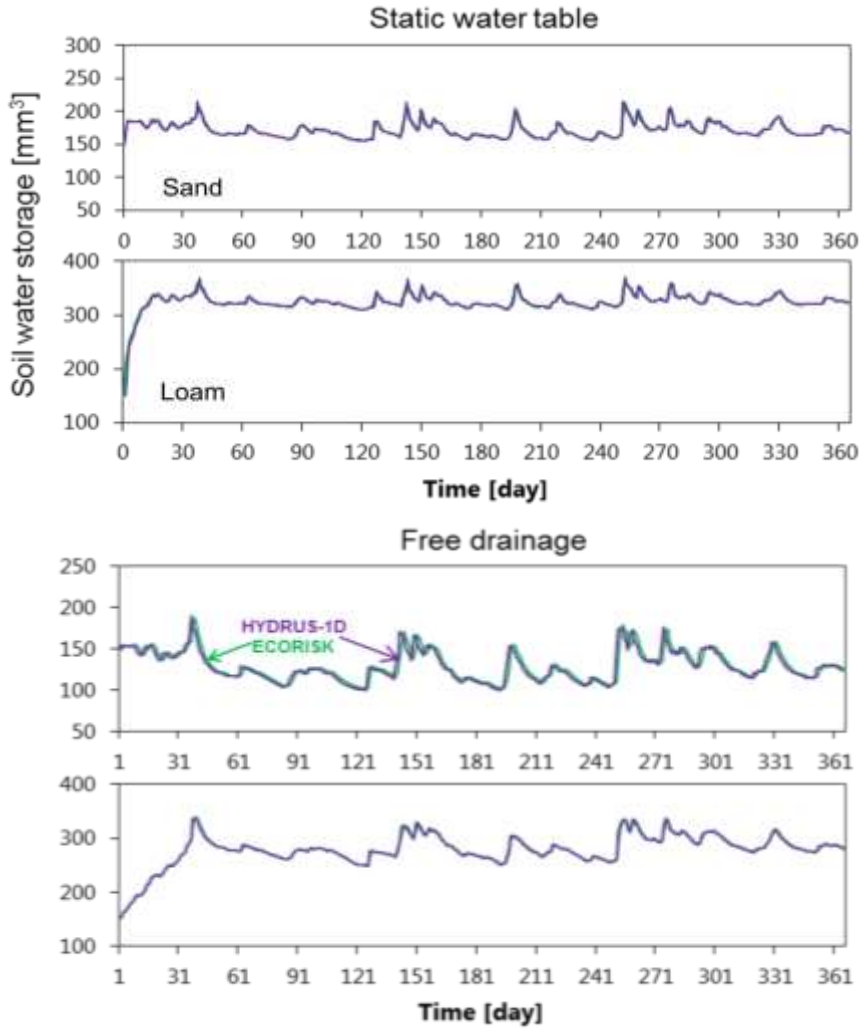

Figure 18. Comparison of our model with HYDRUS-1D with static water table and free drainage under conditions of real precipitation in the Mol forest site.

2.4.3.2. Testing and validation of radionuclide transport submodel

We demonstrated the validity of the solute transport model by comparison with the Ogata banks numerical solution (Figure 18). This figure also shows the effect of using different space derivative approximations (central, upstream and analytical). The following approaches were tested:

Forward in time (explicit): $\frac{\partial u}{\partial t} = \frac{u_i^{n+1} - u_i^n}{\Delta t} = FDS(u)_i^n$

Backward in time (implicit): $\frac{\partial u}{\partial t} = \frac{u_i^{n+1} - u_i^n}{\Delta t} = FDS(u)_i^{n+1}$

Central in time (Crank Nicolson): $\frac{\partial u}{\partial t} = \frac{u_i^{n+1} - u_i^n}{\Delta t} = \frac{FDS(u)_i^{n+1} + FDS(u)_i^n}{2}$

$FDS(u)_i^n$: finite difference approximation for the space derivative of u at i at time n.

In the end, the forward in time explicit method was adopted as it gave on balance of all factors the best results.

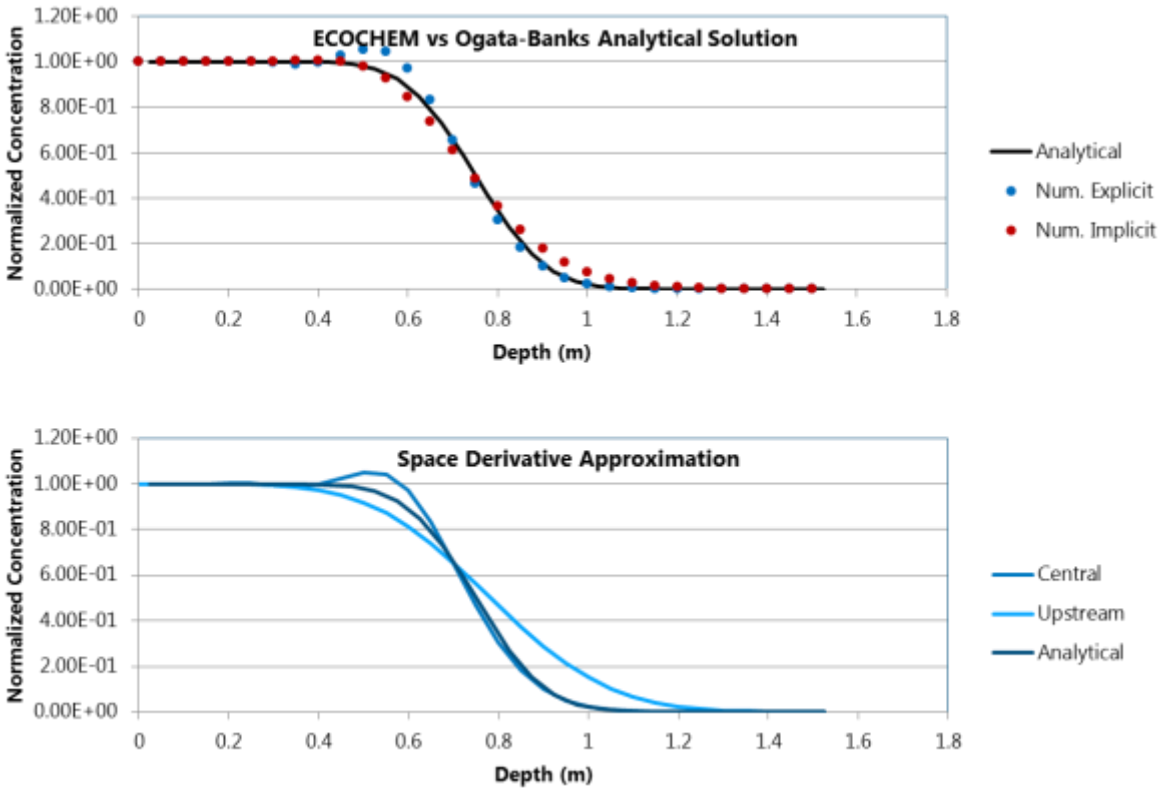

Figure 19: Comparison between analytical solutions and different numerical methods employed in the ECOCHEM solute transport code

Having verified that the solute transport model functioned without error, we focused on improving further the parametric K_d approach. Initially, the parametric K_d equations derived from the literature fitted experimental results poorly, so it was necessary to improve the equations. Using the genetic algorithm analysis and considering cofactors, the parametric K_d equations were optimised to obtain a better fit with the experimental data. The analysis revealed that pH and clay content are the soil variables that explain most of the variability in the K_d data.

An illustration of the improvements in correlation between calculated versus experimental K_d values is given in Figure 20 showing an analysis for uranium (a particularly difficult element to model). Parametric equations with 3, 5 and 7 parameters prior (above) and after (below) improving the models with a genetic algorithm are shown; note the increase in the coefficient of determination R2 before and after optimization.

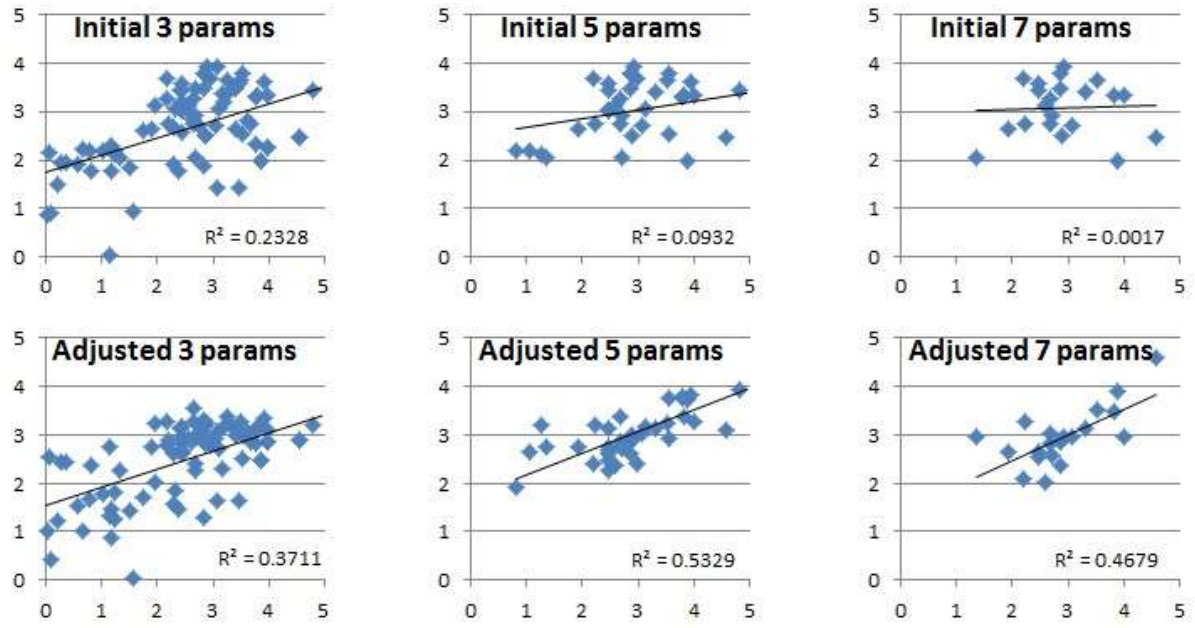

Figure 20: Examples of improvements of various parametric equations before (above) and after (below) adjusting the base parameters. The x axis represents the experimentally measured K_d (from SCK-CEN's proprietary database) whereas the Y axis represents the prediction by the parametric K_d model.

For a limited number of radionuclides, we opted for a co-factor criterion based on the knowledge of interaction mechanisms (for instance, the parametric equation for Cs can be corrected by potassium interference in soil solution). It is possible to use a filter to reduce data uncertainty and variability. Additional analysis is in progress beyond the ECORISK project to see if it is possible to introduce this refinement, with plans for publication if the attempt is successful.

2.4.4. Nutritional constraints modelling

2.4.4.1. Comparison of the simple vs. PHREEQC version

Two treatments of the mineral soil chemistry are included in the new code, the "simple" with only phosphorus and the more general "PHREEQC" that describes the processes affecting all the elements in the mineral soil. We ran both versions on the Brasschaat stand, with

- the current climate conditions,
- the observed soil profile
- the observed and calculated physico-chemical characteristics,
- the original ANAFORE bucket water transfer module
- feedback of N and P status on tree growth,
- no feedback from the other nutrients (Ca, Mg, K) status on tree growth,
- a forest management scenario targeting a 30 m²/ha basal area.

The resulting yield tables are presented below.

year	height	N_bef	DBH_bef	G_bef	V_bef	N_aft	DBH_aft	G_aft	V_aft	N_thin	DBH_thin	G_thin	V_thin
/	m	nbr	m	m^2/ha	m^3/ha	nbr	m	m^2/ha	m^3/ha	nbr	m	m^2/ha	m^3/ha
15	5.4	10000	0.09	70.6	249	5000	0.09	35.3	124	5000	0.09	35.3	124
22	8.2	5000	0.12	58.6	279	2560	0.12	30.0	143	2440	0.12	28.6	136
27	10.8	2560	0.15	43.0	269	1786	0.15	30.0	188	774	0.15	13.0	81
32	13.0	1786	0.16	36.6	268	1463	0.16	30.0	219	323	0.16	6.6	48
37	14.9	1463	0.18	37.9	332	1159	0.18	30.0	263	304	0.18	7.9	69
42	16.5	1159	0.20	35.1	344	991	0.20	30.0	294	168	0.20	5.1	50
47	18.0	991	0.21	34.9	379	852	0.21	30.0	326	139	0.21	4.9	53
52	19.0	852	0.23	35.6	431	718	0.23	30.0	364	134	0.23	5.6	68
57	19.8	718	0.24	33.8	439	637	0.24	30.0	389	81	0.24	3.8	50
62	20.5	637	0.27	35.6	501	537	0.27	30.0	422	100	0.27	5.6	79
67	20.9	537	0.29	34.5	516	468	0.29	30.0	449	69	0.29	4.4	66
72	21.7	468	0.29	31.7	484	444	0.29	30.0	459	24	0.29	1.6	25
77	22.1	444	0.32	35.1	570	380	0.32	30.0	488	64	0.32	5.1	82

year	height	N_bef	DBH_bef	G_bef	V_bef	N_aft	DBH_aft	G_aft	V_aft	N_thin	DBH_thin	G_thin	V_thin
/	m	nbr	m	m^2/ha	m^3/ha	nbr	m	m^2/ha	m^3/ha	nbr	m	m^2/ha	m^3/ha
15	5.4	10000	0.09	70.6	249	5000	0.09	35.3	124	5000	0.09	35.3	124
22	8.2	5000	0.12	57.9	275	2590	0.12	30.0	142	2410	0.12	27.9	133
27	10.8	2590	0.15	43.2	270	1801	0.15	30.0	188	789	0.15	13.1	82
32	13.0	1801	0.16	36.4	264	1486	0.16	30.0	218	315	0.16	6.4	46
37	14.9	1486	0.18	38.1	334	1171	0.18	30.0	263	315	0.18	8.1	71
42	16.5	1171	0.20	35.1	344	1000	0.20	30.0	294	171	0.20	5.1	50
47	18.0	1000	0.21	35.0	380	858	0.21	30.0	326	142	0.21	5.0	54
52	19.0	858	0.23	35.6	432	723	0.23	30.0	364	135	0.23	5.6	68
57	19.8	723	0.24	33.9	440	641	0.24	30.0	390	82	0.24	3.8	50
62	20.5	641	0.27	35.6	503	540	0.27	30.0	423	101	0.27	5.6	79
67	20.9	540	0.29	34.6	518	469	0.29	30.0	450	71	0.29	4.5	68
72	21.7	469	0.29	31.6	484	445	0.29	30.0	460	24	0.29	1.6	25
77	22.1	445	0.32	35.1	572	380	0.32	30.0	488	65	0.32	5.1	84

Table 13: Yield tables for the Brasschaat stand with the "simple" version (top) and "PHREEQC" version (bottom) (bef = before thinning, aft = after thinning, thin = thinned).

The yield tables from the two versions compare well. The difference can be ascribed to the difference in the way the mineral soil processes are implemented, and to the fact that they have not been parameterised to exactly match one another. The initial growth of the stand is high, even for the most productive pine stands. After this initial period, both tables agree quite well with the yield tables established by ENGREF (1984) and by Jansen *et al.* (1996) for a stand with a relatively low site index.

2.4.4.2. Evaluation of the mineralization flux

As a stand develops, it is expected that the litterfall and mineralization fluxes converge to similar, equilibrium, values. Figure 21 shows the litterfall and mineralization fluxes of P, K, Ca and Mg simulated in Brasschaat using the PHREEQC version and the same datasets as in 2.4.4.1.

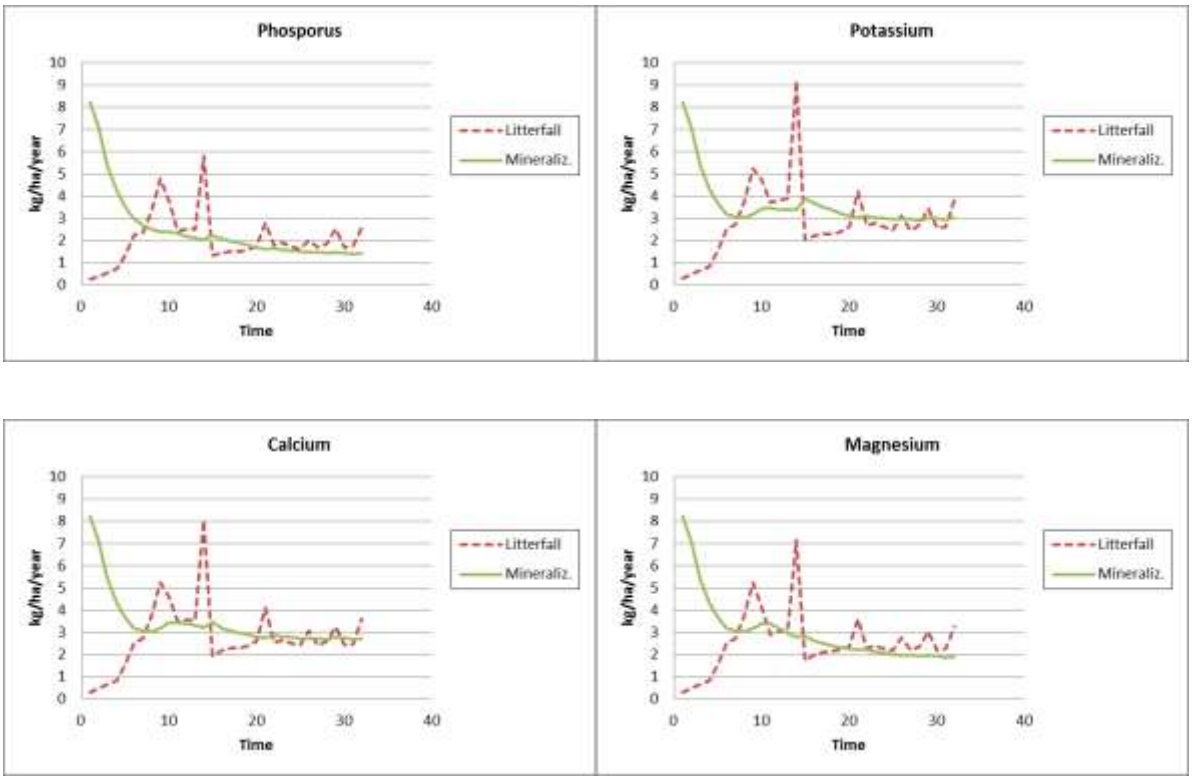

Figure 21. Litterfall and mineralization fluxes of P, K, Ca and Mg.

After the contrasting initial years of the forest growth, the two fluxes indeed converge towards each other after about 30 years, to a common average value for Ca and K, while for P and Mg the litterfall slightly exceeds mineralization.

2.4.4.3. Feedback of the element concentrations on tree growth

A Brasschaat stand simulation with Ca, Mg and K feedback on growth activated was run with, tentatively, the same parameters as for P. It resulted in a severe growth limitation due to shortage, producing trees *ca.* 10 m high instead of the 20 m effectively observed in the Brasschaat stand. This demonstrates the effectiveness of the feedback of the element concentrations on tree growth. However this feedback could not be fully calibrated due to an insufficient number of observations in view of the additional parameters to estimate and possible compensation mechanisms between all the other parameters of the model.

2.5. Results

2.5.1. Response of forest growth to climate change

2.5.1.1. Mean response to change in climate conditions

In order to assess the effect of a changed climate on forest growth, a set of simulations was performed for the Brasschaat forest. As management scenario we used a management where half of the volume increment is removed every 5 years (see Figure 14). For the three climate sets, HIST, RCP45 and RCP85 20 80-year climate sequences were sampled as described in section 2.4.2.2. Also, 15 species parameter sets (concerning photosynthesis, C-allocation, ...) were selected from a Bayesian optimization simulation according to a latin-hypercube selection. The climate and parameter set were combined into a total of 3 x 15 x 20 = 900 simulations. By parallelising the simulations on the supercomputer infrastructure of the University of Antwerp, the total simulation time was kept under a day. Carbon dioxide concentrations were kept constant throughout the simulations, with 390 ppm for HIST, 622 for RCP45 and 1100 for RCP85. As the response is likely to be not only sensitive to the changed climatic conditions (mostly temperature and precipitation) but also to the changed CO_2 concentrations, we added an extra set of 2 x 15 x 20 for the two RCP runs where we kept the CO_2 levels at historical levels (390 ppm), adding another 600 simulations.

Results for change in wood biomass [%] are shown in Figure 22. Every grey dot represents a relative difference in percentage for the given parameter set (x-axis) and two climate sequences (RCP-HIST)/RCP. The blue (RCP45), the red (RCP85) bands show the variance of the grey dots around the mean, which is represented by the coloured horizontal dash. For every parameter set, 4 sets of 20 (equal to the number of climate sequences) grey dots are shown: the first two sets show the results for a changed climate, but historical CO_2 concentrations of 390 ppm, the last two for changed climate and changed CO_2 concentrations.

The single grey dots are scattered around the zero point, which means that for a single historical climate sequence and a single future climate sequence, the biomass change signal can project both an increase or a decrease (see section 2.4.2.2). The different parameters sets react very differently to climate change, indicating that an extended parameter optimization process is useful.
Most of the mean signals are positive, indicating an average increase in wood biomass due to the given climate changes.

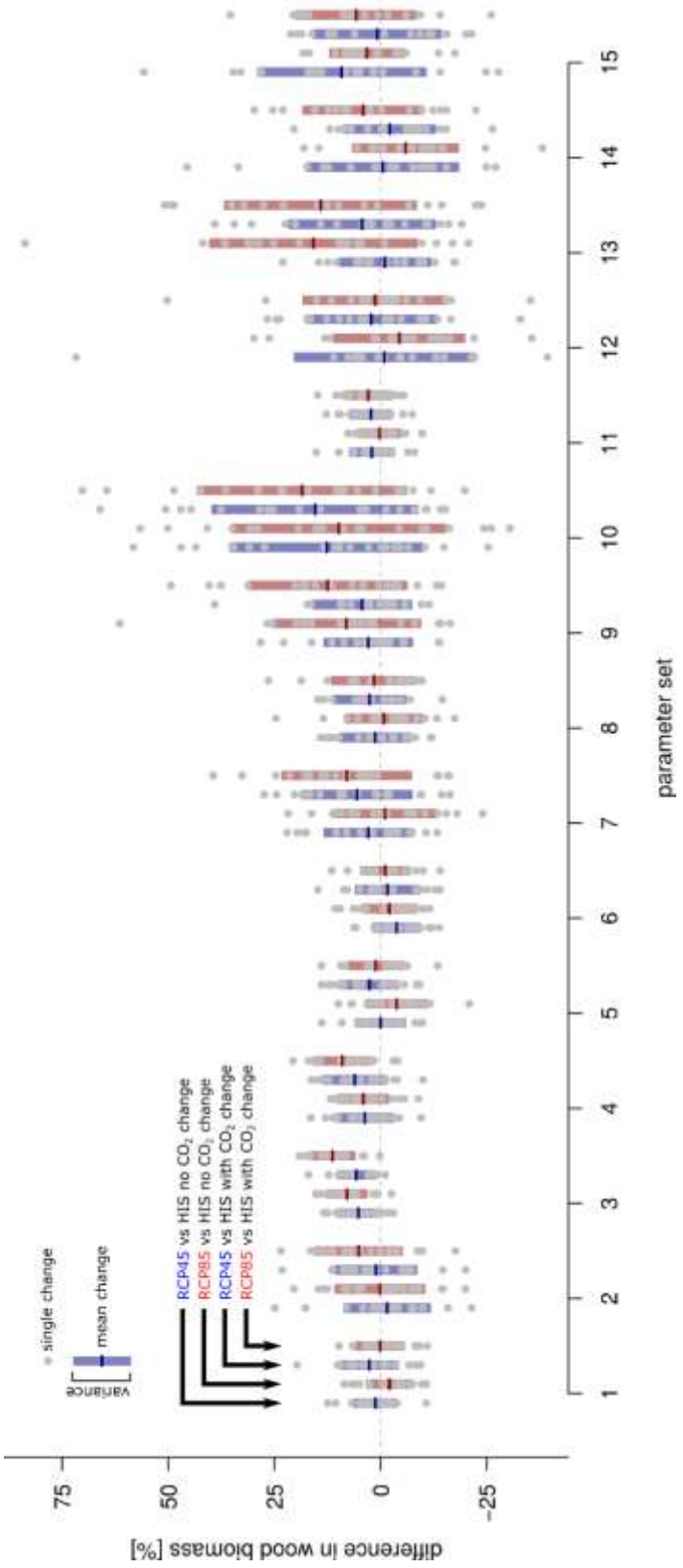

Figure 22. Effects of climate change on forest wood biomass.

The mean change and 95% confidence intervals of a simple t-test for all parameters sets and all climate sequences is given in Table 14. For the simulations without an increase in CO_2 there is a slight but significant increase in wood biomass (95% confidence interval [0.76%,3.72%] for RCP45 and [0.36%,3.58%] for RCP85) which

indicates the changes in climatic features on average cause an increase in wood biomass of about 1-2%. The simulations with an increase in CO_2 show an even more robust increase in wood biomass (95% confidence interval [2.04%,4.90%] for RCP45 and [4.64%,7.96%] for RCP85). This shows that the increased CO_2 is responsible for a larger approximately 5% increase in mean wood biomass.

The change in climate patterns is thus responsible for a significant but small increase, which is even larger when the projected CO_2 concentrations are also present in the forest ecosystem. Single realizations of climate sequences should be handled with caution as their change signal might interpreted wrongly.

experiment	**mean change**	**95% confidence interval**
RCP45 (no CO_2 increase)	2.24	[0.76, 3.72]
RCP85 (no CO_2 increase)	1.97	[0.36, 3.58]
RCP45 (with CO_2 increase)	3.47	[2.04, 4.90]
RCP85 (with CO_2 increase)	6.30	[4.64, 7.96]

Table 14. Change in mean wood biomass under climate change

2.5.1.2. Analysis of the difference between extreme results

From the average results and their uncertainty it is clear that the response of the forest to global change is positive on average (increased biomass and productivity), but some combinations of weather and parameters lead to severe reduction in growth. Comparing the most positive and the most negative response yields some insight to understand what is happening.

In Figure 23 the difference between the most positive and the most negative prediction of biomass development is given: with a difference of $>30\%$. The reduction appears linked to GPP (Gross Primary Production) as expected, with the first years overlapping and large differences around 20 years of age (Figure 24, left).

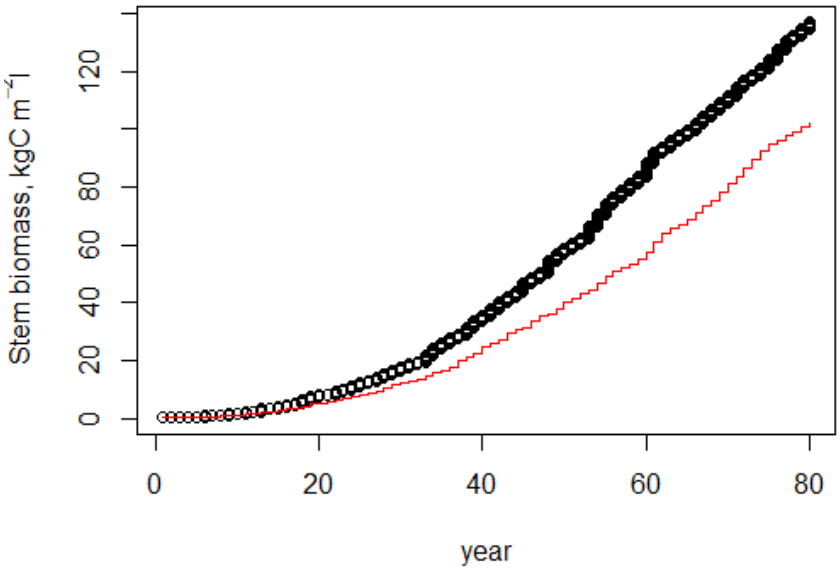

Figure 23: Stem biomass development in Brasschaat forest (Pinus sylvestris) under Global Change conditions for the most positive (black) and the most negatively responding parameter sets (red)

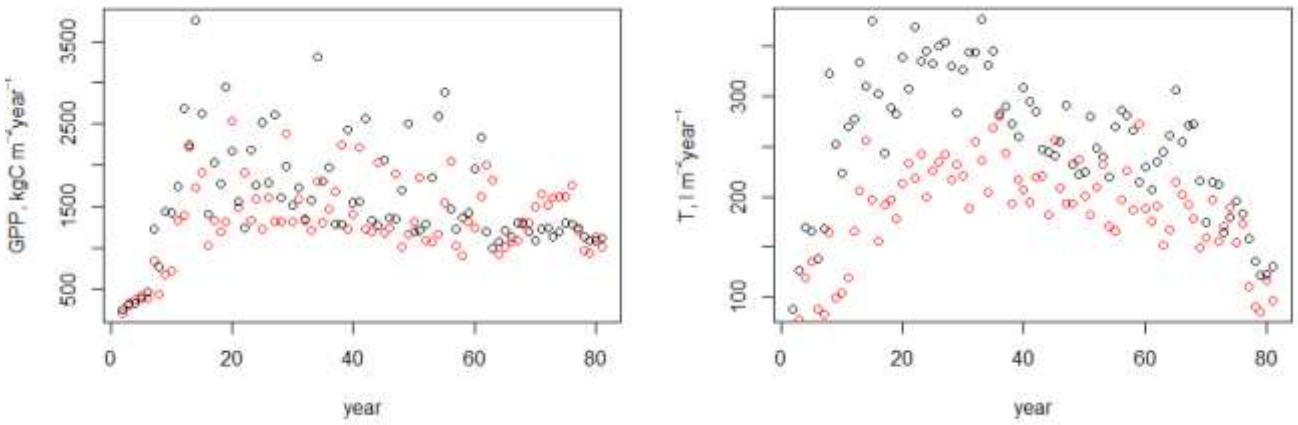

Figure 24. **Left**: Difference in GPP between the most positive and the most negatively responding parameter sets in the Brasschaat forest (Pinus sylvestris) in response to global climate change over an entire rotation (80 years). **Right**: Difference in transpiration between the most positive and the most negatively responding parameter sets in the Brasschaat forest (Pinus sylvestris) in response to global climate change over an entire rotation (80 years).

One possible explanation for reduced can be drought, and indeed GPP is closely linked to canopy transpiration (Figure 24, right).

The difference in transpiration is even bigger than in GPP, but this was not linked to a difference in soil water which was equally stable for both runs. It appears that transpiration is reduced by stomatal closure because photosynthesis is reduced.

The reduction in photosynthesis is caused by P-depletion as can be seen in Figure 25 for years 15-18.

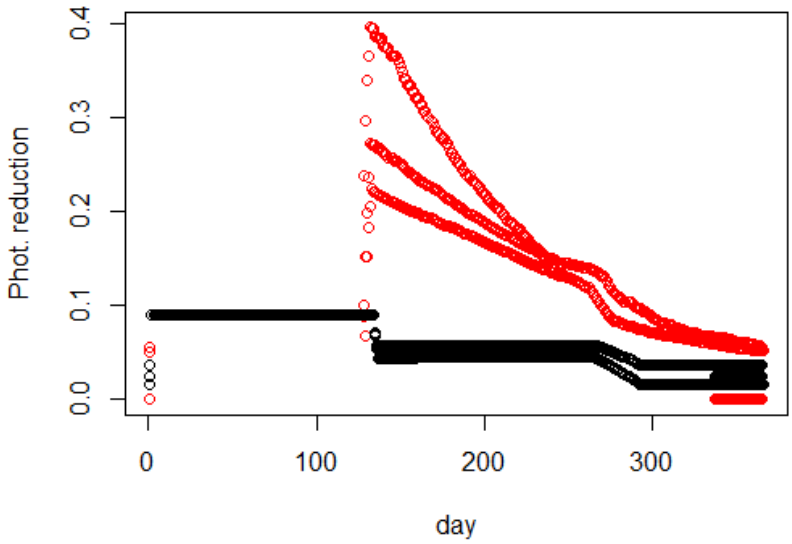

Figure 25 Difference photosynthetic reduction due to P depletion between the most positive and the most negatively responding parameter sets in the Brasschaat forest (Pinus sylvestris) in response to global climate change over an entire rotation (80 years)

This P depletion is caused by a combination of colder soil temperature, dryer soil (both leading to reduced P mineralisation) and lower P uptake efficiency (due to the chosen species parameters). This clearly indicates that for the Brasschaat site P limitation is a potential risk.

2.5.2. Modification of the harvest practices to minimise nutritional constraints

One of the questions addressed in this project was the potential effect of harvesting branches for wood energy. Four simulations were performed on the Brasschaat stand with Scots pine (*Pinus sylvestris*) and the following common inputs:

- observed soil profile,
- observed and calculated physico-chemical characteristics,
- original ANAFORE bucket water transfer module,
- feedback from N and P status on tree growth,
- no feedback from the other nutrients (Ca, Mg, K) status on tree growth,
- initial plantation density of 2500 trees per hectare,
- a forest management targeting a 30 m²/ha basal area,

and different scenarios:

- branch harvesting: 0% (B0) or 100% (B1),
- one climate scenario leading to lower production (V0) and one leading to a higher production (V1).

a. Effect of branch harvesting (B0, B1) in a high production context (V1)

Table 15 shows the yield table for the cross-scenario no branch harvest (B0) with high production (V1), and Table 16 the yield table for the cross-scenario full branch harvest (B1) with high production (V1).

year	height	N_bef	DBH_bef	G_bef	V_bef	N_aft	DBH_aft	G_aft	V_aft	N_thin	DBH_thin	G_thin	V_thin
/	m	nbr	m	m^2/ha	m^3/ha	nbr	m	m^2/ha	m^3/ha	nbr	m	m^2/ha	m^3/ha
15	5.3	2500	0.15	45.9	132	1250	0.15	23.0	66	1250	0.15	23.0	66
22	8.2	1250	0.19	35.2	150	1065	0.19	30.0	128	185	0.19	5.2	22
27	10.8	1065	0.22	38.7	214	827	0.22	30.0	166	238	0.22	8.6	48
32	13.1	827	0.23	34.5	220	720	0.23	30.0	191	107	0.23	4.5	28
37	15.2	720	0.24	33.5	242	645	0.24	30.0	217	75	0.24	3.5	25
42	16.8	645	0.26	34.2	284	566	0.26	30.0	249	79	0.26	4.2	35
47	18.3	566	0.27	33.4	310	508	0.27	30.0	278	58	0.27	3.4	32
52	19.4	508	0.30	35.5	382	430	0.30	30.0	323	78	0.30	5.4	59
57	20.3	430	0.32	34.4	409	376	0.32	30.0	358	54	0.32	4.3	51
62	21.0	376	0.34	33.4	429	338	0.34	30.1	385	38	0.34	3.4	43
67	21.4	338	0.34	30.9	403	329	0.34	30.1	392	9	0.34	0.8	11
72	21.7	329	0.35	32.2	439	307	0.35	30.1	410	22	0.35	2.2	29
77	21.7	307	0.37	33.4	483	276	0.37	30.1	434	31	0.37	3.4	49

Table 15. Yield table high production V1, no branch harvest B0.

year	height	N_bef	DBH_bef	G_bef	V_bef	N_aft	DBH_aft	G_aft	V_aft	N_thin	DBH_thin	G_thin	V_thin
/	m	nbr	m	m^2/ha	m^3/ha	nbr	m	m^2/ha	m^3/ha	nbr	m	m^2/ha	m^3/ha
15	5.3	2500	0.15	45.9	132	1250	0.15	23.0	66	1250	0.15	23.0	66
22	8.2	1250	0.19	35.2	150	964	0.19	27.2	116	286	0.19	8.1	34
27	10.8	964	0.22	35.5	199	764	0.22	28.2	157	200	0.22	7.4	41
32	13.1	764	0.23	32.4	209	670	0.23	28.4	183	94	0.23	4.0	26
37	15.2	670	0.25	31.7	231	602	0.25	28.5	207	68	0.25	3.2	23
42	16.8	602	0.26	32.5	272	531	0.26	28.6	240	71	0.26	3.8	32
47	18.3	531	0.28	31.9	297	480	0.28	28.8	269	51	0.28	3.1	29
52	19.4	480	0.30	34.2	370	415	0.30	29.6	320	65	0.30	4.6	50
57	20.3	415	0.32	33.8	404	372	0.32	30.3	363	43	0.32	3.5	42
62	21.0	372	0.34	33.7	433	342	0.34	31.0	398	30	0.34	2.7	35
67	21.4	342	0.34	31.8	416	335	0.34	31.1	407	7	0.34	0.7	9
72	21.7	335	0.36	33.3	454	318	0.36	31.6	431	17	0.36	1.7	23
77	21.7	318	0.37	35.1	506	295	0.37	32.6	470	23	0.37	2.5	37

Table 16 Yield table high production V1, full branch harvest B1.

The two yield tables are very similar in height and diameter of the trees, and in the number of trees thinned to achieve the target basal area. Harvesting the branches or not does not appear to have an effect on the tree growth. The simulated basal area in the first years of the stand growth is high, and close to the most productive pine stands.

The phosphorus content of the individual mean tree (Figure 26, left) has a similar variation in both branch export scenarios.

And as the number of standing trees is nearly the same, the immobilisation of P in the whole stand is also very close in both branch scenarios (Figure 26,right).

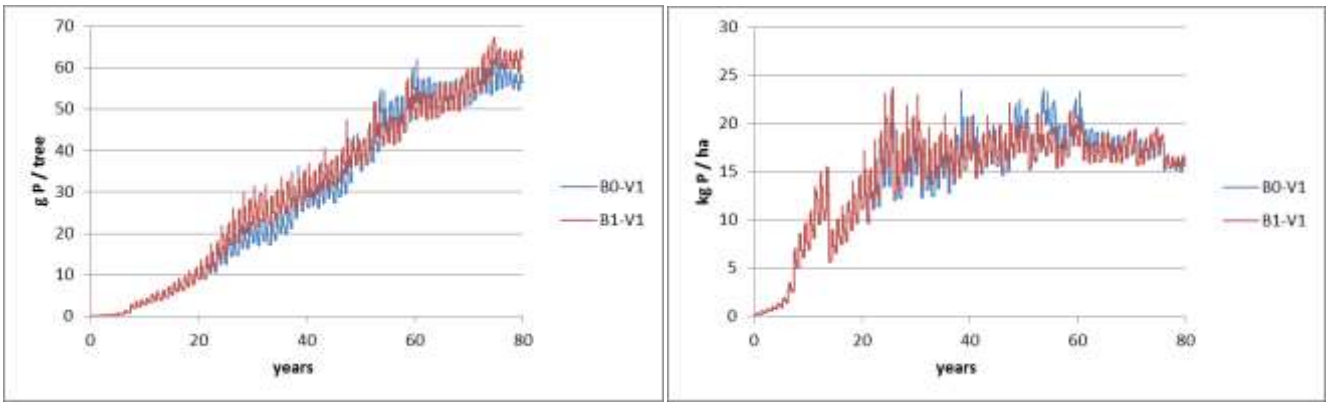

Figure 26. **Left**: P content of the individual tree (scenarios B0- and B1-V1). **Right**: P immobilisation at stand level (scenarios B0-V1 and B1-V1).

The exportation of P by thinning operations is shown in Figure 27: left for the no branch harvesting (B0) and right for the full branch harvesting (B1) scenario with P in stem from B0 for comparison. None of the branches exported at thinning have a diameter over 4 cm, all these branches fall in the diameter class 0-4 cm. The P exportation in the stem is also similar in both cases for the same reasons as above. The exportation of P in branches in the B1 scenario represents an additional 8 to 15% of the exportation in the stem wood. The contribution of the branch bark is negligible.

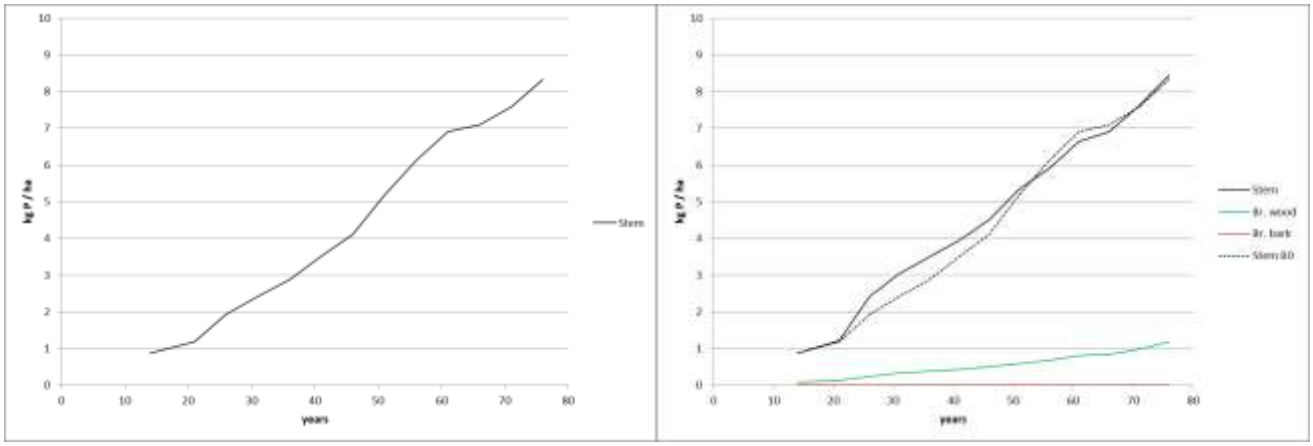

Figure 27. Cumulated P exportation at stand level, left scenario B0-V1; right scenario B1-V1.

At the end of the rotation, the P exported in thinned trees is 0.11 kg/ha/year in the no branch and 0.12 kg/ha/year in the full branch export scenario. The P immobilized in the remaining standing trees represents 0.21 kg/ha/year.

The variation of the soil organic P content over time in the holorganic layer and in the (organo)mineral soil profile are presented in Figure 28. Organic phosphorus in the (organo)mineral soil is strongly depleted, in a similar way in the two scenarios, suggesting a disequilibrium between the initial organic pools in the mineral soils with respect to the stand conditions. Organic P content in the holorganic layer initially

decreases due to net mineralization, then returns to about the same level and stabilises. At the end of the rotation, soil organic P content in the full branch harvesting scenario is 3 kg/ha lower than in the no branch harvesting scenario, mainly due to the difference in the holorganic P content.

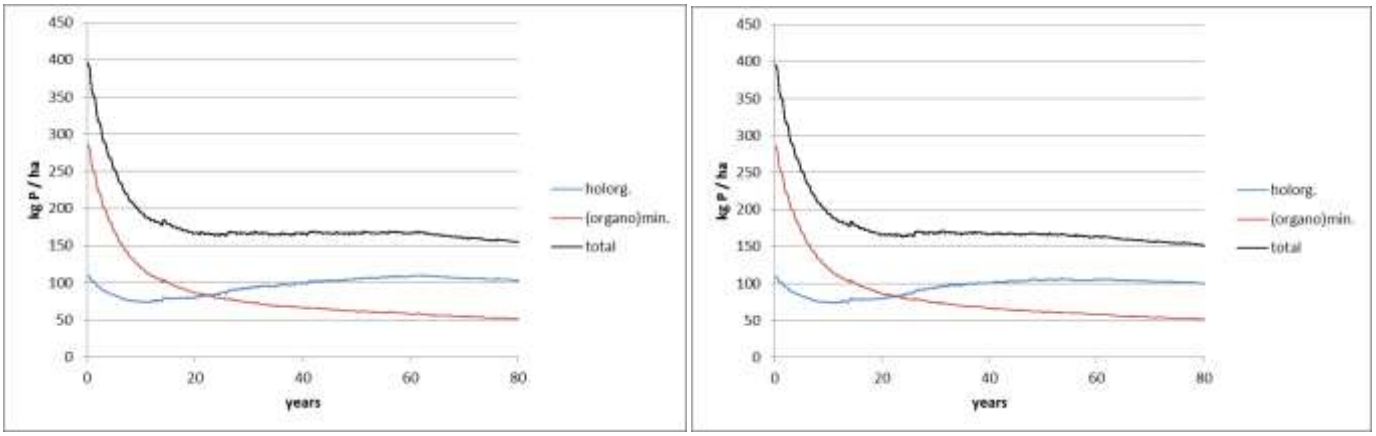

Figure 28. Organic P content in the soil, left scenario B0-V, right scenario B1-V1

P in litterfall and P released by mineralization are presented in Figure 29. P released by mineralization from the holorganic horizon differs only slightly between the two scenarios.

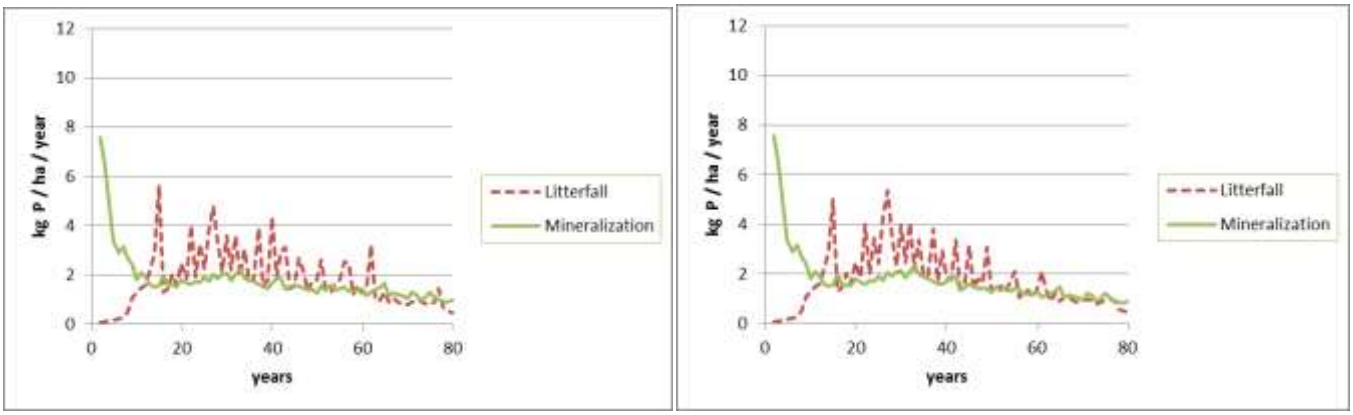

Figure 29 P in litterfall and mineralized in holorganic layer (scenario B0-V1).

Initially, P released by mineralization exceeds P in litterfall. Then as the trees grow P brought by litterfall is higher than P released by mineralization up to about 50 years. After 40 years, P released by mineralization and P in litterfall both decrease. Release by mineralization very slightly exceeds litterfall in the no branch export scenario in average, while they are similar in the full branch export scenario.

b. Effect of branch harvesting (B0, B1) in a low production context (V0)

Table 17 shows the yield table for the cross-scenario no branch harvest (B0) with low production (V0), and Table 18 the yield table for the cross-scenario full branch harvest (B1) with low production (V0).

year	height	N_bef	DBH_bef	G_bef	V_bef	N_aft	DBH_aft	G_aft	V_aft	N_thin	DBH_thin	G_thin	V_thin
/	m	nbr	m	m^2/ha	m^3/ha	nbr	m	m^2/ha	m^3/ha	nbr	m	m^2/ha	m^3/ha
15	5.3	2500	0.11	24.6	74	1250	0.11	12.3	37	1250	0.11	12.3	37
22	8.5	1250	0.14	19.9	90	1250	0.14	19.9	90	0	0.14	0.0	0
27	10.7	1250	0.16	25.0	138	1250	0.16	25.0	138	0	0.16	0.0	0
32	13.0	1250	0.17	29.6	195	1250	0.17	29.6	195	0	0.17	0.0	0
37	15.0	1250	0.18	32.2	232	1166	0.18	30.0	216	84	0.18	2.2	16
42	16.6	1166	0.19	33.1	265	1058	0.19	30.0	241	108	0.19	3.1	25
47	18.3	1058	0.20	33.7	306	943	0.20	30.0	272	115	0.20	3.7	33
52	19.6	943	0.21	33.7	342	840	0.21	30.0	305	103	0.21	3.7	37
57	20.8	840	0.23	33.8	382	746	0.23	30.0	339	94	0.23	3.8	43
62	21.8	746	0.23	32.2	386	695	0.23	30.0	360	51	0.23	2.2	26
67	22.2	695	0.25	33.4	433	625	0.25	30.0	389	70	0.25	3.4	44
72	22.8	625	0.26	32.5	446	577	0.26	30.0	412	48	0.26	2.5	34
77	23.2	577	0.27	32.8	477	528	0.27	30.1	436	49	0.27	2.8	40

Table 17. Yield table low production V0, no branch harvest B0.

year	height	N_bef	DBH_bef	G_bef	V_bef	N_aft	DBH_aft	G_aft	V_aft	N_thin	DBH_thin	G_thin	V_thin
/	m	nbr	m	m^2/ha	m^3/ha	nbr	m	m^2/ha	m^3/ha	nbr	m	m^2/ha	m^3/ha
15	5.3	2500	0.11	24.6	74	1250	0.11	12.3	37	1250	0.11	12.3	37
22	8.5	1250	0.14	19.9	90	1250	0.14	19.9	90	0	0.14	0.0	0
27	10.7	1250	0.16	25.0	140	1250	0.16	25.0	140	0	0.16	0.0	0
32	13.0	1250	0.17	29.5	197	1250	0.17	29.5	197	0	0.17	0.0	0
37	15.0	1250	0.18	32.0	231	1173	0.18	30.0	217	77	0.18	2.0	14
42	16.7	1173	0.19	33.7	277	1044	0.19	30.0	246	129	0.19	3.7	30
47	18.3	1044	0.20	33.1	301	947	0.20	30.0	273	97	0.20	3.1	28
52	19.6	947	0.21	33.6	341	845	0.21	30.0	305	102	0.21	3.6	37
57	20.8	845	0.22	33.5	376	756	0.22	30.0	336	89	0.22	3.5	40
62	21.7	756	0.23	32.3	385	703	0.23	30.0	358	53	0.23	2.3	27
67	22.2	703	0.25	33.4	431	633	0.25	30.0	388	70	0.25	3.3	43
72	22.9	633	0.26	32.6	445	584	0.26	30.0	411	49	0.26	2.5	34
77	23.2	584	0.27	33.0	478	532	0.27	30.0	435	52	0.27	2.9	43

Table 18. Yield table low production V0, full branch harvest B1.

With this low production scenario, the mean tree is taller by 1.5 m, but smaller in diameter by 10 cm, resulting in a mean tree volume half of the high production scenario. The yield tables for both branch export scenarios are very similar, as they were for the high production scenario. The number of trees left standing to achieve the basal area target is about the double of the high production scenario.

The phosphorus content of the individual mean tree (Figure 30, left) has a similar variation in both branch export scenarios.
It is half that of the high production scenario. The number of standing trees being nearly the same, the immobilisation of P in the whole stand is also very close in both branch scenarios (Figure 30, right). Moreover, as the P content of the individual tree in scenarios V0 is half that of scenarios V1 and the number of standing tree in V0 the double of V1, phosphorus immobilized at stand level is rather similar in average.

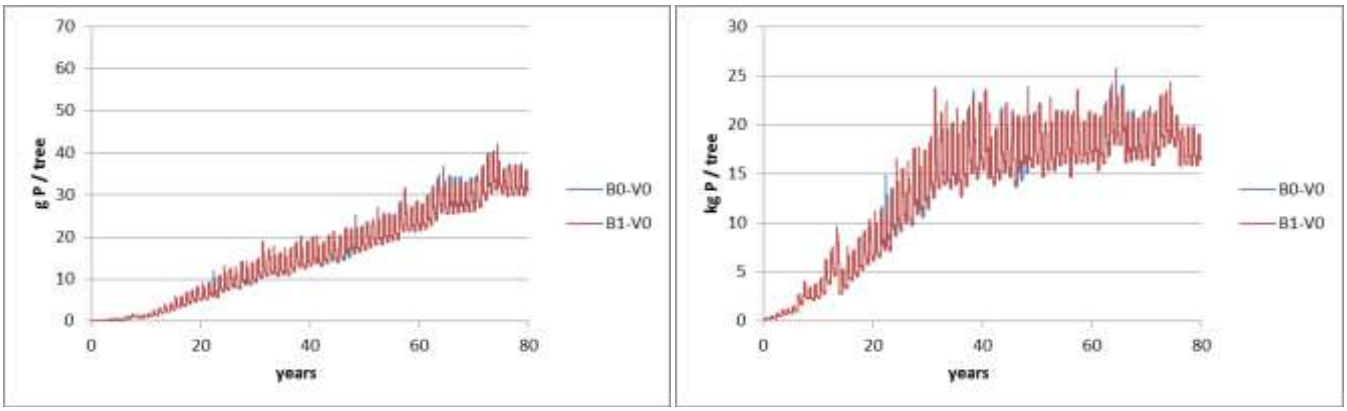

Figure 30. **Left**: P content of the individual tree (scenarios B0-V0 and B1-V0). **Right**: P immobilisation at stand level (scenarios B0-V0 and B1-V0).

The exportation of P in thinned material is shown in Figure 31 for the no branch harvesting (B0, left) and for the full branch harvesting (B1, right) scenario with P in stem from B0 for comparison. All the exported branches are in the diameter class 0-4 cm. The difference between the B0 and B1 scenarios is about 6 to 9% in the last 30 years of the rotation.

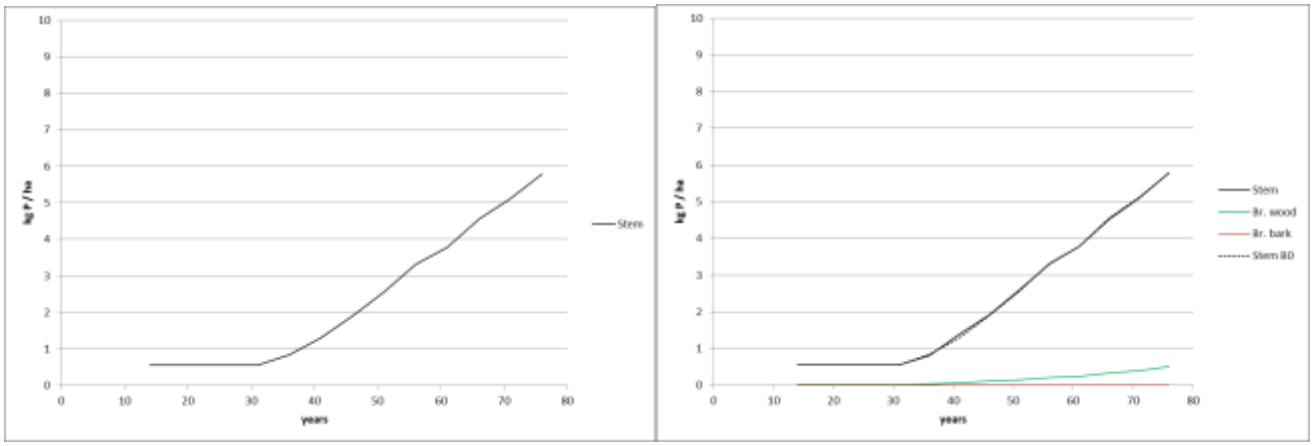

Figure 31 Cumulated P exportation at stand level for scenario B0-V0 on the left and scenario B1-V0 on the right.

At the end of the rotation, the P exportation in thinned trees is 0.07 kg/ha/year in the no branch and 0.08 kg/ha/year in the full branch export scenario. The remaining standing trees represent 0.21kg/ha/year as in the V1 scenarios.

The variation of the soil organic P content over time in the holorganic layer and in the (organo)mineral soil profile are presented in Figure 32. As in the high production scenarios, organic phosphorus in the (organo)mineral soil is strongly depleted, in a similar way in the two branch export scenarios. Organic P content in the holorganic layer initially decreases due to P release by mineralization whereas P supply by

litterfall is low in the first years, then it increases again, finally reaching a value 50% higher than the initial one. At the end of the rotation, organic P in the full branch harvesting scenario is 2.4 kg/ha lower than in the no branch harvesting scenario.

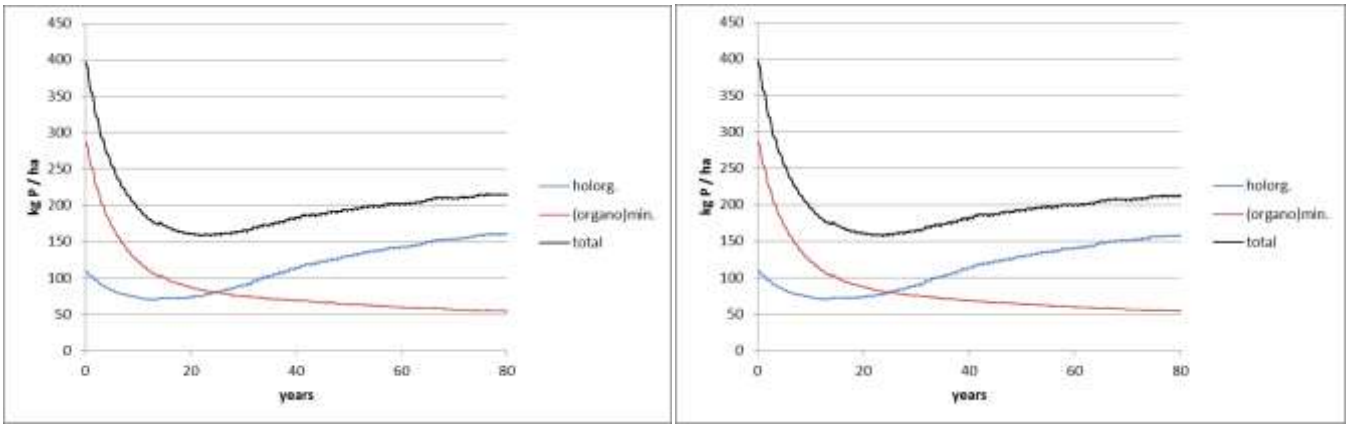

Figure 32 Organic P content in the soil for scenario B0-V0 on the left and scenario B1-V0 on the right.

P supply by litterfall and P released by mineralization are presented in Figure 33. As in the high production scenarios, P released by mineralization from the holorganic horizon differs only slightly between the two branch export scenarios. But contrarily to the high production scenarios, mineralization does not decrease towards the end of the rotation but remains at a constant level.

After the first 20 years, P in litterfall exceeds P from mineralization, leading to the increase of P content in the holorganic layer observed in Figure 32.

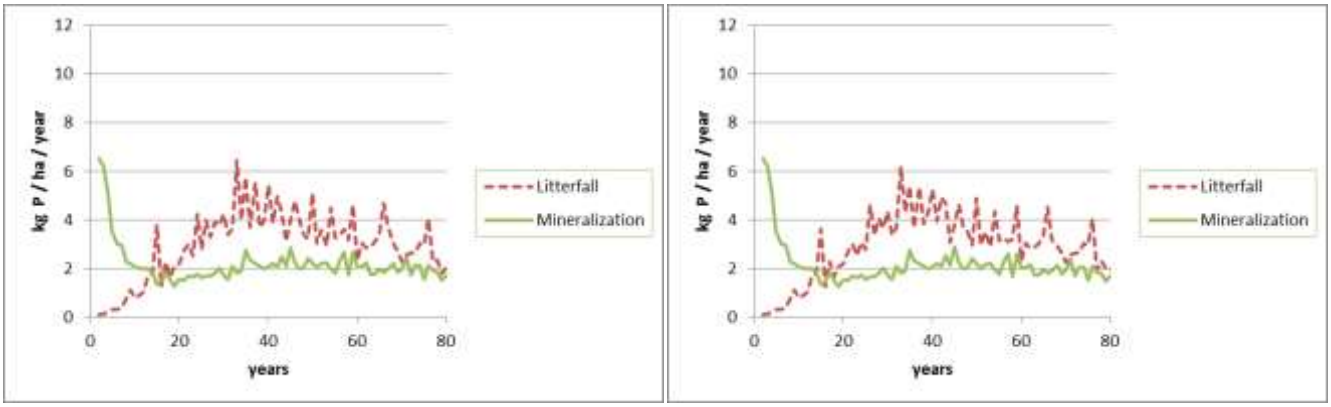

Figure 33 P in litterfall and mineralized from holorganic layer for scenario B0-V0 on the left and scenario B1-V0 on the right.

Either in the low or in the high production scenarios, the exportation of branches has no significant influence on the stand production or on the soil P status. The low/high production scenario impacts the P content in the holorganic horizon. In all scenarios,

organic P in the mineral soil rapidly and strongly decreases, globally decreasing the P content of the soil system.

2.5.3. Radionuclide transfer through forest ecosystems

2.5.3.1. Measurements at the Mol site

The relative distribution of the mass of Mg, Al, Cl, Ca, Mn and K in Scots pines from the forest stand in Mol, Belgium (average of 6 trees) was determined, as shown in Figure 34. A very simple linear, first-order compartment 'box' model of the tree then used to obtain some indication of the likely transfer rates (flow per unit mass, in d^{-1}) between vegetation compartments. This simple model has 5 compartments (foliage, wood, floor, roots and soil, linked to the observed element distributions) and 11 parameters (the inter-compartmental transfer rates). Initial parameter values were chosen based on the model from Van den Hoof and Thiry (2012), originally designed to study the cycling of ^{36}Cl. Then, the transfer rates were modified iteratively until the deviation between the simulated content in the model compartments and the experimentally measured content in forest floor, soil, roots, wood and foliage reached a minimum level. Full details are given elsewhere (Gielen, Vives i Batlle *et al*. 2016). The kinetic parameters are given in Table 19.

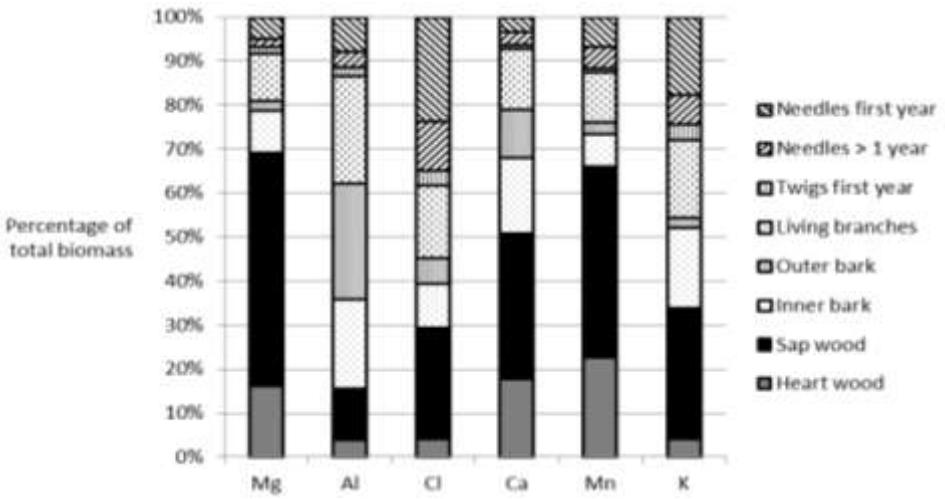

Figure 34: Relative distribution of the mass of Mg, Al, Cl, Ca, Mn and K in Scots pines from the forest stand in Mol, Belgium (average of 6 trees)

Table 19: Model-fitted inter-compartment transfer rates and mass flows for different elements. N/A: not assessed.

From	To	Transfer rate (d^{-1})						Selectivity coefficient				
		H_2O	Mg	Cl	Ca	Mn	K	Mg	Cl	Ca	Mn	K
Litter	Roots	N/A	5.0E-06	1.2E-05	5.0E-05	6.0E-05	9.0E-05	N/A	N/A	N/A	N/A	N/A
Litter	Soil	6.3E-04	3.6E-05	2.0E-05	6.1E-05	3.5E-05	2.1E-04	5.7E-02	3.2E-02	9.7E-02	5.6E-02	3.3E-01
Leaves	Litter	1.3E-02	1.2E-03	5.0E-04	3.0E-03	2.1E-03	1.6E-03	9.1E-02	3.8E-02	2.3E-01	1.6E-01	1.2E-01
Leaves	Wood	6.2E-02	4.0E-04	3.0E-04	1.0E-04	2.0E-03	7.0E-04	6.5E-03	4.8E-03	1.6E-03	3.2E-02	1.1E-02
Roots	Litter	N/A	5.0E-05	1.0E-04	6.0E-05	9.0E-04	5.5E-04	N/A	N/A	N/A	N/A	N/A
Roots	Soil	N/A	5.0E-05	1.0E-04	6.0E-05	9.0E-04	5.5E-04	N/A	N/A	N/A	N/A	N/A
Roots	Wood	1.5E+00	7.5E-04	5.0E-04	2.2E-03	5.2E-03	3.2E-03	5.1E-04	3.4E-04	1.5E-03	3.5E-03	2.2E-03
Soil	Roots	2.2E-04	2.3E-06	1.8E-06	2.8E-06	2.0E-06	6.2E-06	1.0E-02	8.2E-03	1.3E-02	9.1E-03	2.8E-02
Wood	Litter	2.4E-04	1.4E-05	3.0E-05	3.2E-05	1.4E-05	1.0E-05	5.8E-02	1.2E-01	1.3E-01	5.8E-02	4.1E-02
Wood	Leaves	1.5E+00	1.1E-04	4.0E-04	2.0E-04	5.5E-04	7.0E-04	7.5E-05	2.7E-04	1.4E-04	3.7E-04	4.7E-04
Wood	Roots	6.2E-02	2.7E-05	2.5E-04	1.0E-05	3.2E-03	2.3E-04	4.4E-04	4.0E-03	1.6E-04	5.2E-02	3.7E-03

The ratios of these element-derived kinetic rates to those originally developed for ^{36}Cl (Van den Hoof and Thiry 2012) give an indication of the differential mobility of Mg, Al, Cl, Ca, Mn and K compared to Cl, which is treated here as surrogate for the mobility of water within the tree. These ratios are expressed as multiplicative coefficients for the fluxes, following the concept introduced by Casadesus *et al.* (Casadesus, Sauras-Yera *et al.* 2008) in which the transfer of radionuclides between two compartments is calculated as the transfer of a known element (e.g. a nutrient) multiplied by the ratio of concentrations of RN to nutrient, corrected by a selectivity coefficient. The calculated coefficients are also given in Table 19.

The hydrology measurements produced at the Mol site were used in combination with generic literature data to parameterise the water transport sub-model.
The selectivity coefficients have been delivered for use within ANAFORE, as part of a Master project that, due to timing, continues beyond this project.

2.5.3.2. First results with the simplified ECOFOR model

Previous research (Vincke and Thiry 2008) estimated pine transpiration to be < 1.85 mm d^{-1}, 25% of PET. Understory evaporation was estimated as 18 – 20% of total ET. The soil water reserve is found at 2.5 m, with an extractable water table at 1.45 m below surface. The contribution of the water table to forest transpiration was 61% (98.5% in dry periods), signalling its potential as a contaminant source in dry periods where the predominant water transport direction is upwards. Although the capillary flow through the soil was not measured, upward flow rates of more than 2 mm day^{-1} are common, and values range from 0.5 to 8 mm day^{-1} (Raes and Deproost 2003). The model successfully predicted these main observed trends in evapotranspiration in comparison with the average monthly PET values for grass and coniferous tree-covered

surfaces based on the climatological data for Mol (Belgium) in the period 1984-88 (Mallants 2005), as shown in Figure 35. The use of real irradiance data taken on a daily basis somewhat improves the sinusoidal expression used to predict monthly irradiance. The model also successfully predicts the mean soil water content of ~ 25%, as evidenced in Vincke's study (Vincke and Thiry 2008), and that most of the water is stored in the roots, followed by the rest of the plant and leaf outer surfaces. The simulated water table height below ground fluctuated between 2.1 and 2.6 m (the measured water table floor is between 1.8 – 2 m). Transpiration was calculated to be < 1.2 mm/day (expected < 2 mm/d). At peak periods transpiration is ~ 15% of PET compared with 20% in the study. The predicted maximum capillarity flow of 0.4 mm per day is compatible with our estimations.

Validation of the model following its coupling to a previous stand-alone ^{36}Cl model (Van den Hoof and Thiry 2012) is ongoing. Although the results are too tentative to be fully given here, the solution for a constant water table is consistent with the predictions of that original model.

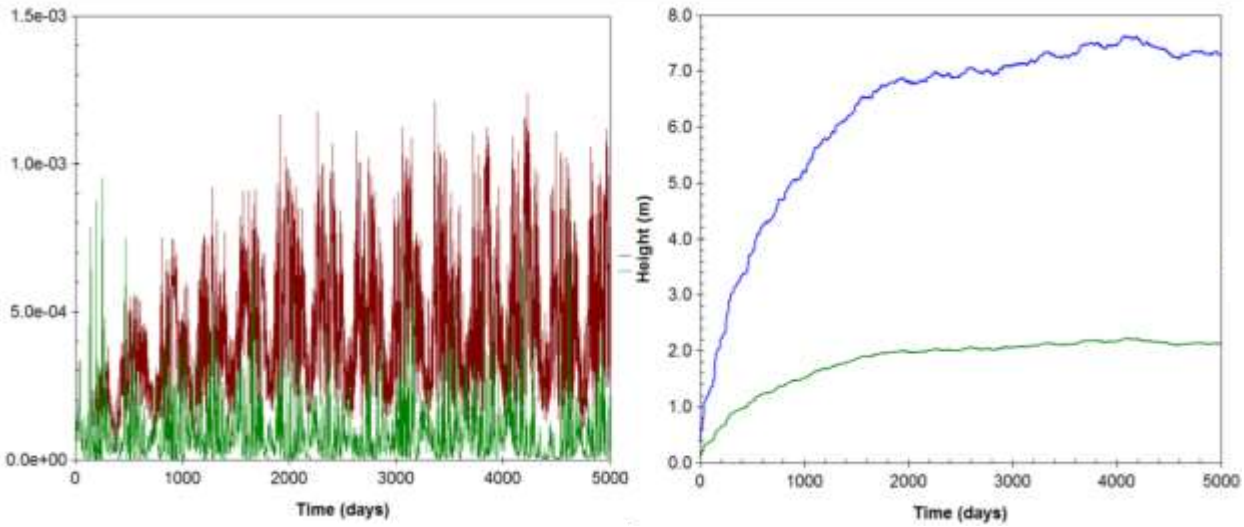

Figure 35: (a) Model-predicted evaporation (brown) and transpiration (green) – (b) Water table (blue) and capillary front (green) heights (simulation starting from empty compartments)

2.5.3.3. Risks of radionuclide transfer in forest ecosystems

Description of the management approach

This section describes the applicability of the radionuclides/pollutants model for the management of pollution in forests. The objective is to show how the models can be used to see the relative effects of different climate scenarios on the transport of radionuclides. In other words, we are not applying the model as an assessment tool to

determine absolute levels or risk, but as means to evaluate how much radioactivity gets across the soil profile for different scenarios starting from the same source term.

After the model simulations are conducted, it is possible to link-up with the ERICA tool (Environmental Risk from Ionising Contaminants: Assessment and Management - a European Commission/European Atomic Energy Community EURATOM)-funded project) (Beresford, Brown *et al*. 2007, Brown, Alfonso *et al*. 2008, ERICA 2009, Brown, Alfonso *et al*. 2016). ERICA provides the approach to convert activity concentrations in tree (Bq kg^{-1}) to internal and external dose rate (μGy h^{-1}) for a series of reference organisms (including trees) and from there into a risk factor, linking dose to exposure via a dose coefficient DC (a list of DC's for terrestrial vegetation for the radionuclides cited in the ECORISK proposal is given in Table 20 for the purposes of illustration).

Radionuclide	DC for internal exposure (μGy h^{-1} per Bq kg^{-1})			
	Lichen/briophytes	Grasses/herbs	Shrub	Tree
Cl-36	1.23E-04	3.13E-03	1.56E-04	2.27E-04
Ca-41	8.64E-06	1.27E-06	7.91E-07	3.17E-06
Sr-90	1.47E-03	4.00E-04	9.18E-05	3.10E-04
Nb-94	2.48E-06	1.39E-07	1.33E-07	6.96E-06
Sn-126	2.90E-04	4.02E-04	4.02E-04	9.75E-04
Cs-137	4.47E-04	1.56E-04	2.75E-04	4.34E-05
U-238	2.20E-02	3.07E-03	1.46E-03	1.58E-04

Table 20: Dose conversion coefficients for internal exposure from the ERICA tool

The risk factor is the ratio of the dose rate to a predicted no effects dose rate (PNEDR) which is calculated using a species sensitivity distribution approach, basically the PNEDR is the dose rate for which at least 5% of the species in an ecosystem would reach 10% effects (measured as mortality, morbidity or reproduction effects, based on data from the associated FREDERICA database (FREDERICA 2006, Copplestone, Hingston *et al*. 2008, Garnier-Laplace, Copplestone *et al*. 2008)), corrected by a safety factor, as shown in Figure 36. For the ERICA approach, this PNEDR IS 10 μGy h^{-1}, meaning that below this level it is possible to screen-out assessment sites from further study. In technical terms, the approach proposed for a particular climate event is:

To determine for a given radionuclide a risk factor for a 'reference' model simulation containing 'standard' climatic conditions.

To calculate the activity concentration in tree (Bq kg^{-1}) per unit (nominal) activity concentration in soil (Bq kg^{-1}), i.e. a kind of "biosphere conversion factor" (BCC) similar to that used in radiological assessment.

To convert to dose rate (μGy h^{-1}) using the ERICA tool (i.e. by multiplying (a) by a dose coefficient for tree.

To derive risk quotient as follows: $$RQ = \frac{A_{wholetree}[Bq] \times DC[\mu Gy h^{-1} \text{per } Bq kg^{-1}]}{M_{wholetree}[kg] \times PNEDR[= 10\ \mu Gy h^{-1}]}$$.

2 – Determine the enhancement of the risk factor for climate event.

In other words, the target is not so much the absolute risk factor itself, but how it changes for a particular climate event. This is for now the best way to proceed, given the state of advancement and validation of the modelling system.

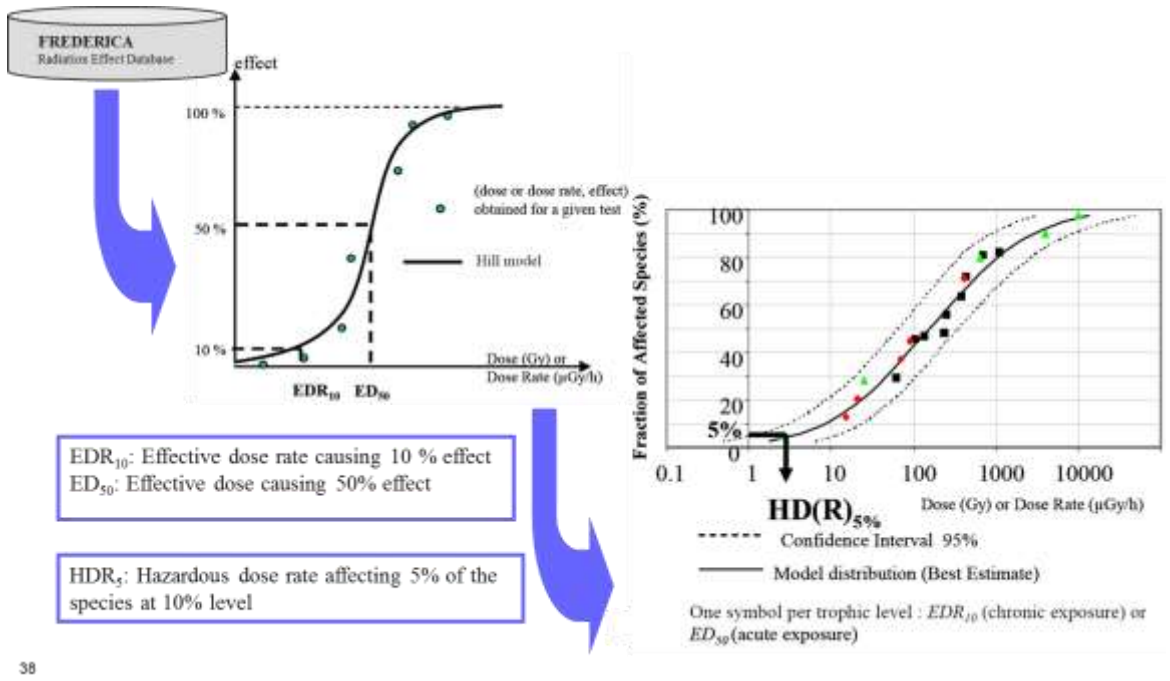

Figure 36: Schematic of the ERICA approach for deriving a benchmark level for protection from radiation in an ecosystem

The above approach is demonstrated by means of examples, involving the radionuclides ^{238}U, ^{137}Cs and ^{90}Sr. Options for future analysis would include considering different bottom boundary conditions including free drainage where water flows downwards under the force of gravity and a static water table at the bottom where water could move upward or downward depending on the pressure head gradient, giving concentration of contaminated groundwater flowing into the unsaturated zone. The constant bottom boundary condition serves the purpose of a routine release scenario, whereas the pulse release can be used to simulate an accident scenario.

Examples of BCC calculation

For this example, we link the element U to an element in the tree and we set constant bottom boundary conditions instead of a pulse release. We used a constant groundwater concentration and we produced two model runs for Mol: Pulse for uranium at year 2, and constant unit concentration source of U at the bottom boundary which starts to be transported with water from day 1. We took a soil profile of 80 cm till the water table, with 40 2-cm thick layers, and we used the results to calculate the Ratio of uranium from plant to top soil (transfer factor) and the ratio between the concentration in the tree and the bottom layer of soil (BCC).

Activity concentrations of U in different surface soil fractions and activity concentration of U in different tree fractions are shown in Figures 37 and 38.

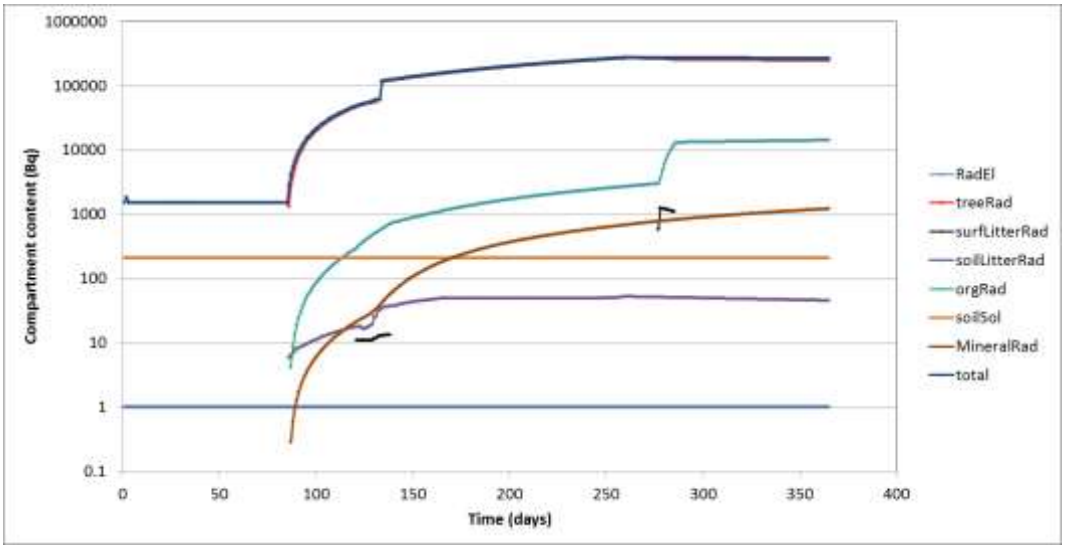

Figure 37: Activity concentrations of U in different surface soil fractions

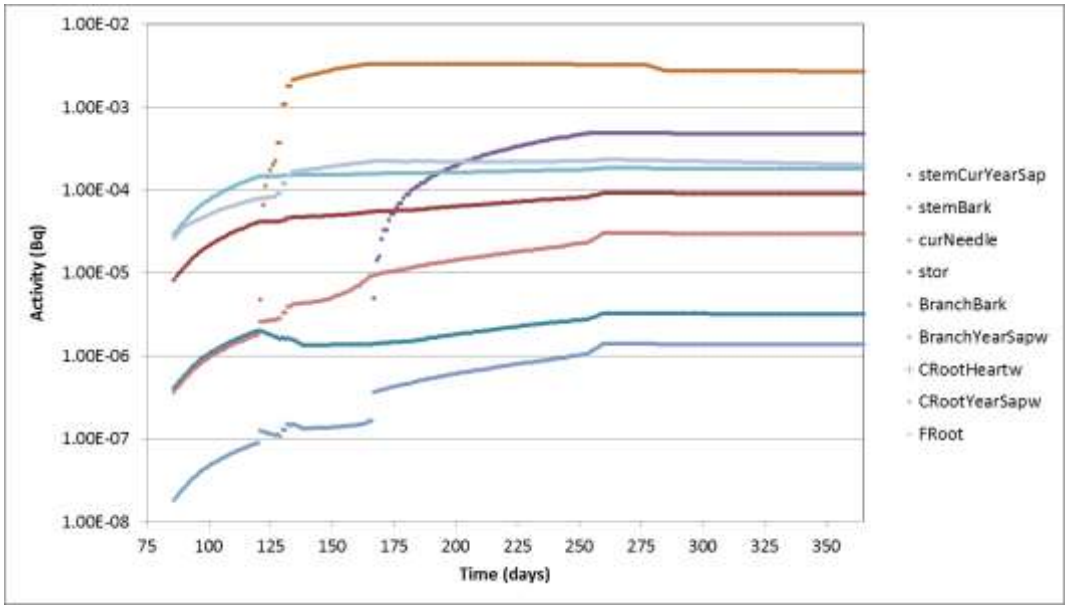

Figure 38: Activity concentration of U in different tree fractions

The U concentration ratio of soil solution at the top of the soil column relative to the bottom is calculated by the model as $\sim 10^{-20}/10^{-15} = 10^{-5}$. This seems reasonable after 1 year, given the high K_d of U; hence, soil column transport seems to be realistically calculated by the model.

The wood to roots concentration ratio after 1 year can be deduced from Cwood = 1.23×10^{-4} Bq kg^{-1} (all except needles) and Croot = 1.78×10^{-4} Bq kg^{-1}.
Hence the ratio of wood/root is 0.69 compared with a measured value of 0.08 (Roivainen, Makkonen *et al.* 2011). This higher ratio shows that ANAFORE calculates U plant uptake over-conservatively. The reason for this is the established link of U to phosphorous in ANAFORE. To achieve more realistic results, the flux from roots to wood in the model can be corrected by a selectivity coefficient = 0.08/0.69 = 0.12, which can be retrofitted in model.

A further test done with the radionuclides ^{238}U, ^{137}Cs and ^{90}Sr show that, starting with equal concentrations in the bottom boundary layer, the model yields concentrations in the proportions 1: 0.9: 0.8, respectively, in soil solution. The fact that U is more available in soil solution than Sr is in agreement with the fact that at pH < 5.5 and the low clay content prevalent in Mol soils (Vincke 2006), uranium is more soluble (has a lower K_d) than strontium as calculated by the parametric K_d approach. The fact that ^{137}Cs (which has a higher K_d than the other two elements) has comparable mobility relates to the fact that sorption is not the only factor affecting transport. The transport equation considers both advection and diffusion processes, And Cs having the highest diffusion coefficient of the 3 elements considered (see Table 21), given the low flow vertical rate considered in the simulation and hence the relative importance of diffusive transport, assists in enhancing the vertical migration of this radionuclide.

Element	pH	Silt	Clay	Sheppard formula	K_d (L kg^{-1})	D_c (m^2 s^{-1})
U	4.2	0.061	0.015	$\text{Log}(K_d) = 1.75 + 0.0145\cdot(\text{clay})\cdot(\text{pH})$	5.64E+01	1.00E-09
Cs	4.2	0.061	0.015	$\text{Log}(4.2\cdot K_d) = 3.03 + 0.101\cdot(\text{pH}) + 0.0117\cdot(\text{clay})$	6.80E+02	2.06E-09
Sr	4.2	0.061	0.015	$\text{Log}(K_d) = 2.93 - 0.224\cdot(\text{pH}) + 0.0217\cdot(\text{clay})$	9.76E+01	7.91E-10

Table 21: Parametric Kd's and diffusion coefficient (Dc) data for U, Cs and Sr for sandy soil (Buffle, Zhang et al. 2007, Sheppard 2011)

Climate simulation

For the following test, which provides our fullest example of application of the radionuclide transport module in context of assessing changes in radiation risk to a forest due to changes of climate, we devised a simulation with ^{238}U, ^{137}Cs and ^{90}Sr for

the Mol scenario, with two types of climate: climate type A (10 dry summers) and B (10 wet summers).

Figure 39 shows, for the Mol location, a the time-series of the 30 years of monthly mean precipitation (mm d^{-1}) for all months in the HIST simulations done by ALARO-0 (see section 2.4.1.2), as connected points. Against a white/grey background for different years, red points represent JJA (= June, July, August) months and small black points represent non-JJA months. The height of the dark grey bars in the background denotes the mean JJA precipitation for each year (high = wet; low = dry). The numbers above the graph show the ranking of these bar, from driest to wettest. The seven driest summers are shown with red labels on the x-axis. Likewise, the seven wettest summers are shown in blue. To generate the climate files for the model, climate sequences of 10 years were sampled from the red (dry climate) and blue (wet climate) years. As proved in section 2.4.2.2, results of ANAFORE depend on inter-annual variability and we have generated 4 dry climates sequences and 4 wet climate sequences requiring to perform 8 model runs, for the purposes of analysing the mean difference between dry ("A") and wet ("B") climate, independent of the exact sequence.

The results of the simulation are shown in Table 22. The results are expressed in relative terms, namely, the activity concentrations in soil solution for a given dry or wet simulation (Ai or Bi, respectively, for i = 1…4) divided by the overall mean A1…A4 to B1…B4, which would represent the 'mean climate'.

Year	Isotope	A1	A2	A3	A4	B1	B2	B3	B4	Mean A	Mean B	% diff.
7	^{238}U	1.00	1.00	1.00	1.00	1.00	1.00	1.00	1.00	1.00	1.00	0
	^{137}Cs	1.00	1.00	1.00	1.00	1.00	1.00	1.00	1.00	1.00	1.00	0
	^{90}Sr	1.00	1.00	1.00	1.00	1.00	1.00	1.00	1.00	1.00	1.00	0
8	^{238}U	0.99	0.99	0.99	0.99	0.99	1.08	0.99	0.99	0.99	1.01	-2.3
	^{137}Cs	0.13	0.13	0.13	0.13	0.13	7.07	0.13	0.13	0.13	1.87	-170
	^{90}Sr	1.00	1.00	1.00	1.00	1.00	1.03	1.00	1.00	1.00	1.00	-0.91
9	^{238}U	0.22	0.22	0.22	2.12	0.22	4.59	0.22	0.22	0.69	1.31	-62
	^{137}Cs	0.00	0.00	0.00	2.41	0.00	5.59	0.00	0.00	0.60	1.40	-79
	^{90}Sr	0.41	0.41	0.41	1.85	0.41	3.70	0.41	0.41	0.77	1.23	-46
10	^{238}U	0.14	0.70	1.09	2.27	0.14	2.86	0.32	0.47	1.05	0.95	10
	^{137}Cs	0.00	0.65	1.10	2.48	0.00	3.17	0.21	0.38	1.06	0.94	12
	^{90}Sr	0.30	0.75	1.08	2.05	0.30	2.53	0.44	0.56	1.04	0.96	8.7

Table 22 : Results of climate simulations for the scenarios from Figure 3

Our interpretation is as follows. The effect of climate variation appears to be cumulative. For the first few years there are no observable differences, probably because the detrimental effect of the wet compared with dry conditions operates at lower speed that the main processes of advection and transport and cannot manifest in just a few years. By year 9, wet climate concentrations of radionuclides in soil solution exceed dry climate by around 60%. By year 10, dry climate concentrations of radionuclides in soil solution exceed wet climate by around 10%. This behaviour depends on the bulk annual volume of precipitation, as well as the short-term variations, which vary for each model simulation even within the dry (A) and wet (B) category. In dryer periods, upward transport of radionuclides is slower, whereas in generally wet conditions upward transport is less restricted because the soil is more saturated opening the pathway for radionuclide migration through diffusion, even if the general direction of the flow is slowly downwards. This facilitates the increase in concentration of elements with a high diffusion coefficient like ^{137}Cs.

In the most extreme case, corresponding to model run B2, year 8 (1983) registers a very high precipitation during June to August and a result there is an order of magnitude enhancement of the concentration of ^{137}Cs. Assuming the concentration of ^{137}Cs in the tree is linearly proportional to the concentration in the soil solution (from which it proceeds by root uptake), an assumption reasonably valid at low molar concentrations, one can expect the radiation dose rate to the tree to increase by a factor of 10, even though in practice the dose rate will be small.

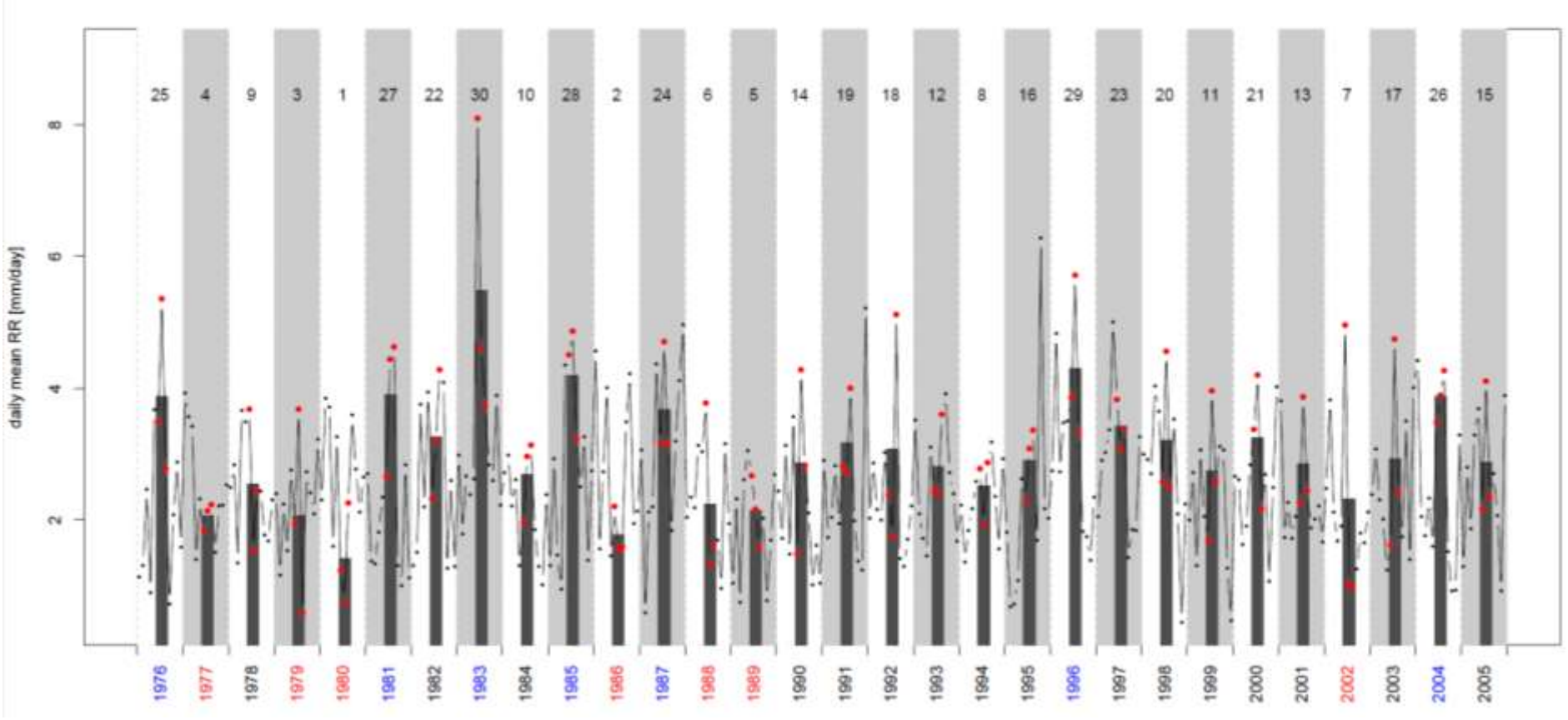

Figure 39: Projected Mol climate scenario for use in radionuclide transport model simulations comprising 10 dry (type A) and 10 wet (type B) summers.

3. POLICY SUPPORT

3.1. Model availability

At the start of this project it was not certain whether we it would be possible or not to have a single modelling system running in real time including all the calculations of the different submodels. We finally managed to realise a fully linked model system instead of a database with model results. In this way, we are now able to run out model to answer specific questions concerning the effects of global climate change on Belgian forests.

ANAFORE

The ANAFORE forest model and a short user manual and input files for the Brasschaat Scots pine forest can be requested. We realise that this model is not the most user friendly for non-specialists, but at the University of Antwerpen the modelling team is available for training or help (contact: gaby.deckmyn@uantwerpen.be)

ALARO-0 CORDEX data

All Climate data is available through the Earth System Grid Federation data nodes (ESGF, website: http://esgf.llnl.gov/). For support contact olivgiot@meteo.be.

Radiological risk assessment

It is in principle possible to link model output to the ERICA assessment tool for the calculation of radiation dose to the trees, for the purpose of assessing environmental impact under different climate scenarios, although this requires manual transfer of the output (the calculated activity concentrations for the selected radionuclides) given that ERICA is a separate and independent piece of software. The software is free to download and use, but it is necessary to register using a valid e-mail address. This registration will enable the user to keep you informed of new updated versions, also available free of charge. The download link for ERICA is: http://www.erica-tool.com/erica/download/

PHREEQC

The latest standalone versions of the geochemical equilibrium and reaction code PHREEQC are available at the dedicated USGS webpage: www.brr.cr.usgs.gov/projects/GWC_coupled/phreeqc/ (accessed 3 January 2017).

Concerning PHREEQC and nutrient allocation in the tree: a specific user manual is available on request through quentin.ponette@uclouvain.be or mathieu.jonard@uclouvain.be.

3.2. Possible applications

The integrated version of the model can be used to investigate climate change responses of forest stands concerning:

- Tree growth, yield and C stocks
- Any tree species after parameterisation; oak, beech, spruce and Scots pine have been parameterised
- All C, H_2O, N, P, (K, Ca, Mg are not fully parameterised) fluxes from half-hourly to yearly scale
- Detailed management simulations:
    - Detailed thinning and cutting options, rotation length
    - Removal of branches/bark/tree tops at harvest
    - Dead wood options
    - Regeneration options
    - liming
- Calculation of the transport of selected radionuclides after point pollution or pollution through a contaminated water table.
- Evaluating the effect of site fertility, including internal and external element fluxes, and tree nutritional status on tree growth, quantifiying the contribution of fluxes and stocks to nutrient cycling and storage in forest ecosystems.

3.3. Impact of results

Our results show the importance of paying attention to soil nutrients and pollutants when making decisions concerning forest management under a changing climate. Small changes such as leaving branches on site at harvest, can have a (small) significant impact on retaining soil nutritional balance.

Past emphasis was either only on the aboveground biomass or on soil carbon storage but resent findings and this study clearly show the necessity of including more nutrients and pollutants to come to a correct interpretation of the risks of climate change to forest ecosystems. These results should have an impact on future management plans and we hope (and will try to ensure) these findings are use.
We showed that the inclusion of random weather variations in models with climate scenarios has a significant effect on the results.
This is a good option to get a correct idea of the risks of a particular climate (even if the average effect is positive, the risk of a very negative effect can be enhanced under global change for example by three consecutive dry years). Past studies generally used only one run of each climate scenario which results in a rather random output.

A third important conclusion from our study is the high sensitivity of the predicted results to soil temperature and soil moisture changes. These drivers need to be

monitored as key drivers at risk by the changing climate. Soils where changes in groundwater availability or soil temperature (depending on ground cover, humidity) are expected are at a higher risk for changes in nutrient turnover leading to major effects on ecosystem functioning.

3.4. Policy oriented conclusions

Belgium will become warmer and have wetter winters in future according to detailed predictions, available through the RMI. Although random selection of weather has a significant effect on the results the main conclusions concerning the vulnerability of Belgian forests are clear and quite consistent over all parameter sets used. Early growth (establishment of the stand) is very sensitive and very cold, dry or hot conditions during the first 10 years tend to influence final productivity, mainly through effects on the soil leading to reduced nutrient availability.

At the Brasschaat site, adult trees have access to ground water and are not vulnerable to drought. Increased CO_2 concentration and temperature increase the productivity of this stand under global warming. Only drought during the first 10 years can result in a reduced productivity. In conclusion: the risk for a bad establishment and yield is higher under changing climate, but the average predicition is a 3-6 % increase in productivity.

Phosphorus in the soil is close to limiting or limiting in Brasschaat. The simulations suggest a depletion of the organic P pools in the holorganic layer as well as in the mineral soil, which would cause a risk to the next forest rotations.

On humid soils radionuclides are able to enter the ecosystem through diffusion from the groundwater table and can be taken up by trees.

4. DISSEMINATION AND VALORISATION

4.1. Final meeting

The final meeting for our Steering Committee members where the final results were presented, has been in Antwerpen. We welcome new opportunities to use the developed tools together with our Steering Committee members.

4.2. Presentations at scientific meetings and summer schools

Deckmyn, G. Lecturer Coimbra Summer School (Portugal) on soil ecology 'Soil models: the good, the bad and the ugly', 5-7/10/2016.

Deckmyn, G. Presentation 'Soil models: lessons learned and future '. COST meeting TARTU, 17-19/1/2017.

Vives i Batlle, J. (2016). Process and data identification in a radionuclide forest model. COMET Workshop 3 (session on fit for purpose models and data for terrestrial forests), Sevilla, June 15-17, 2016.

Vives i Batlle, J., Gielen, S., Vandenhove, H. (2015). Modelling water and Cl cycling in forests: ECOFOR development. COMET WP3 meeting, Oslo, 29-30 January 2015.

Vives i Batlle, J., Al Mahaini, T., Sarioglu, S. (2014). Project ECORISK – latest developments in flow and transport modelling. BIOPROTA Annual Workshop - Key Issues in Biosphere Aspects of Assessment of the Long term Impact of Contaminant Releases Associated with Radioactive Waste, London, United Kingdom.

Andivia, E., Genon, J.G., Jonard, M., Deckmyn, G., Ceulemans R., Ponette Q.. Oral presentation 'A process-based soil-plant model to assess nutritional limitations on forest growth within a changing environment'. 27th International Biennial Conference of the IUFRO Research Group 7.01, "Global Challenges of Air Pollution and Climate Change to Forests", conference session 4 "Health and growth of forests: bridging monitoring and modelling". Nice 2-5/6/2015.

4.3. New initiatives

The consortium is trying for new projects using the modelling tools developed in ECORISK. The 'FORHOPE' project was submitted to SBO for funding, but was unfortunately not funded.

The PLECO team (University of Antwerp) is involved in three ongoing European COST actions based on the work accomplished during this project:

- BIOLINK: linking belowground diversity. G. Deckmyn is workgroup leader of workgroup 4, Soil modelling
- KEYSOM: role of soil fauna on SOM. G. Deckmyn is management committee member.
- PROFOUND: towards robust projections of European forests. J. Horemans is Steering Committee member of this COST action.

G. Deckmyn is workgroup leader of an international consortium working on a new soil simple modelling design, the prototype model is expected by summer 2017.

The SCK team is part of a successful proposal for project TERRITORIES under the EC programme CONCERT (http://www.concert-h2020.eu/), where it will continue working on development of the ECOFOR model applied to a Belgian NORM-radionuclide contaminated site. SCK-CEN has also announced a PhD project on forest modelling "Field and modelling studies on the transfer of radionuclides to vegetation in the NORM-contaminated Tessenderlo site" (http://academy.sckcen.be/en/Your_thesis_internship/PhD_thesis/Topics) where the SVAT modelling research theme started under WP3 weill be continued. We plan in future to write jointly with UA, KMI a paper on the development and optimization of the forest model – this should be done between Talal and Olivier, when both become available. There is also the possibility to mention that UA as leaders of the project will write jointly with everybody an umbrella paper' on the project, which could be easily derived from the final report. We should keep this in mind.

SCK's involvement in forest modelling will continue through research including further development of ECOFOR in a new PhD project on Field and modelling studies on the transfer of radionuclides to vegetation in the NORM-contaminated Tessenderlo site (http://academy.sckcen.be/en/Your_thesis_internship/AllTopics/Field-and-modelling-studies-on-the-transfer-of-radionuclides-to-vegetation-in-the-NORM-contaminated-Tessenderlo-site-1675).

The forest science group (UCL) is also involved in the EUMIXFOR COST action with Q. Ponette as working group 1 leader and in the PROFOUND COST action with M. Jonard as management committee member.

The RMI is a part of the CORDEX.be project (www.euro-cordex.be) which is a 2-year BELSPO project that aims to gather existing and ongoing Belgian research activities in the domain of climate modelling to create a coherent scientific basis for future climate services in Belgium.
The PLECO team is involved in the new international soil modelling platform ICSM (International Soil Modelling Consortium) https://soil-modelling.org/governance.

5. PUBLICATIONS

Gielen, S., Vives i Batlle, J., Vincke, C., Van Hees, M. and Vandenhove, H. (2016). Concentrations and distributions of Al, Ca, Cl, K, Mg and Mn in a Scots pine forest in Belgium. Ecological Modelling 324: 1–10.

Giot, O., Termonia, P., Degrauwe, D., De Troch, R., Caluwaerts, S., Smet, G., Berckmans, J., Deckmyn, A., De Cruz, L., De Meutter, P., Duerinckx, A., Gerard, L., Hamdi, R., Van den Bergh, J., Van Ginderachter, M., and Van Schaeybroeck, B. (2016). Validation of the ALARO-0 model within the EURO-CORDEX framework, Geosci. Model Dev., 9, 1143-1152, doi:10.5194/gmd-9-1143-2016.

Vives i Batlle, J., Vandenhove, H., Gielen, S. (2014). Modelling water and ^{36}Cl cycling in a Belgian pine forest. In: Proc. ICRER 2014 - 3rd International Conference on Radioecology & Environmental Radioactivity, 7-12 September 2014, Barcelona, Spain. Electronic proceedings Session: 05.1. Radioactive Waste Management & Disposal, Paper OP-035. Available from: http://radioactivity2014.pacifico-meetings.com/.

Deckmyn, G., Meyer, A., Smits, M. M., Ekblad, A., Grebenc, T., Komarov, A., Kraigher, H. (2014). Simulating ectomycorrhizal fungi and their role in carbon and nitrogen cycling in forest ecosystems
Revue canadienne de recherche forestière-issn 0045-5067-44, p. 535-553 http://hdl.handle.net/10067/1183700151162165141

Horemans, J., Bosela, M., Dobor, L., Barna, M., Bahyl, J., Deckmyn, G., Fabrika, M., Sedmak, R., Ceulemans, R. (2016). Variance decomposition of predictions of stem biomass increment for European beech: contribution of selected sources of uncertainty Forest ecology and management-issn 0378-1127-361, p. 46-55 http://hdl.handle.net/10067/1289580151162165141

Schaubroeck, T., Deckmyn, G., Giot, O., Campioli, M. *et al.* (2016). Environmental impact assessment and monetary ecosystem service valuation of an ecosystem under different future environmental change and management scenarios : a case study of a Scots pine forest, Journal of environmental management 173 - ISSN 0301-4797-173, p. 79-94

Bortier, M. F. M., Enrique, A., Genon, J., Deckmyn, G. (2017). Simulating phosphorus cycling in forest ecosystem models: a process-based approach. In preparation

6. ACKNOWLEDGEMENTS

The computational resources and services used in this work were partly provided by the VSC (Flemish Supercomputer Center), funded by the Research Foundation - Flanders (FWO) and the Flemish Government – department EWI. We thank the Steering Committee members for their useful feedback and input.

7. REFERENCES

Andivia, E., Genon, J., Jonard, M., Deckmyn, G., Ceulemans, R., and Q. Ponette (2015). A process-based soil-plant model to assess nutritional limitations on forest growth within a changing environment. Oral presentation at the 27th International Biennial Conference of the IUFRO Research Group 7.01, "Global Challenges of Air Pollution and Climate Change to Forests", conference session 4 "Health and growth of forests: bridging monitoring and modelling". Nice on June 2-5, 2015.

ALADIN International Team (1997). The ALADIN project: Mesoscale modelling seen as a basic tool for weather forecasting and atmospheric research. WMO Bull., 46, 317–324

Appelo, C.A.J. (1994). Cation and proton exchange, pH variation, and carbonate reactions in a freshening aquifer. Water Resources Res. 30(10):2793-2805.

Baes, C. F. and R. D. Sharp (1983). "A proposal for estimation of soil leaching and leaching constants for use in assessments models." Journal of Environmental Quality 12: 17-28.

Beresford, N. A., Brown, J., Copplestone, D., Garnier-Laplace, J., Howard, B., Larsson, C.-M., Oughton, O., Pröhl, G., and I. Zinger (2007). D-ERICA: An integrated approach to the assessment and management of environmental risks from ionising radiation. Description of purpose, methodology and application. A deliverable of the ERICA project (FI6RCT-2004-508847). Available via http://wiki.ceh.ac.uk.

Blanco, J.A., Zavala, M.A., Bosco Imbert, J., and F.J. Castillo (2005). Sustainability of forest management practices: Evaluation through a simulation model of nutrient cycling. For. Eco. Manag. 213: 209-228.

Brakensiek, D. L., Rawls, W..J., and G. R. Stephenson (1984). Modifying SCS hydrologic soil groups and curve numbers for rangeland soils. In: Proc. Annual meeting of the American society of agricultural engineers, Pacific northwest region. Kennewick, WA, USDA-ARS, Paper Number PNR-84-203, 13 pp.

Brission, N., Seguin, B., and P. Bertuzzi (1992). "Agrometeorological soil water balance for crop simulation models." Agricultural and Forest Meteorology 59: 267–287.

Brown, J., Alfonso, B., Avila, R., Beresford, N., Copplestone, D., and A. Hosseini (2016). "A new version of the ERICA tool to facilitate impact assessments of radioactivity on wild plants and animals." Journal of Environmental Radioactivity 153: 141-149.

Brown, J. E., Alfonso, B., Avila, R., Beresford, N. A., Copplestone, D., Pröhl, G., and A. Ulanovsky (2008). "The ERICA Tool." Journal of Environmental Radioactivity 99(9): 1371-1383.

Bubnova, R., Hello, G., Bénard, P., and J.-F. Geleyn (1995). Integration of the fully-elastic equations cast in the hydrostatic pressure terrain-following coordinate in the framework of the Arpge/Aladin NWP system. Mon. Wea. Rev., 123, 515–535.

Buffle, J., Zhang, Z., and K. Startchev (2007). "Metal flux and dynamic speciation at (bio)interfaces. Part I: Critical evaluation and compilation of physico-chemical parameters for complexes with simple ligands and fulvic/humic substances." Environmental Science & Technology 41(22): 7609-7620.

Campioli, M., Vincke, C., Jonard, M., Kint, V., Demarée, G., and Q. Ponette (2012). Current status and predicted impact of climate change on forest production and biogeochemistry in the temperate oceanic European zone : review and prospects for Belgium as a case study, Journal of forest research - 17:1, p. 1-18

Casadesus, J., Sauras-Year, T., and V. R. Vallejo (2008). "Predicting soil-to-plant transfer of radionuclides with a mechanistic model (BioRUR)." Journal of Environmental Radioactivity 99(5): 864-871.

Ceulemans, R., Kowalski, A.S., Berbigier, P., Dolman, A.J., Grelle, A., Janssens, L. A., Lindroth, A., Moors, E., Rannik, U., and T. Vesala (2003). "Coniferous forests (Scots and Maritime pine): carbon and water fluxes, balances, ecological and ecophysiological determinants." Ecological Studies 163: 71-97.

Charlton, S.R., and D.L. Parkhurst (2011). Modules based on the geochemical model PHREEQC for use in scripting and programming languages. Computers and Geosciences 37(10):1653-1663.3.

Copplestone, D., Hingston, J.L., and A. Real (2008). "The development and purpose of the FREDERICA radiation effects database." Journal of Environmental Radioactivity 99(9): 1456-1463.

Curtin, D., and H.P.W. Rostad (1997). Cation exchange and buffer potential of Saskatchewan soils estimated from texture, organic matter and pH. Can. J. Soil Sci. 77:621-626.

Deckmyn, G., Campioli, M., Muys, B., and H. Kraigher (2011). Simulating C cycles in forest soils: Including the active role of micro-organisms in the ANAFORE forest model. Ecological Modelling 222:1972–1985.

Deckmyn, G., Verbeeck, H., Op de Beeck, M., Vansteenkiste, D., Steppe, K., and R. Ceulemans (2008). ANAFORE: A stand-scale process-based forest model that includes wood tissue development and labile carbon storage in trees. Ecological Modelling 215:345–368.

Deckmyn, G., Meyer, A., Smits, M. M., Ekblad, A., Grebenc, T., Komarov, A., and H. Kraigher (2014). Simulating ectomycorrhizal fungi and their role in carbon and nitrogen cycling in forest ecosystems
Revue canadienne de recherche forestière-issn 0045-5067-44,p. 535-553.

Dee, D. P., Uppala, S. M., Simmons, A. J., Berrisford, P., Poli, P., Kobayashi, S., Andrae, U., Balmaseda, M., et al. (2011). The ERA-Interim reanalysis: configuration and performance of the data assimilation system. Q.J.R. Meteorol. Soc., 137: 553–597. doi:10.1002/qj.828

Déqué, M., Marquet, P., and R.G. Jones (1998). Simulation of climate change over Europe using a global variable resolution general circulation model. Clim. Dyn. 14, 173–189.

De Troch, R., Hamdi, R., Van de Vyver, H., Geleyn, J.F., and P. Termonia (2013). "Multiscale Performance of the ALARO-0 Model for Simulating Extreme Summer Precipitation Climatology in Belgium." Journal of Climate 26 (22): 8895–8915.

De Vries, W., and M. Posch (2003). Derivation of cation exchange constants for sand, loess clay and peat soils on the basis of field measurements in the Netherlands. Alterra -Report 701, Alterra, Green World Research, Wageningen.

ENGREF (1984). Tables de production pour les forêts françaises. 2e édition. Nancy, France.159 pp.

ERICA (2009). "Environmental Risk from Ionising Contaminants: Assessment and Management (ERICA)." The ERICA ASSESSMENT TOOL (version May 2009): [Online] http://www.project.facilia.se/erica/download.html.

Fernandez-Martinez, M., Vicca, S., Janssens, I.A., et al. (2014). Nutrient availability as the key regulator of global forest carbon balance. Nature Climate Change 4:471–476.

FREDERICA (2006). FREDERICA Radiation Effects Database. Available from: http://www.frederica-online.org/mainpage.asp [Accessed 11 July 2016].

Fuentes, J. P., Bustamante, V., and H. Bown (2010). Comparison of soil water repellency and sorptivity between an Acacia caven (highly-perturbed) and Cryptocarya alba (slightly-perturbed) dominated ecosystem. In: Proc. Soil Solutions for a Changing World: 19th World Congress of Soil Science, 1 – 6 August 2010, Brisbane, Australia.

Garnier-Laplace, J., Copplestone, D., Gilbin, R., Alonzo, F., Ciffroy, P., Gilek, M., Agüero, A., Björk, M., Oughton, D.H., Jaworska, A., Larsson, C.M., and J. L. Hingston (2008). "Issues and practices in the use of effects data from FREDERICA in the ERICA Integrated Approach." Journal of Environmental Radioactivity 99(9): 1474-1483.

Gear, C. W. (1971). Numerical initial value problems in ordinary differential equations, Prentice-Hall, NJ.

Gerard, L. and J-F. Geleyn (2005). Evolution of a subgrid deep convection parametrization in a limited-area model with increasing resolution. Q.J.R. Meteorol. Soc., 131: 2293–2312. doi:10.1256/qj.04.72

Gerard, L., Piriou, J., Brožková, R., Geleyn, J., and D. Banciu (2009). Cloud and Precipitation Parameterization in a Meso-Gamma-Scale Operational Weather Prediction Model. Mon. Wea. Rev., 137, 3960–3977, doi: 10.1175/2009MWR2750.1.

Gielen, S. (2013). Element cycling in a Belgian pine forest. MSc Thesis, XIOS Hogeschool Limburg, Hasselt, Belgium, 153 pp.

Gielen, S., Vives i Batlle, J., Vincke, C., Van Hees, M. and H. Vandenhove (2016). "Concentrations and distributions of Al, Ca, Cl, K, Mg and Mn in a Scots pine forest in Belgium." Ecological modelling 324: 1-10.

Giorgi, F., and L. O. Mearns (1999), Introduction to special section: Regional Climate Modeling Revisited, J. Geophys. Res., 104(D6), 6335–6352, doi:10.1029/98JD02072.

Giorgi, F., Jones, C. and G. R. Asrar. (2009). Addressing climate information needs at the regional level: the CORDEX framework. Bulletin of the World Meteorologic Organization 58, 175-183.

Hamdi, R., Van de Vyver, H., and P. Termonia (2012). New cloud and microphysics parameterisation for use in high-resolution dynamical downscaling: application for summer extreme temperature over Belgium. Int. J. Climatol., 32, 2051–2065, doi:10.1002/joc.2409

Helling, S.H., Chester, G., and R.B. Corey (1964). Contribution of organic matter and clay to soil cation exchange capacity as affected by the pH of the saturation solution. Soil Sci. Soc. Am. Proc. 28:517-520.

Hyvönen, R., Agren, G. I., Linder, S., et al. (2007). The likely impact of elevated [CO2], nitrogen deposition, increased temperature and management on carbon sequestration in temperate and boreal forest ecosystems: a literature review. New Phytologist. 173 (3): 463-480

Giot, O., Termonia, P., Degrauwe, D., De Troch, R., Caluwaerts, S., Smet, G., Berckmans, J., Deckmyn, A., et al. (2016). Validation of the ALARO-0 model within the EURO-CORDEX framework, Geosci. Model Dev., 9, 1143-1152, doi:10.5194/gmd-9-1143-2016.

Haylock, M.R., Hofstra, N., Klein Tank, A.M.G, Klok, E.J., Jones, P.D. and M. New. (2008). A European daily high-resolution gridded dataset of surface temperature and precipitation. J. Geophys. Res (Atmospheres), 113, D20119, doi:10.1029/2008JD10201

Hölttä, T., Vesala, T., Sevanto, S., Perämäki, M., and E. Nikinmaa (2006). "Modelling xylem and phloem water flows in trees according to cohesion theory and Münch hypothesis." Trees – structure and function 20(1): 67-78.

IAEA (2009). Quantification of radionuclide transfer in terrestrial and freshwater environments for radiological assessments, IAEA-TECOC-1616, Vienna, 616 pp.

IPCC (2013). Climate Change 2013: The Physical Science Basis. Contribution of Working Group I to the Fifth Assessment Report of the Intergovernmental Panel on Climate Change [Stocker, T.F., D. Qin, G.-K. Plattner, M. Tignor, S.K. Allen, J. Boschung, A. Nauels, Y. Xia, V. Bex and P.M. Midgley (eds.)]. Cambridge University Press, Cambridge, United Kingdom and New York, NY, USA, 1535 pp.

Jansen, J.J., Stevenster, J., and P.J. Faber (1996). Opbrengst tabellen voor belangrijke boomsoorten in Nederland. IBN rapport nr. 221. 240 pp.

Jonard M. (2005). Dynamique des litières foliaires en peuplements purs et mélangés de chêne et de hêtre : Retombées foliaires et premières étapes de la décomposition. Ph.D. Thesis, UCL, Louvain-la-Neuve, 205 pp.

Jonard, M., Legout, A., Nicolas, M., et al. (2012). Deterioration of tree vitality despite a sharp decline in acid deposition: a long-term regional perspective. Global Change Biology 18:711-725.

Jonard, M., Fürst, A., Verstraeten, A., Thimonier, A., Timmermann, V., Potočić, N., Waldner, P., Benham S., et al. (2015). Tree mineral nutrition is deteriorating in Europe, Global Change Biol. 21(1):418-430.

Ketterings, Q. M., Coe, R., Noordwijk, M., Ambagau, Y., and C. A. Palm (2001). "Reducing uncertainty in the use of allometric biomass equations for predicting above-ground tree biomass in mixed secondary forests." Forest Ecology and Management 146: 199-209.

Kotlarski, S., Keuler, K., Christensen, O. B., Colette, A., Déqué, M., Gobiet, A., Goergen, K., Jacob, D., Lüthi, D., van Meijgaard, E., Nikulin, G., Schär, C., Teichmann, C., Vautard, R., Warrach-Sagi, K., and V. Wulfmeyer (2014). Regional climate modeling on European scales: a joint standard evaluation of the EURO-CORDEX RCM ensemble, Geosci. Model Dev., 7, 1297-1333, doi:10.5194/gmd-7-1297-2014.

Lane, L. (2012). "Lane, L. Sucrose solutions, composition, viscosity, density at 20oC. Available from: http://lclane.net/text/sucrose.html (Accessed 18 April 2012)."

Li, K. Y., Boisvert, J.B., and R. De Jong (1999). "An exponential root-water-uptake model." Canadial Journal of Soil Science 79: 333–343.

Mallants, D. (2005). Data collection in support of biosphere calculations concerning water and radionuclide uptake by plant roots from shallow groundwater. Report SCK•CEN-R-4199, 27 pp.

Meerts, P. (2002). Mineral nutrient concentrations in sapwood and heartwood: a literature review. Ann. For. Sci. 59, 713-722.

Millard, P. and G.A. Grelet (2010). Nitrogen storage and remobilization by trees: ecophysiological relevance in a changing world. Tree Physiol. 30: 1083-1095.

Mollier, A., De Willigen, P., Heinen, M., Morel, C., Schneider, A., and S. Pellerin (2008). A two-dimensional simulation model of phosphorus uptake including crop growth and P-response. Ecological Modeling 210:453-464.

Monteith, J., and M. Unsworth (2007). Principles of Environmental Physics, Third Ed. Academic press, 418 pp.

Nonweilwer, T. R. F. (1975). Flow of biological fluids through non-ideal capillaries. Encyclopedia of Plant Physiology 1: 474-477 (New series).

Overloop, S., and L. Meiresonne (1999). Basiskarakteristieken van het proefvlak Brasschaat, domeinbos De Inslag. Mededelingen IBW 1999/1 11

Parkhurst, D.L., and C.A.J. Appelo (2013). Description of input and examples for PHREEQC version 3 - A computer program for speciation, batch-reaction, one-dimensional transport, and inverse geochemical calculations. Chapter A43 in U.S. Geological Survey Techniques and Methods, book 6..

Pausas, J. (1997). "Litter fall and litter decomposition in Pinus sylvestris forests of the eastern Pyrenees." Journal of Vegetation Science 8: 643-650.

Peñuelas, J., Poulter, B., Sadans, J., et al. (2013). Human-induced nitrogen-phosphorus imbalances alter natural and managed ecosystems across the globe. Nature Communications 4:1-10.

Perez-Sanchez, D., Thorne, M.C., and L. M. C. Limer (2012). "A mathematical model for the behaviour of Se-79 in soils and plants that takes account of seasonal variations in soil hydrology." Journal of Radiological Protection 32: 11–37.

Philip, J. R. (1957). "The theory of infiltration: 4. Sorptivity and algebraic infiltration equations." Soil Science 77: 153–157.

Posch, M., and D. Kurz (2007). A2M - a program to compute all possible mineral modes from geochemical analyses. Computers Geosci. 33(4): 563-572.

Prein, A. F., Langhans, W., Fosser, G., Ferrone, A., Ban, N., Goergen, K., Keller,M., Tölle, M., Gutjahr, O., Feser, F., et al. (2015). A review on regional convection-permitting climate modeling: Demonstrations, prospects, and challenges, Rev. Geophys., 53, 323–361. doi:10.1002/2014RG000475.

Raes, D. and P. Deproost (2003). "Model to assess water movement from a shallow water table to the root zone." Agricultural Water Management 62: 79-91.

Riahi, K., Gruebler, A., and N. Nakicenovic (2007). Scenarios of long-term socio-economic and environmental development under climate stabilization. Technological Forecasting and Social Change 74, 7, 887-935.

Rigas, M. L. (2000). "Software Review: Modelmaker 4.0." Risk Analysis 20(4): 543-544.

Roivainen, P., Makkonen, S., Holopainen, T., and J. Juutilainen (2011). "Soil-to-plant transfer of uranium and its distribution between plant parts in four boreal forest species." Boreal Environment Research 16: 158-166.

Rummukainen, M. (2010). State-of-the-art with regional climate models. WIREs Clim Change, 1: 82–96. doi:10.1002/wcc.8

Rushforth, K. (1981). Pocket Guide to Trees. Simon & Schuster, 215 pp.

Saupe, S. G. (2009). "Solute Transport: Phloem Structure & Function. In: Plant Physiology (Biology 327). Available from: http://employees.csbsju.edu/ssaupe/biol327/lecture/phloem.htm (Accessed: 16 April 2012)."

Schroeder, P. R., Dozier, T.S., Zappi, P.A., McEnroe, B.M., Sjostrom, J.W., and R. L. Peyton (1994). The Hydrologic Evaluation of Landfill Performance (HELP) Model -Engineering Documentation for Version 3. USEPA, Cincinnati, Ohio, USA, 116 pp.

Sheppard, S. C. (2011). "Robust Prediction of Kd from Soil Properties for Environmental Assessment." Human and Ecological Risk Assessment 17(1): 263-279.

Šimůnek, J., Van Genuchten, M.T., and M. Šejna (2008). "Development and applications of the HYDRUS and STANMOD software packages, and related codes." Vadose Zone Journal 7(2): 587-600.

Taylor, K.E., Stouffer, R..J., and G.A. Meehl (2012). An Overview of CMIP5 and the experiment design." Bull. Amer. Meteor. Soc., 93, 485-498, doi:10.1175/BAMS-D-11-00094.1.

Teutschbein, C. and J. Seibert, J. (2010). Regional Climate Models for Hydrological Impact Studies at the Catchment Scale: A Review of Recent Modeling Strategies, Geogr. Comp., 4, 834–860, doi:10.1111/j.1749-8198.2010.00357.x.

Teutschbein, C. and J. Seibert (2013). Is bias correction of regional climate model (RCM) simulations possible for non-stationary conditions?, Hydrol. Earth Syst. Sci., 17, 5061-5077, doi:10.5194/hess-17-5061-2013.

Van den Hoof, C. and Y. Thiry (2011). Modelling Natural Chlorine Cycling in a Coniferous Stand: Model Development and Applications. Contract report for ANDRA SCK•CEN-R-XX (in preparation), 50 pp.

Van den Hoof, C. and Y. Thiry (2012). "Modelling of the natural chlorine cycling in a coniferous stand: implications for chlorine-36 behaviour in a contaminated forest environment." Journal of Environmental Radioactivity 107: 56–67.

van der Zee, S.E.A.T.M., Fokkink, L.G.J., and W.H. van Riemsdijk (1987). A new technique for assessment of reversibly adsorbed phosphorus. Soil Sci. Soc. Am. J. 51:599-604.

Van Ranst, E., De Coninck, F., Roskams, P., and N. Vindevogel. (2002). Acid-neutralizing capacity of forest floor and mineral topsoil in Flemish forests (North Belgium). Forest Eco. Manage. 166:45-53.

van Vuuren, D., den Elzen, M., Lucas, P., Eickhout, B., Strengers, B., van Ruijven, B., Wonink, S., and R. van Houdt (2007). Stabilizing greenhouse gas concentrations at low levels: an assessment of reduction strategies and costs. Climatic Change, doi:10.1007/s/10584-006-9172-9.

Vereecken, H., Maes, J., Feyen, J., and P. Darius (1989). "Estimating the soil moisture retention characteristic from texture, bulk density and carbon content." Soil Science 148(6): 389-403.

Vereecken, H., Schnepf, A., Hopmans, J.W., et al. (2016). Modeling Soil Processes: Review, Key Challenges and New Perspectives. Vadose Zone Journal 15(5):1-57.

Vidal, M., Rigol, A. and C. J. Gil-Garcia (2009). "Soil radionuclide interactions. In: IQuantification of radionuclide transfer in terrestrial and freshwater environments for radiological assessments, IAEA-TECOC-1616, Vienna, pp. 71-102."

Vincke, C. (2006). Technical report of the post-doc programme "Contribution to long term biosphere impact modelling in a geological disposal scenario through measurements of soil-tree-atmosphere water transfer and related ecophysiological parameters". Belgian Nuclear Research Centre Report SCK•CEN-I-90, Mol, Belgium, 63 pp. http://hdl.handle.net/2078.1/95302.

Vincke, C. and Y. Thiry (2008). "Water table is a relevant source for water uptake by a Scots pine (Pinus sylvestris L.) stand: Evidences from continuous evapotranspiration and water table monitoring." Agricultural and Forest Meteorology 148(10): 1419-1432.

Wise, M.A., Calvin, K.V., Thomson, A.M., Clarke, L.E., Bond-Lamberty, B., Sands, R.D., Smith, S.J., Janetos, A.C., and J.A. Edmonds (2009). Implications of Limiting CO2 Concentrations for Land Use and Energy. Science. 324:1183-1186. May 29, 2009.

Wright, T. M. and G. M. Will (1958). "The Nutrient Content of Scots and Corsican Pines Growing on Sand Dunes." Forestry 31(1): 13 - 25.

Xiao, C. W. and R. Ceulemans (2004). "Allometric relationships for below- and aboveground biomass of young Scots pines." Forest Ecology and Management 203: 177–186.

Yang, X. and W. M. Post (2011). Phosphorus transformations as a function of pedogenesis: A synthesis of soil phosphorus data using Hedley fractionation method. Biogeosciences 8, 2907–2916.

8. ANNEXES

ANNEX 1 - COPY OF THE PUBLICATIONS

ANNEX 2 - MINUTES OF THE FOLLOW-UP COMMITTEE MEETINGS

ANNEX 3 - NEDERLANDSE SAMENVATTING // RÉSUMÉ FRANÇAIS

The annexes are available on our website

http://www.belspo.be/belspo/SSD/science/pr_risk_en.stm